Quantifying the impact of loads on connections between segments of an immersed tunnel
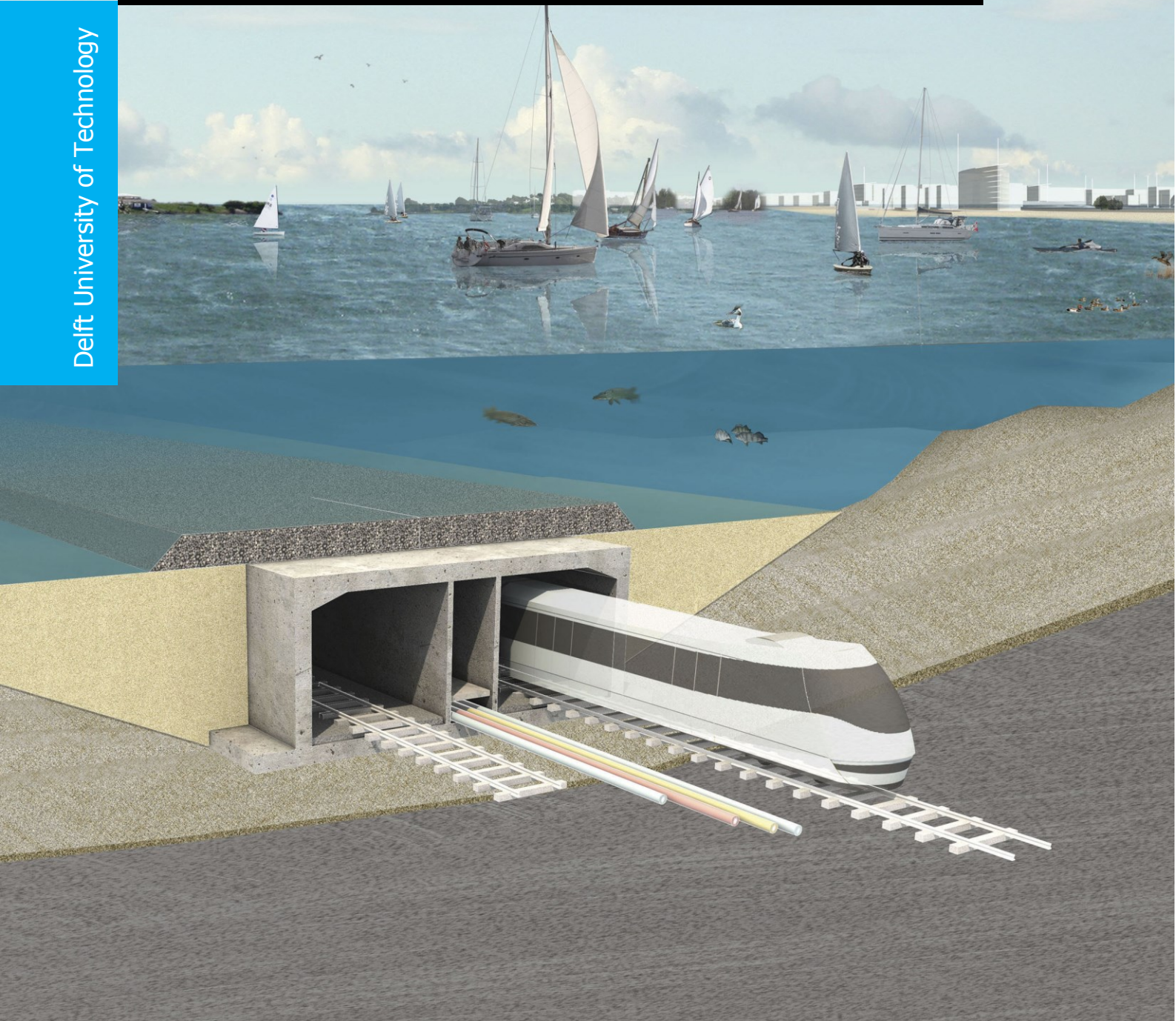
Kamakshi Parwani

QUANTIFYING THE IMPACT OF LOADS ON CONNECTIONS BETWEEN SEGMENTS OF AN IMMERSED TUNNEL

THESIS

submitted in partial fulfillment of the
requirements for the degree of

MASTER OF SCIENCE in
CIVIL ENGINEERING

by

KAMAKSHI PARWANI

Concrete Structures Group
Department of Structural Engineering
Faculty CITG
Delft University of Technology
Delft, the Netherlands
www.citg.tudelft.nl

Group of Structural Reliability
TNO
Van Mourik Broekmanweg 6
Delft, Netherlands
www.tno.nl

iv

QUANTIFYING THE IMPACT OF LOADS ON CONNECTIONS BETWEEN SEGMENTS OF AN IMMERSED TUNNEL

AUTHOR : KAMAKSHI PARWANI

STUDENT ID : 4244095

EMAIL ID : K.Parwani@student.tudelft.nl

DATE OF DEFENSE : AUGUST 19TH

THESIS COMMITTEE:

Chair : Prof. dr. ir. D.A. Hordijk, TU Delft, TU Delft

University supervisor : Dr. ir. drs. R. Braam, TU Delft

Committee Member : Dr. ir. P.C.J. Hoogenboom, TU Delft

Company Supervisor : Ir. G.G.A Dieteren, TNO

ABSTRACT

Immersed tunnels have become an integral part of the modern day society. Their serviceability and maintenance are of prime importance. In recent years, monitoring of immersed tunnels for deformations showed the necessity for the analysis of certain tunnels due to an unexpected and local increase of settlements and rotations. With the Kiltunnel in the Netherlands, settlements observed at a segment joint of the tunnel were higher than expected. This master thesis focuses on the structural behavior of the segment joint of this immersed tunnel.

Developing a 3-D FEM model consisting of the two segments of the tunnel coming together at the connection/joint is described in this thesis. The model is fixed on one end and forces are applied at the other end. The forces which are expected to occur are calculated with the available values of settlement and rotation on site. Various schemes of the combination of forces are studied in this work.

First, the behavior of the joint is observed when the connection is subjected to a shear force only. It is found that the shear force at the joint is concentrated in the walls and almost equal percentages of force flows through each wall. The shear stress values are highest at the middle wall. The middle wall is less thick than the outer walls making it more vulnerable to damage and cracking.

It is also found that in a linear analysis, the tunnel joint is capable of carrying the estimated shear force without the activation of reinforcement. This is applicable to both the top tooth and the bottom tooth of the tunnel. The concrete tensile stresses are far below the concrete tensile strength. It is expected that the actual capacity would be much higher if detailed non-linear analysis is carried out.

When a combination of shear force and bending moment is applied, it was noticed that the DIANA model becomes unstable and there is loss of equilibrium. This implies that soil should be modeled as elastic foundation in order to come to a conclusion about the capacity of the tunnel connection.

ACKNOWLEDGEMENTS

Table of contents

List of figures

8

List of Tables

Chapter 1

Introduction

1.1   Backgrounds of immersed tunnels

Underground facilities for transportation have now become an integral part of the modern day society. Tunneling techniques can be broadly divided into three categories- driven tunnels, immersed tunnels and submerged floating tunnels. Driven tunnels (4) as the name suggests are tunnels which are driven into the ground. Immersed tunnels (3) are used for crossing a water body when construction of a bridge is not feasible or when movement of ships is required. They are placed on the bed of a river or a lake which needs to be crossed. Submerged tunnels (2) are relatively new and are also known as floating tunnels. They are constructed when the bed of the river/ocean is too deep and hence the tunnels are submerged at a particular level in the water body and held in place by anchors. **Figure 1.1** focuses on the various types of tunnels. This research work will focus on immersed tunnels and criteria which are important for their serviceability.
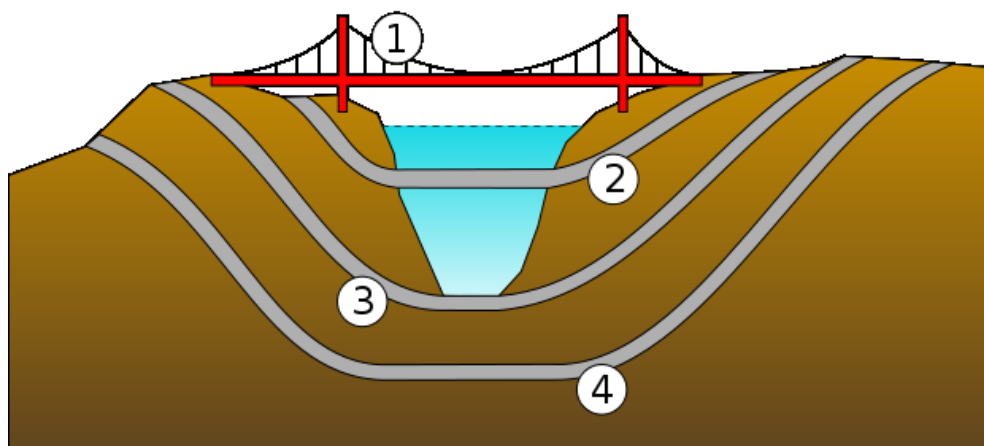
Figure 1.1 - 1-Bridge, 2- Submerged tunnel, 3- Immersed tunnel, 4- Driven tunnel [Ref Image 1]

The first immersed tunnel in the world was the Michigan Central Rail Road tunnel built in the U.S.A in 1910. The shell of this tunnel was made in riveted steel, lapped and ship caulked. The

first immersed tube tunnel in Europe was the Maastunnel in Rotterdam, completed in the year 1943. This tunnel was made in concrete with a rectangular cross-section. Since then, over 200 immersed tunnels have been constructed all over the world with about 150 being used for road or rail transport [1].

The number of immersed tunnels around the world has been increasing and so is the age of the existing tunnels. The tunnels, generally constructed for a lifetime of 100 years, are expected to perform well during their design life without much requirement for maintenance. The high design life is provided because of difficulties involved in the underwater maintenance of the tunnel from the outside. The inner-side can still be maintained regularly during its lifetime.

1.2 Immersed tunnel design in Netherlands

The design of the immersed tunnels varies with the country due to the different soil conditions and local practices followed. The immersed tunnels in the Netherlands generally consist of elements of 100-120 meters (**Figure 1.2**). These elements in turn consist of segments of 20-30 meters. In the joints between the elements, GINA rubber profiles are mounted. The GINA profile is used as a construction seal and acts as a secondary seal during the functional lifespan. OMEGA profiles are mounted on the inside of the joint as primary seal to ensure that the tunnel stays water tight (**Figure 1.3**).The tunnel element is divided into segments because it was found that by casting tunnel elements in segments of 20-30 meters, the problems of concrete shrinkage and creep leading to cracks could be effectively avoided [1] (**Figure 1.4**). The end of each segment is finished as a half joint and provides a spigot and socket type connection between the tunnel segments (**Figure 1.5 & Figure 1.6**). Since the joint is match cast, there are fewer problems with tolerances on bearing surfaces. Each new segment of an element is cast against the previous segment, separated by a thin bituminous layer to prevent adhesion.

After casting, the segments are joined together by post-tensioning wires, making it possible to transport the element. Once the element is lowered into the water and placed next to the previous element, the post-tensioning wires are cut. The entire tunnel alignment is like a chain and each segment can behave like a link in the chain **Figure 1.7**. The wires are cut to prevent the development of large forces/displacements/rotations in the connections of the segments. In this manner, freedom of movement is also provided to the tunnel segments in case of the occurrence of settlement or rotation, although this movement is limited. Even though it is assumed that the rotation/settlement is considerable, the actual value is not known. It is therefore difficult to estimate the segment connection capacity when using only the data of rotation or settlement obtained on site.

A Typical foundation for immersed tunnels can be made in two ways-1) A bed prepared before an element is placed and 2) A bed made after element is placed. The first method is to place the tunnel elements on a gravel bed. This provides higher foundation stiffness but requires more accuracy during the construction of the foundation layer. In the second method, the foundation is prepared by the sand jetting method. In this method, a mixture of sand and water is injected under the element. In the Netherlands, a majority of the tunnels are prepared by the sand-jetting method.

Figure 1.2 - Elements of an immersed tunnel [Ref Image 2]
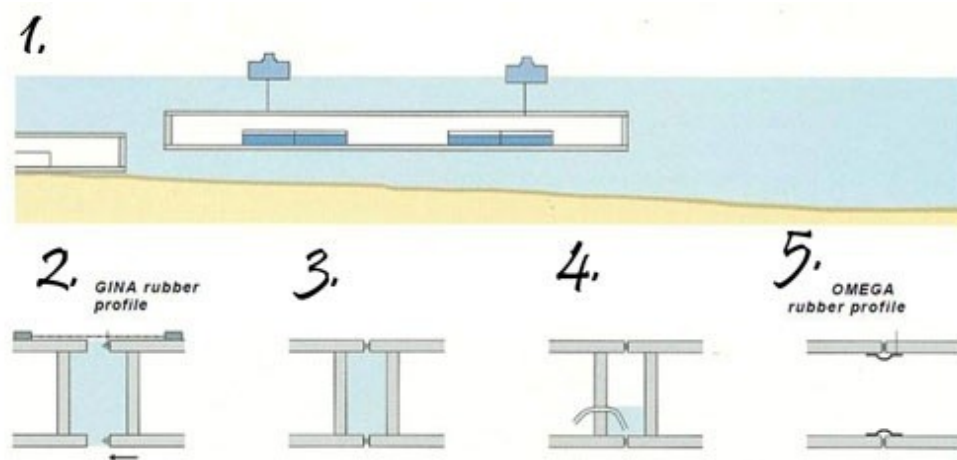
Figure 1.3 - Connections of an immersed tunnel element with GINA and OMEGA profile [Ref Image 2]
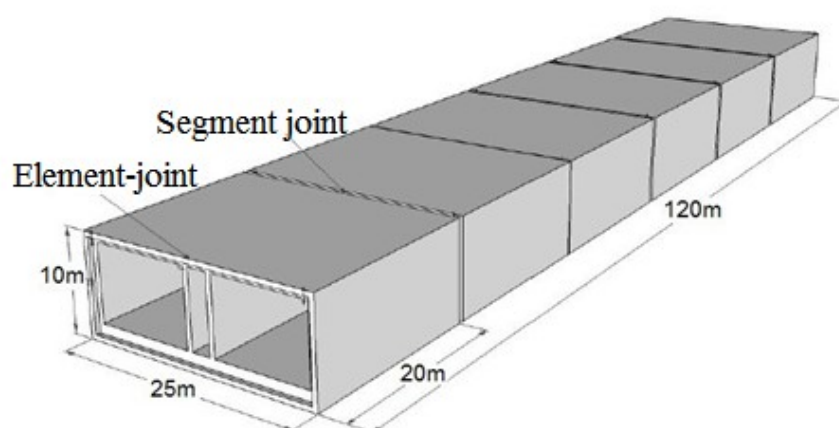
Figure 1.4 - Immersed tunnel element and segments [3]
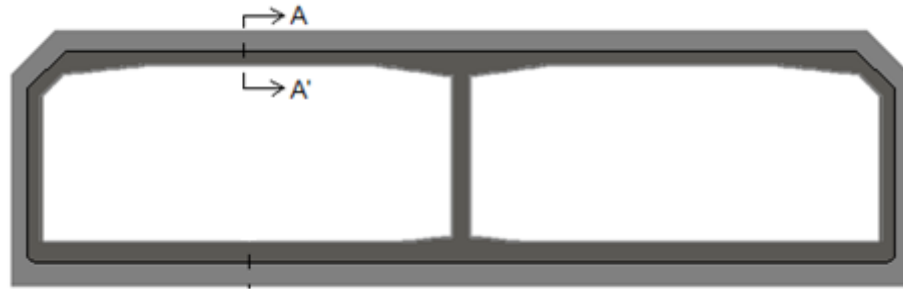
Figure 1.5 - Typical cross-section at the joint between two segments [3]
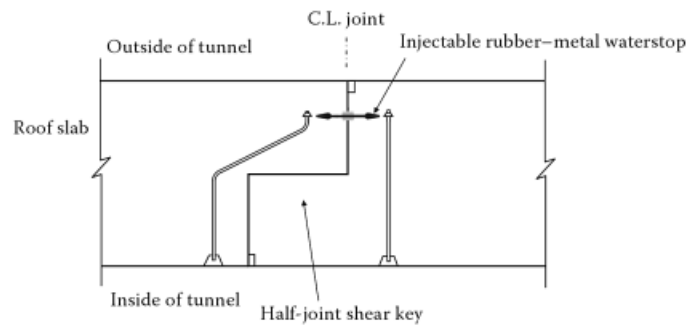
Figure 1.6 - Typical cross-section A-A as shown in **Figure 1.5** [1]
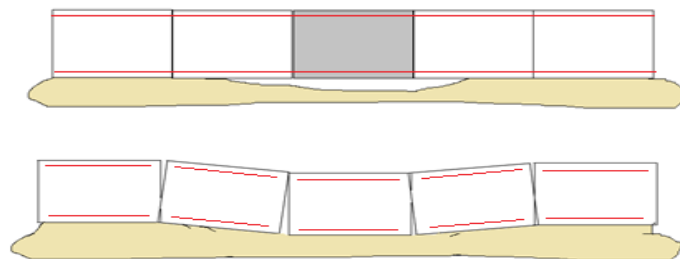
Figure 1.7 – Segments of an immersed tunnel after the prestressing wires are cut [3]

1.3 Challenges with the current design

So far, it had been assumed that the magnitude of settlement and rotation which the segments undergo relative to each other (after the post-tensioning wires are cut) are limited and the connections are able to withstand them easily. However, in some cases, the settlements observed in the connections were higher than expected. A question which rose from high settlement values is- whether there is any form of leakage present in the tunnels? Leakage can lead to problems like corrosion in the reinforcing steel, water in the tunnels which can lead to life-long pumping costs making tunnels unfit for use, shown in **Figure 1.8**. The amount of water leakage may or may not be critical depending upon the case. It is expected that a leak flow of about 4m^3/hr can be pumped out but higher values may cause problems.

One of the most influential factors affecting the settlements of the tunnel segments is the stiffness of the supporting soil layers. Thick layers of compressible soils can lead to high magnitudes of

settlements, shown in **Figure 1.9**. However if this settlement is uniform across the element, the service life of the structure is not affected. On the other hand, high relative displacements of the segments can lead to leakage and make the structure unusable **[2]**. The Netherlands is one of the first countries to have immersed tunnels on soft soils such as clay and peat. The development of settlements with time remains a big question. A majority of tunnels have been monitored for settlements over the years in the Netherlands by Rijkswaterstaat. In one such case, namely the Kiltunnel, leak water was found in the tunnel segment connection. This lead to an extensive recording of displacements and rotations of the tunnel segments on site. A matter of apprehension on this case was that in the leak water, sand was also present, indicating that the sand from the tunnel foundation was washed out. This was a concern since, if the foundation sand is displaced, it could lead to more settlements in the tunnels segments. The segment settlements and rotations were monitored and a first study was performed to determine whether the connections were capable of resisting the extra load **[3]**. It was found that the segment connections were able to resist shear-force generated by the displacements.

The measurements on the tunnel elements showed that rotation in longitudinal and transverse direction also occured. However, the combined effect of rotations and displacement was not studied in the earlier work (**Figure 1.10**). Since the tunnel was not designed to withstand excessive longitudinal and transverse axis rotation of segments along with the shear-force, it is important to study all the effects in order to come to a realistic conclusion about the capacity of the tunnel segments (**Figure 1.11**).

Figure 1.8 - Water leakage in the connections of the Kiltunnel (left) and Drechttunnel (right) [3]

Figure 1.9 –View of cross-section of an Immersed tunnel with surrounding soil [3]
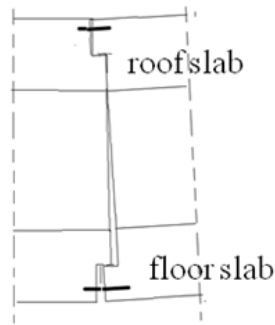
Figure 1.10 – Expected behavior in the segment connection
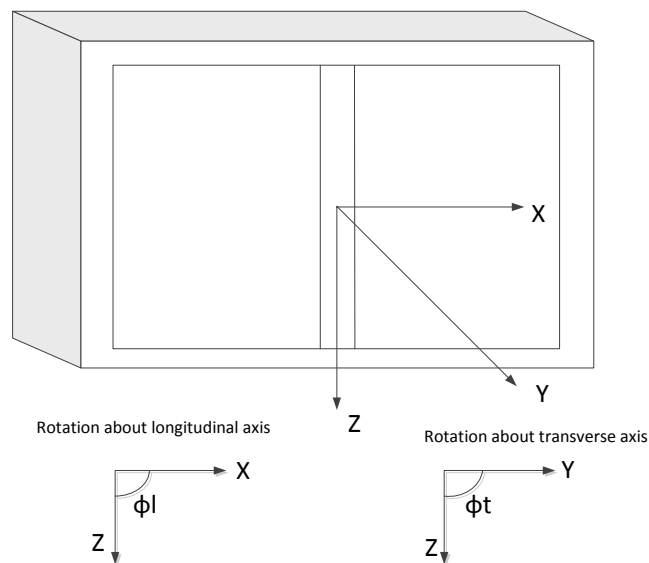
Figure 1.11 - Rotation of the segments along longitudinal and transverse axis

The measurement data available at TNO gives the variation of δ, φ_l, φ_t over the length of the Kiltunnel. It was found that the extreme values of δ, φ_t occurred together but the extremes of φ_l, φ_t did not occur together. In the **Figure 1.12** and **Figure 1.13**, the values of φ_l and φ_t can be observed over the length of the Kiltunnel. The element and segment arrangement of the Kiltunnel can be found in Appendix A1. In the **Figure 1.12** and **Figure 1.13**, the sluitvoeg (closing joint) and zinkvoeg(element joint) represent the connections between the elements. All the remaining locations/positions represent the connections between segments. In this study, only the connection between segments is of interest, the values at the junction of elements are ignored. In the **Table 1.1,** the extreme values which were measured on the field are provided for these three variables. The first entry in the table, D-C (south side) taken in the year 2010 showed the highest value of δ and φ_t. The second entry E-D (south side) had the highest value of φ_l. Consideration of rotations in both directions is very important for the full 3-D analysis. However, due to limitations in terms of time and computing capacity, it was decided to restrict the work to the rotation in transverse direction only. Hence, we will concentrate on the D-C joint of the Kiltunnel, **Table 1.1**. In the current research work, a 3-D FEM model of the segment connection will be proposed and the behavior of the connections subjected to a normal force (N), shear force (V) and rotation about the lateral/transverse axis (φ_t) will be studied.

S no	Description	δ (mm)	φ_l (rad)	φ_t (rad)
1	D-C (South side) 2010 (min)	66	$1.2*10^{-4}$	$-2.1*10^{-3}$
2	E-D (South side) 2010 (min)	18	$5.3*10^{-4}$	$-2.1*10^{-4}$

Table 1.1 - Vertical settlement and rotation of the segments along longitudinal and transverse axis of the Kiltunnel
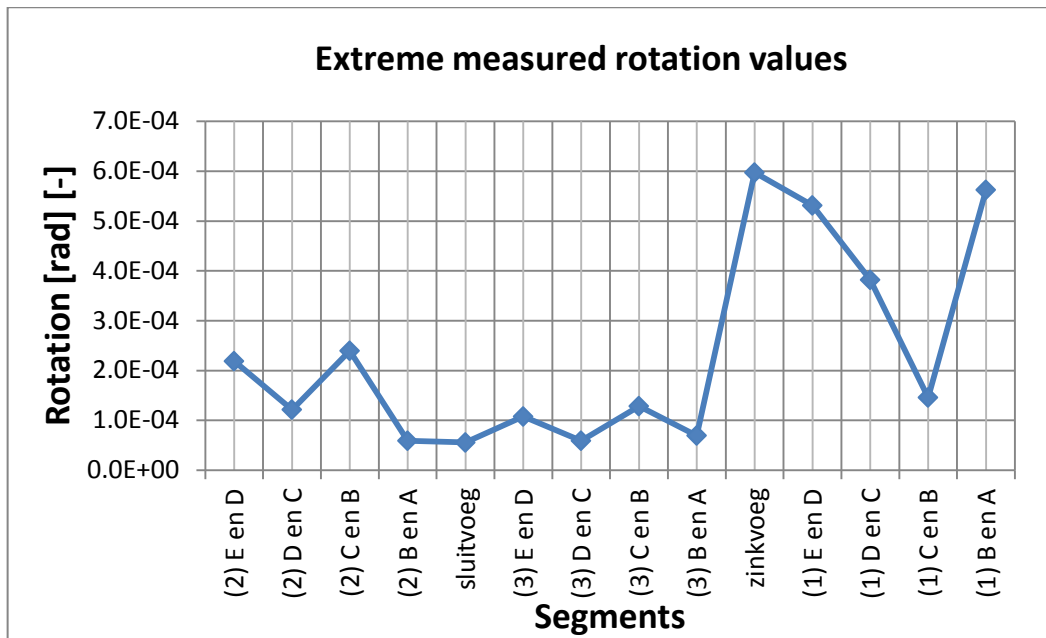
Figure 1.12 – Extreme rotation of the segments along the longitudinal axis (φ_l) in rad along the length of the Kiltunnel [3]
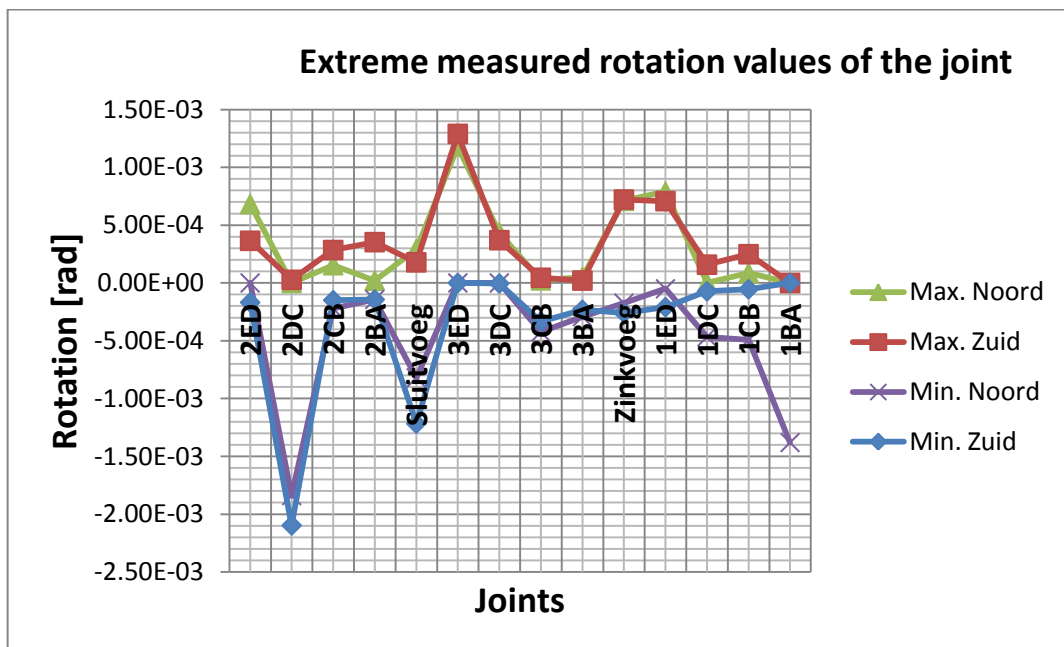
Figure 1.13 – Extreme rotation of the segments along the transverse axis (φ_t) in rad along the length of the Kiltunnel [3]

It is aimed to obtain the limiting combination of rotation and shear force at which the segment connection fails in SLS/ULS. With this study it will be better understood how the connections behave and get an idea about the possible location of the cracks. It is preferred to study the rotation along both the lateral and longitudinal axis of the tunnel. The FEM analysis then enables a better judgment on the behavior of the tunnel. However, due to computational limitations, this will not be included in this research work. Hence, the focus is on the rotation along the lateral axis (**Figure 1.13**). Hence the focus is on rotation along the lateral axis. However, the FE model developed should be able to handle both rotation components. Analyzing the model and tunnel segment joint behavior will be performed using the rotation about the transverse axis only.

1.4 Available literature

The modeling of a tunnel generally consists of two parts. One is the interaction of the tunnel with the soil and the second is the interaction of tunnel segments/elements with each other. In the past, tunnels have been modeled by various methods to understand the two interactions. Examples are the multi-mass-spring model, quasi-three-dimensional model and finite-element model [4]. Despite the availability of extensive methods, it is difficult to model the entire tunnel because of computational limitations [5]. Hence, in most studies only a part of the tunnel is modeled and studied where behavior is most interesting. The majority of the tunnel models consist of soil structure interaction as it is an important part in determining the tunnel behavior. For example, a 3-D FEM model of a driven tunnel was made to study the differential longitudinal settlements in tunnels. Here, the soil was modeled as a set of normal and shear springs around the tunnels elements [6] (**Figure 1.14**). Loads were applied to see how the tunnel behaves in case of differential settlement. In another work, to study the interaction between the segments of a tunnel and between soil and tunnel, a multi-mass-spring model was used to predict the behavior of long immersed tunnels in the event of an earthquake. In this work, the tunnel was modeled as a Winkler elastic foundation beam with joints [7], (**Figure 1.15**). Although some FEM and numerical studies have been done to study the behavior of tunnels due to settlements, not much attention has been given to the behavior of connections in immersed tunnels in particular.
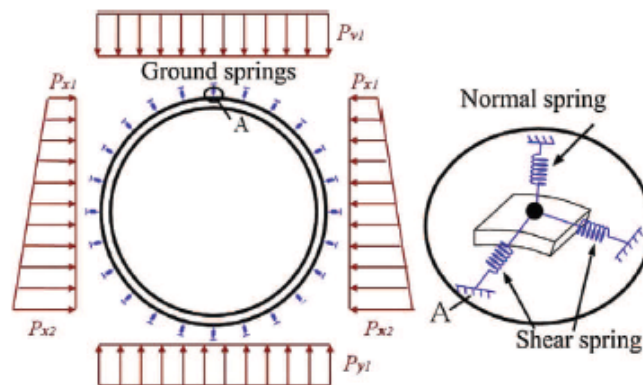
Figure 1.14 - Modeling in 3-D FEM [6]
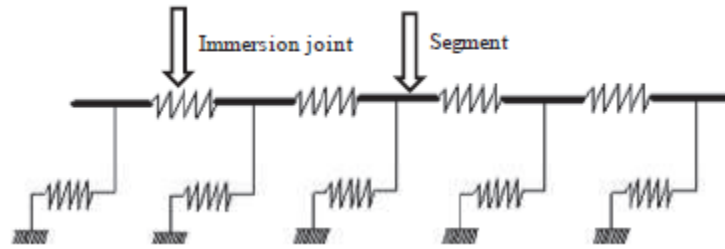
Figure 1.15 - Modeling in 2-D, Multi-mass-spring model [7]

In the first work on the immersed tunnel joints **[3]**, a detailed 2-D analysis for the connections subjected to differential settlement was carried out. First, from the measurements performed in the past, the displacement and rotation of the immersed tunnel were obtained from site (**Figure 1.16**). With the help of setting-line, a beam resting on elastic supports was modeled. The varying spring constant of the elastic supports was back calculated from registered settlement (**Figure 1.17**, **Figure 1.18** & **Figure 1.19**). With this data, the shear-force that occurs in the segment joints was estimated. It is assumed that the shear-force that occurs in the actual structure is close to the value obtained through this 1-D analysis. Once there was an estimate of the forces, a 2-D model was made using FEM. For the 2-D model, the effective width of the tunnel walls was used to determine the part to be modeled. This was arrived at by taking the width of the 3-D model which would be effective in transferring the shear force (**Figure 1.20**). This way it was assumed that the middle wall transfers shear in the form of I-section and the corner walls transfer shear in the form of C-section. Hence 3.5 meters from the outer wall of the tunnel on both sides are effective and 6 meters in the middle wall. With the help of this model, in 2-D, the capacity of the tunnel connection was calculated. It was found that the connection is safe in transferring shear force which occurs due to the current settlement of the tunnel section (**Figure 1.21**). Although it was proved in this study that the tunnel section is safe, the question about the accuracy of the effective width model still remains. Bending moment causing the rotation of the tunnel was not studied in this part of the work. Another point of concern is that the model is effective in ULS, however its overall behavior in 3-D in SLS is not known.
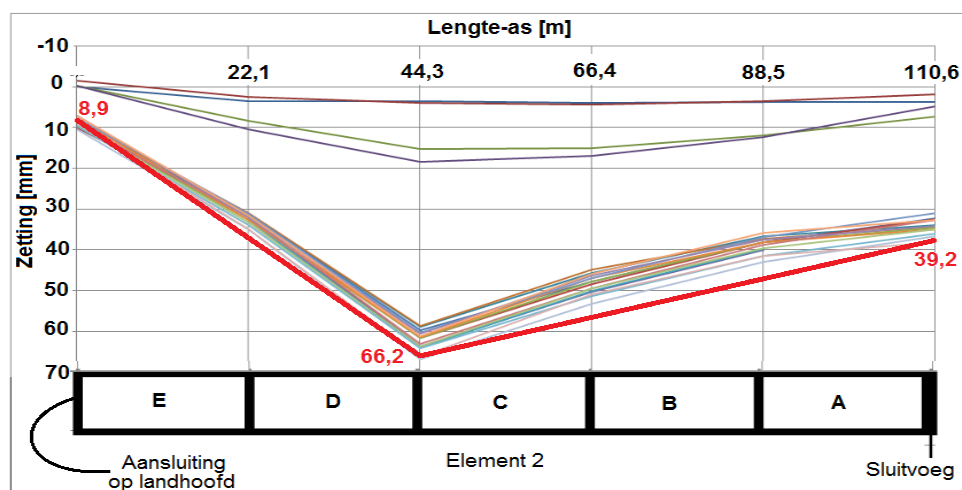
Figure 1.16 – Actual setting line of the Kiltunnel in mm

21

Figure 1.17 – Model of beam resting on elastic foundation [3]
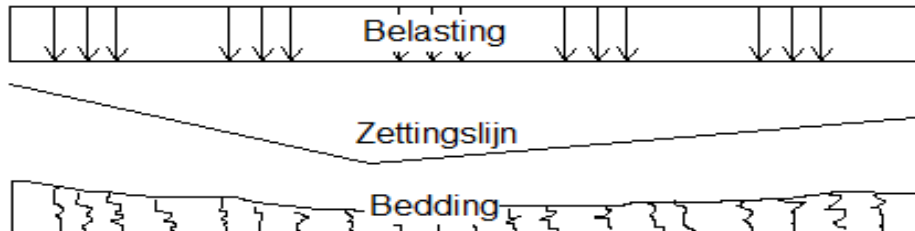
Figure 1.18 – Back-calculation of the elastic spring constant of soil [3]
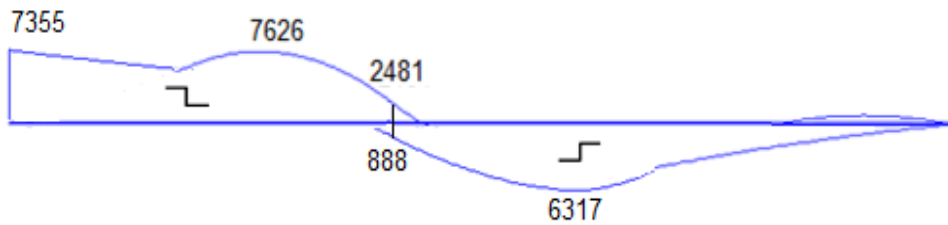
Figure 1.19 – Shear force calculation (kN) from the beam resting on elastic support [3]
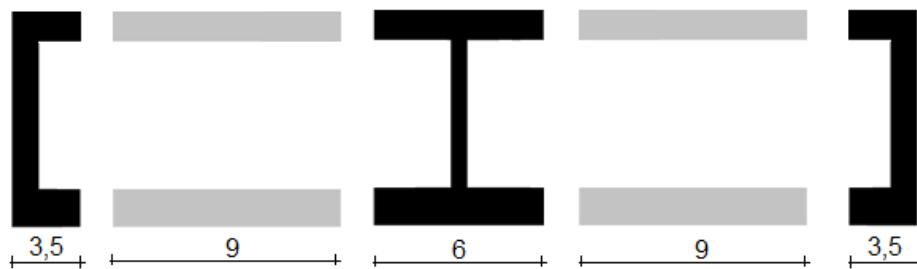
Figure 1.20 – Effective width model (meters)[3]
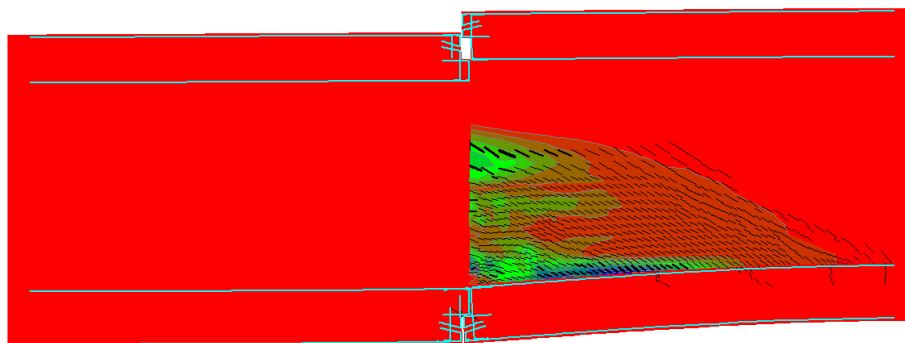
Figure 1.21 – Resultant behavior on shear force application[3]

1.5 Research goals

The findings from the previous section are: Both SLS and ULS behavior are unknown since

1- The effective width model is estimated
2- Possible high local forces from rotation about the longitudinal and transverse axes.

Therefore, it was decided to perform a full 3-D analysis that enables studying the segment joint behavior in SLS and ULS and can be used to validate the applicability of the effective width model. Due to the unavailability of clear data about the soil characteristics, the FEM model will not include soil-structure interaction.

In the current study, a 3-D FEM model will be used to study the behavior of the segment joint of the tunnel. The model will include segment parts which have a length equal to the height of the tunnel. This is included at both sides of the connection. In the previously applied 2-D model, the rotation of the segments in transverse direction was not taken into consideration. Hence, to have a more accurate idea of the tunnel behavior, a 3-D model taking into account all the forces should be made for the connection.

The research questions that follow:

- Are the already existing segment connections capable of resisting the loads that occur due to differential settlement and rotations?
- If yes, what are the limits of settlement or rotation at which they will fail?

The research questions that arise from modeling using the FEM:

- How can the contact/interface between tunnel segments be defined in FEM?
- For which parts of the tunnel segments can the material properties of concrete be assumed to be physically-linear and where is non-linear behavior to be used?

1.6 Key areas in the research

The current research is divided into two major parts with respect to modeling in the FEM software package DIANA. The first part consists of a 2-D model and the second part consists of the 3-D model.

2-D analysis in FEM: In this part of the study, 2-D analyses are performed in order to learn the reinforcement modeling and study the structural behavior of the shear key. The main work here is to determine the behavior of the reinforcement at increasing load (**Figure 1.22**). Another part which is important for 2-D modeling is to understand the interaction at the shear key joint of the two segments. This work will be carried out in chapter 2 and 3 of this thesis.

3-D modeling of connections: In this part, the tunnel connections are modeled in 3-D. Vertical displacement and the rotation about the transverse axis are used for obtaining a situation close to reality. The most important part is the load/displacement versus rotation relationship.
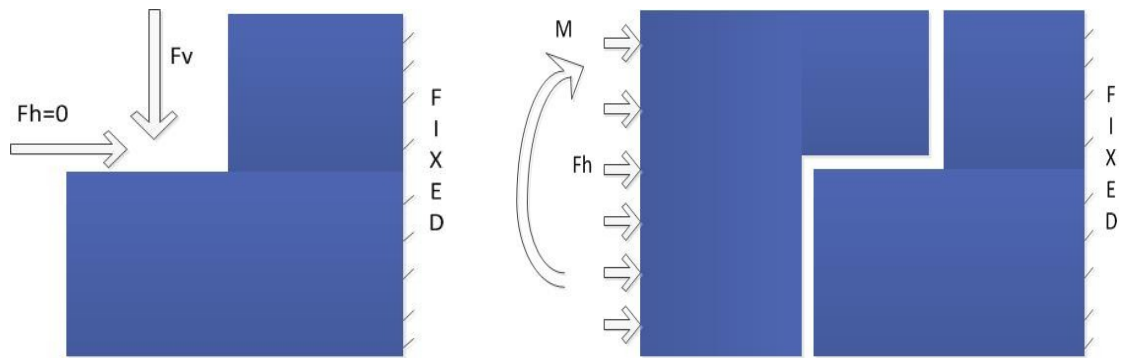
Figure 1.22 - Shear key analysis- Single shear key behavior (left) and shear-key interaction (right)

The input will be provided by applying forces on one end of a segment. This will generate a rotation/settlement on the other end of the segment (**Figure 1.23**). The model will be composed of parts of two segments and the connection between them. The total analyzed length of the segments is assumed to be about 2-3 times the height of the tunnel. This is because the local behavior at the connection does not influence the behavior over the entire length of the segment, only a part of it.

First, the pressure due to water causing compression in the tunnel is applied. Only 60% of the normal force will be applied. The compressive force at time t= t' is assumed to have reduced to 60 % due to relaxation of the GINA profile and time dependent behavior of concrete **[3]**. Next load is the shear force along with the bending moment in the transverse direction. Loads are applied in small steps. These steps represent the situation at an instant of time, t=t'. This analysis would give the combined limit of failure for each variable. This part of the work will be discussed in chapter 5 of the thesis.

Analysis of the 3-D results: Once the segment joint is modeled and its failure load/displacement is known, a prediction of future behavior in terms of loads and deformations can be made. Also, the location and direction of the cracks around the connections can be identified.
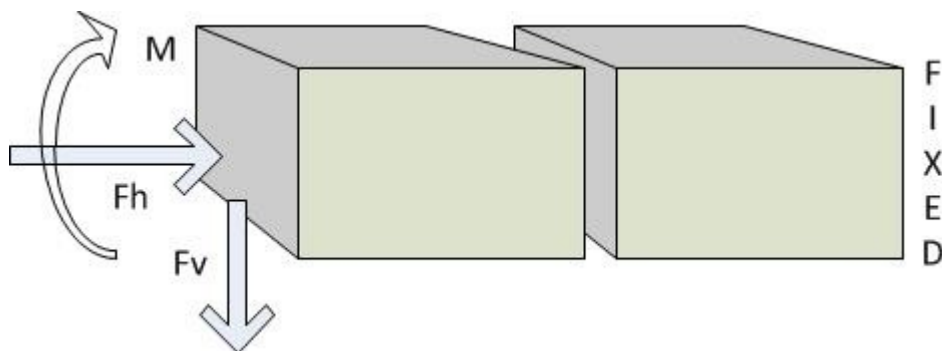
Figure 1.23 - Forces applied on the tunnel segment

Chapter 2

Modeling in DIANA

2.1 Introduction

In the previous chapter, an overview of the topics which would be covered in this thesis was discussed. In this chapter, the first study of the single tooth analysis will be done. The material model for concrete and steel will be discussed, followed by the analysis and results. These results will be reinforced with hand calculations in the end of the chapter. It was necessary to perform the analysis, in order to come to the right material properties and to have an idea about the failure behavior of the tooth. This chapter is also used as a stepping stone to the FEM analysis in DIANA.

2.2 Material model

2.2.1 Introduction

When modeling in FEM, there are certain factors which need to be accounted for such as

- Material models for concrete
- Material models for steel
- The interaction between two concrete segments of tunnel and the degree of interaction.

The material models hold importance because reinforced concrete is a composite material from concrete and steel, two materials with very different physical and mechanical behavior. Concrete exhibits nonlinear behavior even under low level loading due to its material behavior, e.g. environmental effects, cracking, biaxial stiffening and strain softening. Reinforcing steel and concrete interact in a complex way through bond-slip and aggregate interlock **[10]**. Hence accurate definition for bond between concrete and steel is also important for the modeling.

2.2.2   Combination of steel and concrete behavior

Two different approaches have been used so far for the analysis of RC elements by the finite element method: the modified stiffness approach and the layer approach. The first is based on an average moment-curvature relationship which reflects the various stages of material behavior, while the latter subdivides the finite element into imaginary concrete and steel layers with idealized stress-strain relations for concrete and reinforcing steel. In this work, a combination of the two will be adopted with DIANA, where the preprocessor, Fx+, divides the elements into steel and concrete layers. In the processor, the various stages of material behavior are provided. Also, for the current work, complete bond is assumed between steel and concrete for the analysis.

2.2.3   Crack models

The two types of crack models that can be used in DIANA are the smeared crack model and the total strain crack model. The total strain crack model is based on fixed and rotating crack concepts [11]. In the smeared crack model, the strain of the material between the cracks can be sub-decomposed into an elastic part, a creep part and a plasticity part. Also the crack strain can be decomposed into the local crack strains of a number of cracks at different orientations. However, with the smeared crack model, the disadvantage is that, when multiple cracks occur, the internal iteration procedure may fail [12].

Next model is the total strain crack model. It is a constitutive model based on total strain that describes the stress as a function of the strain in the coaxial stress-strain concept. The stress-strain relationships are evaluated in the principal directions of the strain vector. There exist two different ways of fixed or rotating cracks. Both approaches are described in the same framework where the crack directions are either fixed or continuously rotating with the principal directions of the strain vector. The disadvantage with the model is that combinations with creep, shrinkage and thermal strains are not straight forward. Due to the ease of implementation, for this research it was decided to proceed with the total strain crack model. The total strain crack model has two parts, namely the compressive behavior model and the softening model. The options available in DIANA are shown in **Figure 2.1 and Figure 2.2**. The material model considered for steel is shown in **Figure 2.3**. It has two elastic moduli.
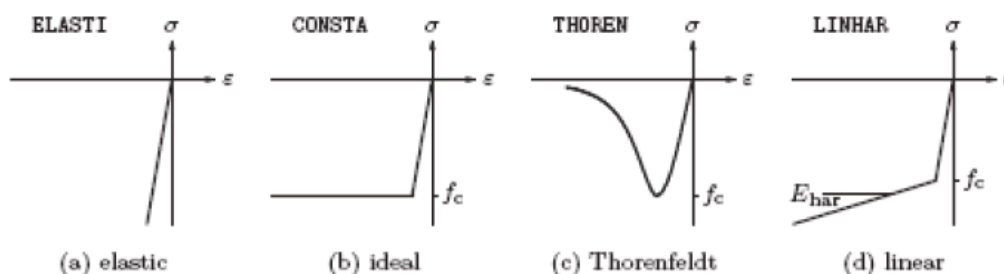
Figure 2.1 - Compressive behavior DIANA; total strain crack model [11]

Figure 2.2 - Tension softening DIANA; total strain crack model **[11]**

Figure 2.3 - Steel stress strain behavior **[10]**

Since the behavior in tension is expected to be governing; the Hordijk model is used in the analysis. The fracture energy GF1 for the concrete class C35 is 0.075 N/mm (maximum size of aggregate-20mm). For the concrete compressive behavior, which is not governing here, the Thorenfeldt model is chosen for the analysis. However, opting for ideal behavior is also not expected to make a difference in the results. The steel behavior is defined with the help of the

27

HARDIA function, which defines the plastic strain of the steel. The bond between steel and concrete was assumed to be perfect for simplicity of the analysis.

2.3 Modeling in FX+

With the information available, a model of a shear key was made in FX+. The shear key forms a small part of the tunnel tooth, **Figure 2.4**. The aim was to understand the load vs deflection plot and to compare it with results of the previously obtained plot, Schols[3]. In general, any load vs deflection plot for a reinforced concrete structure consists of three stages, namely 1-elastic behavior, 2-inelastic behavior and 3-crushing/yielding behavior, **Figure 2.5**. The nonlinear response is caused by two major effects, namely the cracking of concrete in tension and yielding of the reinforcement or crushing of concrete in compression **[10]**.
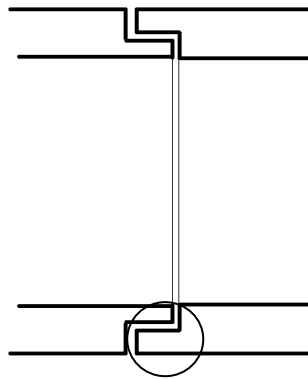
Figure 2.4 – Shear key (As a part of the tunnel)
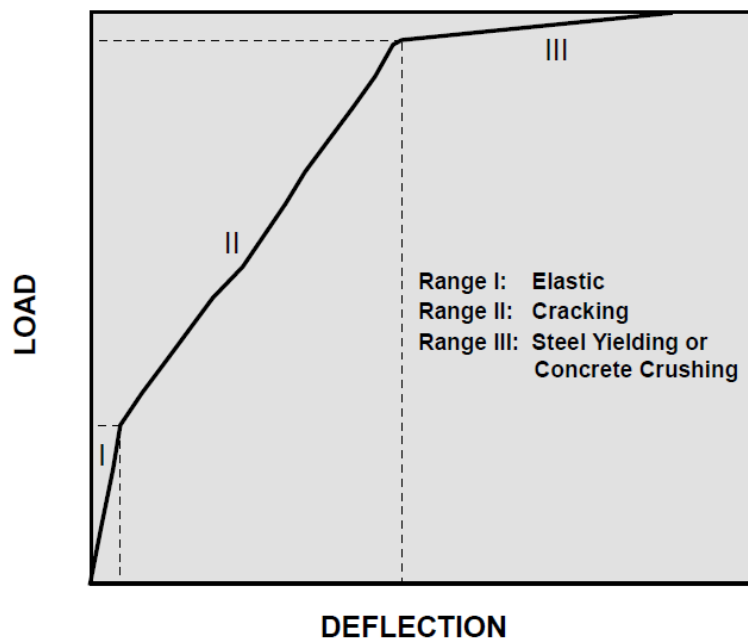
Figure 2.5 - Standard load vs deflection plot for Reinforced concrete **[10]**
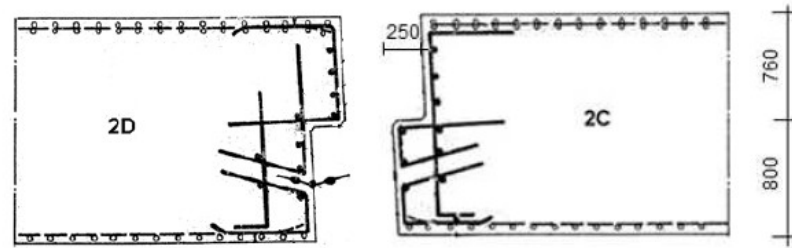
Figure 2.6 - Reinforcement in the shear key in the Floor of the Kiltunnel (dimensions in mm [3])
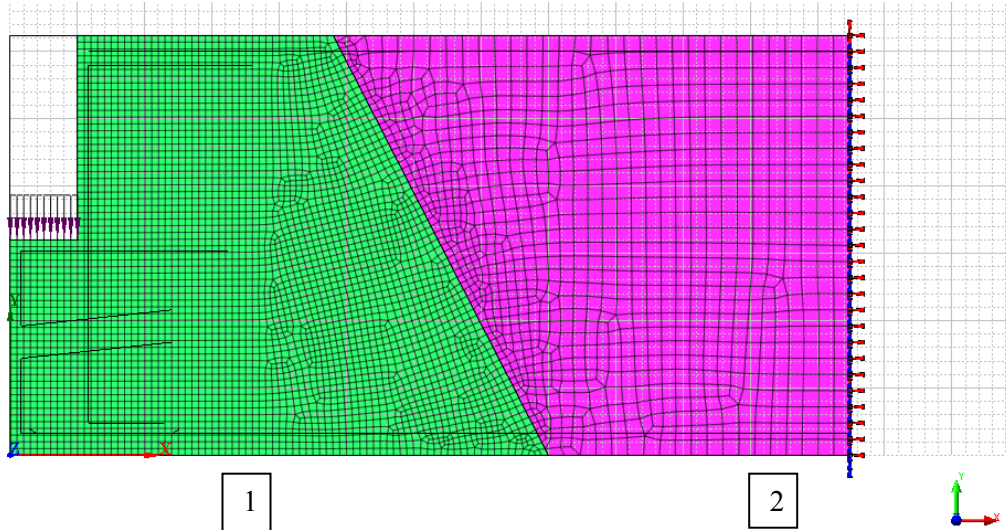
Figure 2.7 - 2-D element with load on left and fixed support on the right

A 2-D model was made in FX+ to understand the behavior of the shear key reinforcement. The model was dimensioned according to the diagram available in the TNO repository as shown in **Figure 2.6**. The 2-D element was meshed with element size 25 mm near the force and 60 mm near the support, **Figure 2.7**. The elements chosen were plane stress elements. The thickness given to the model was 200 mm. The thickness was based on the center to center distance of the reinforcement (200 mm). This work was done to understand and determine:

- Load vs deflection
- Crack propagation in the element
- Reinforcement strains

The most important factors that need to be taken into account are the type of elements and the corresponding mesh used and the iteration procedure as discussed further.

2.3.1   Mesh type

In trial analysis it was found that square meshes perform better than rectangular ones in terms of tracing the post-peak behavior. Hence, the preferable mesh type for concrete analysis is one with a small aspect ratio, which is the ratio between the length and the width of the mesh elements. Another important aspect was the division of the element which was analyzed and has been discussed in further sections.

In such a cantilever beam analysis, failure occurs at the top near the support. Hence, a major portion of the top part was linear (purple in **Figure 2.7**). In this manner, the critical part which may otherwise fail was made linear.

2.3.2 Reinforcement layout

The reinforcement design was derived from the old drawings. The diameter used was φ=16mm. The reinforcement in the perpendicular direction was omitted in this case because its effect is negligible on the behavior of the element. The cover provided was 45 mm for all the bars near the outer slab/floor and 30 mm near the walls. The reinforcement was assumed to be perfectly bonded with the concrete and no specific anchorage length was provided.

2.3.3 Division in linear and non-linear elements

The element was divided into two parts. The one where the force was applied had a non-linear material behavior (**1 in Figure 2.7**). The part near the support had linear material behavior (**2 in Figure 2.7**). This was done in order to ensure that the fixed support at the right end does not influence the behavior of the element on the left to which the load is applied. If this is not done, cracks may be expected near the support at the top (similar to cantilever beam).

2.3.4 Force applied

The force applied was **800N/mm** on the edge as shown in **Figure 2.7** and **Figure 2.8**.

The force was picked because this was used in the earlier analysis [3] and the aim is to compare the two analyses. As the force was applied, force control was used for the analysis.

Total Force=800 *250=200kN
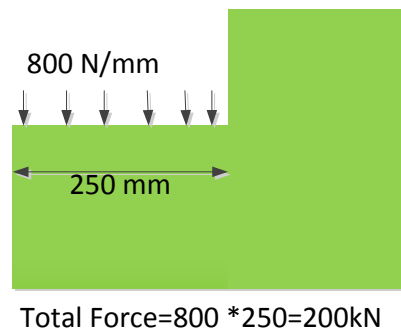
Figure 2.8 – Force applied

2.3.5 Property of materials

The summary of the properties of element near the application of force (non-linear) is described in **Table 2.1** and the properties of the elements near the support (linear) in **Table 2.2**. It should be noted that the material factors were used since this calculation is not about the actual behavior in practice. It is more about the comparison of DIANA vs ATENA. Therefore, Schols' data set was used.

Properties of Concrete used **[3]:**

$$f_{cd} = \alpha_{cc} * \frac{f_{ck}}{\gamma_c} = 1.0 * \frac{35}{1.5} = 23.3 \; MPa$$

$$f_{ctd} = \alpha_{ct} * \frac{f_{ctk}}{\gamma_c} = 1.0 * \frac{2.2}{1.5} = 1.5 MPa$$

Properties of Steel used **[3]:**

$$f_{yd} = \frac{f_{yk}}{\gamma_s} = \frac{400}{1.15} = 348\ MPa$$

$$f_{td} = f_t = \frac{500}{1.15} = 435 MPa$$

$$\varepsilon_{ud} = 0.9 * \varepsilon_{uk} = 0.9 * 5 = 4.5\%$$

$$\varepsilon = \frac{f_{yd}}{E} = \frac{348}{2.1 * 10^5} = 0.174\%$$

Calculation of Gf1 (fracture energy of concrete):

$$G_f = G_{fo} * \left(\frac{fcm}{fcmo}\right)^{0.7}$$

$$fcm = 23.3 + 10 = 33.3 \frac{N}{mm^2}$$

$$fcmo = 10 \frac{N}{mm^2}$$

$$G_{fo} = 0.035 \frac{N}{mm}\ (for\ 20\ mm\ aggregate)$$

$$G_f = 0.035 * \left(\frac{33.3}{10}\right)^{0.7} = 0.075\ N/mm$$

Property	Data Value	
Element	2-D plane stress elements, CQ16M	
Mesh size (auto)	25 mm	
Element thickness	200 mm	
Reinforcement used	16mm φ	
Reinforcement mesh	1division	
E modulus of concrete	34000 N/mm2	
E modulus of steel	210000 N/mm2	
Poisson s ratio (Concrete & steel)	0.2	
Tensile strength	1.5 N/mm2	
Compressive strength	23.3 N/mm2	
Cracking model	Total strain crack model	
Type of crack	Fixed and rotating	
Tensile softening curve	Hordyk	
Compression curve	Constant/Thoren	
Tensile strength of concrete	1.5 N/mm2	
Gf1	0.075 N/mm	
Yield of steel	348 N/mm2	Strain = 0.0017
	435 N/mm2	Strain = 0.045
Constraint	Fixed on the right	

Table 2.1- Details of the input for DIANA mesh near the force-nonlinear (1)

Property	Data Value
Element	2-D plane stress elements, CQ16M
Mesh size (auto)	60 mm
Element thickness	200 mm
E modulus of concrete	40000 N/mm2
Poisson s ratio (Concrete & steel)	0.2

Table 2.2- Details of the input for DIANA mesh near the support-linear (2)

2.3.6   Convergence procedure

The factors which can be varied during the iterations are:

- Control- arc length/ simple force control
- Type of Norm- Energy/Force/Displacement
- Iteration procedure- Newton Raphson regular/modified

In non-linear analysis, due to the presence of cracks there will be deformations and hence, displacement and force norm together should not be used. It is generally recommended to opt for energy norm during the analysis. Between Newton Raphson regular and modified, the modified one is much faster as the matrix is calculated at every step. In the regular Newton Raphson, the matrix is calculated at each iteration which makes it slower. The final result slightly varied when any of these factors were changed. It was found that for the current analysis, the best results were obtained with Force control, energy and force norm and the Newton Raphson Modified iteration procedure. Both Energy norm and Force norm need to be satisfied consecutively in the analysis. This was done to ensure that the plot does not return back to its origin**. Table 2.3** summarizes the parameters used.

Convergence criteria	Method used
Control	Force control
Displacement norm	No
Force norm	Yes(0.01)
Energy norm	Yes(0.001)
Procedure	Newton –Raphson (modified)
Number of iterations	50
Load steps	0.05(8) 0.005(120)

Table 2.3- Details of the convergence procedure used

2.4 Results of the 2-D analysis

The load vs. deflection plot was made for the analysis. The load steps in the analysis were 0.05(8) 0.005(120). Small steps were used for the analysis so it is easy to model the post peak behavior of the shear key. A comparison was also drawn to the analysis carried out earlier [3]. The plots of stresses were obtained for certain load steps and the crack width diagrams were also plotted. It was noticed that no cracks were formed in the first few load steps. Increasing the load further increased the number of cracks.

It was found that the reinforcement near the loading point yields and results in the failure of the element. Three types of analysis were performed with the model. In the first analysis, a rotating crack model was used. In the second analysis, a fixed crack model was analyzed. In the third type of analysis, the division of the two parts of the element was adjusted. **Table 2.4** gives the summary of the three analyses. It was found that varying a single parameter leads to a change in the force displacement plot. For all the load displacement plots, the corner most node was selected as shown in **Figure 2.9**. Another factor which can affect the results of the modeling is the position of the reinforcement. Due to the lack of accurate details of the reinforcement placement in the drawings, an estimate was made for it. It is understood that the main reinforcements which are placed at a right angle to each other, take up tensile stresses occurring due to the crack formation. A minute change in their position should not affect the final load-displacement behavior as both have the same area of steel.

Property	Analysis 1	Analysis 2	Analysis 3
Total strain model	Rotate	Fixed	Rotate
Division line	3 lines	3 lines	1 line

Table 2.4- Difference in the three analyses carried out
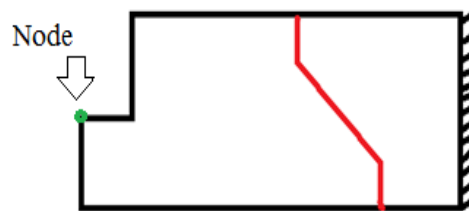
Figure 2.9- Node selected for the load displacement plot

2.5 Results of analysis 1

In this case, the element was divided into two parts, with the help of three lines, **Figure 2.10**. The part near the support has linear properties whereas the part near the force has non-linear properties. The load displacement plot of the element is shown in **Figure 2.11**.

A plot of the maximum reinforcement stress was made with respect to the load steps (**Figure 2.12**) for the reinforcement element 33510 as shown in **Figure 2.13**. It was noticed that till a certain point, the steel stresses were very low. After that, there was large increase in the steel stresses. This was expected because, after a certain point, the concrete tensile strength is reached. The concrete cracks, and the load is taken by the steel reinforcement. In **Figure 2.12**, the load step marked as point 1, occurs at a load of 424 N/mm. The tensile stress plot is shown in **Figure 2.14**.

According to the input, the steel starts to yield at 348 N/mm^2 and has a plastic behavior till 435 N/mm^2. In the analysis, it was observed that once the steel starts to yield, the concrete fails. A through crack is obtained and no further convergence occurs. Hence, it is not possible to see the

steel stress reaching 435 N/mm^2, which is the maximum plastic stress that the steel can have. Another anomaly which can be observed in the steel stress plot is the flat plateau around the stress of 250 N/mm2 between points 2 and 3. This local snap-back was observed because the crack passes the tip of the reinforcement, **Figure 2.13** . There is localized increase of the steel stress around those load steps. In the **Appendix B1**, the plot of reinforcement stresses, concrete compressive stresses and tensile stresses can be found for the three data points, shown in **Figure 2.12** as 1, 2 and 3. The tip of the reinforcement which is in the crack direction can be clearly observed in **Figure 2.13**. The stress in reinforcement element 33510 is 348 N/mm^2 at load step 55 (Applied force of 508 N/mm) and the steel yields. However, the maximum stress is found in the reinforcement tip with a value of 359 N/mm^2. This can be seen in **Figure 2.13** in the bar diagram on the right.

The diagram with the reinforcement stresses (**Figure 2.13**) also shows that there is no problem with the assumption of no anchorage length. This is because the steel stresses are governing in zones around the crack and the two perpendicular reinforcements have sufficient anchorage length there. Although the reinforcement tip is an exception to this case, it is not governing for the failure of the element. The tensile stresses for load step 34 and 48 can be seen in **Figure 2.14** and **Figure 2.15**. In **Figure 2.15**, it is noted that the crack has almost penetrated the shear key.
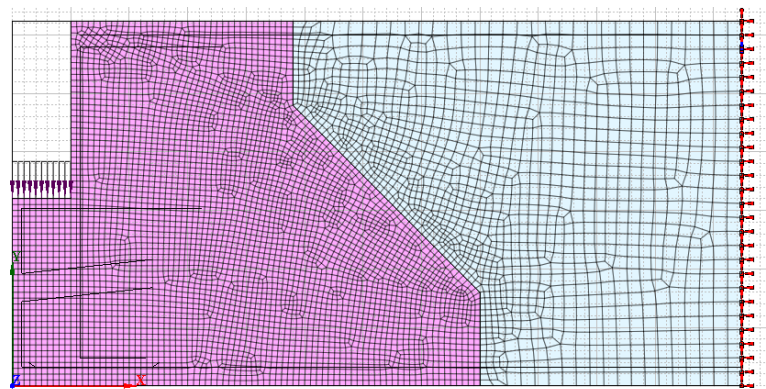
Figure 2.10 -2-D element with load on left and fixed support on the right
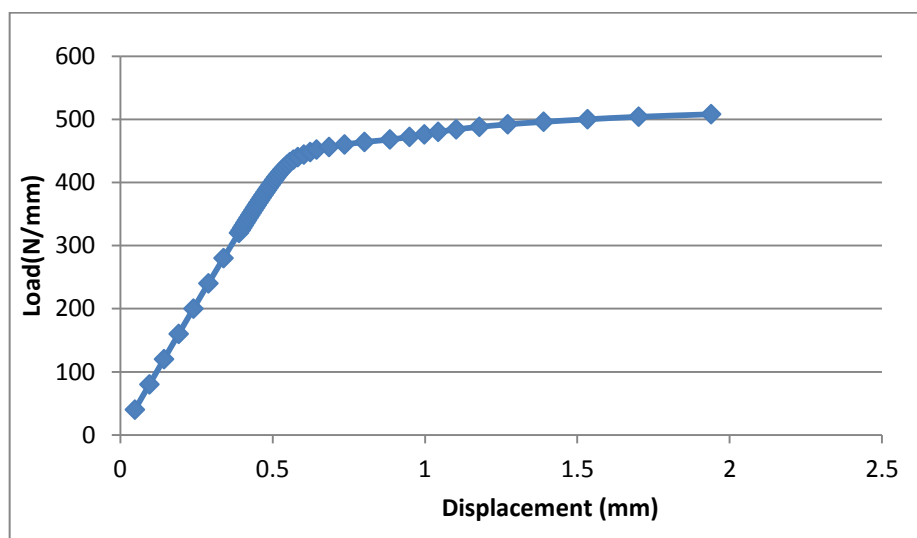
Figure 2.11 -Load vs displacement plot for Analysis 1
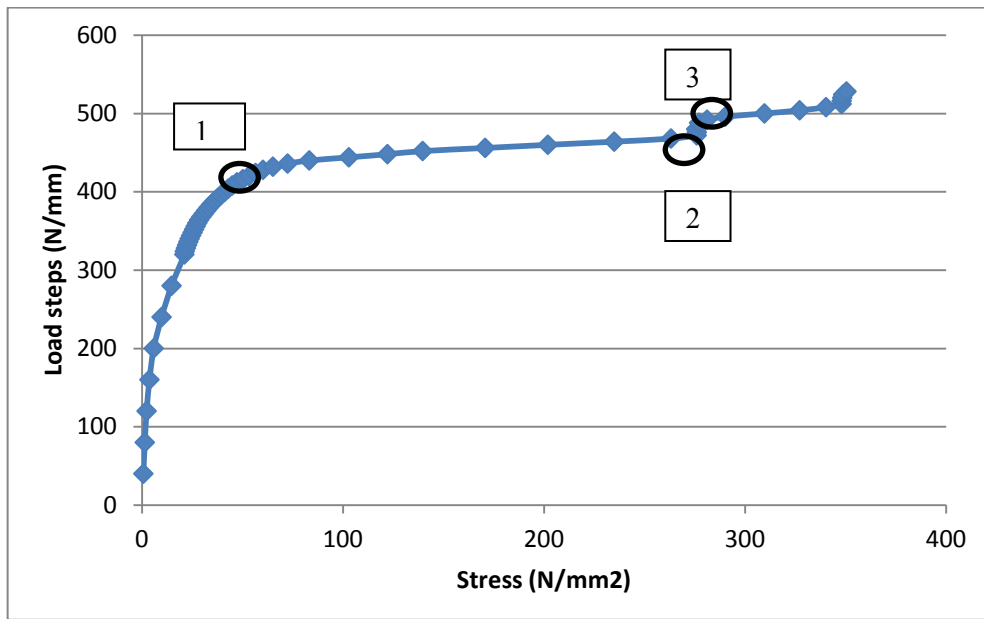
Figure 2.12 -Steel stress vs load steps for Analysis 1 for element 33510

[UNIT] N , mm
[DATA] Structural Nonlinear , Sxx Nodes , Load Step 55(0.635)
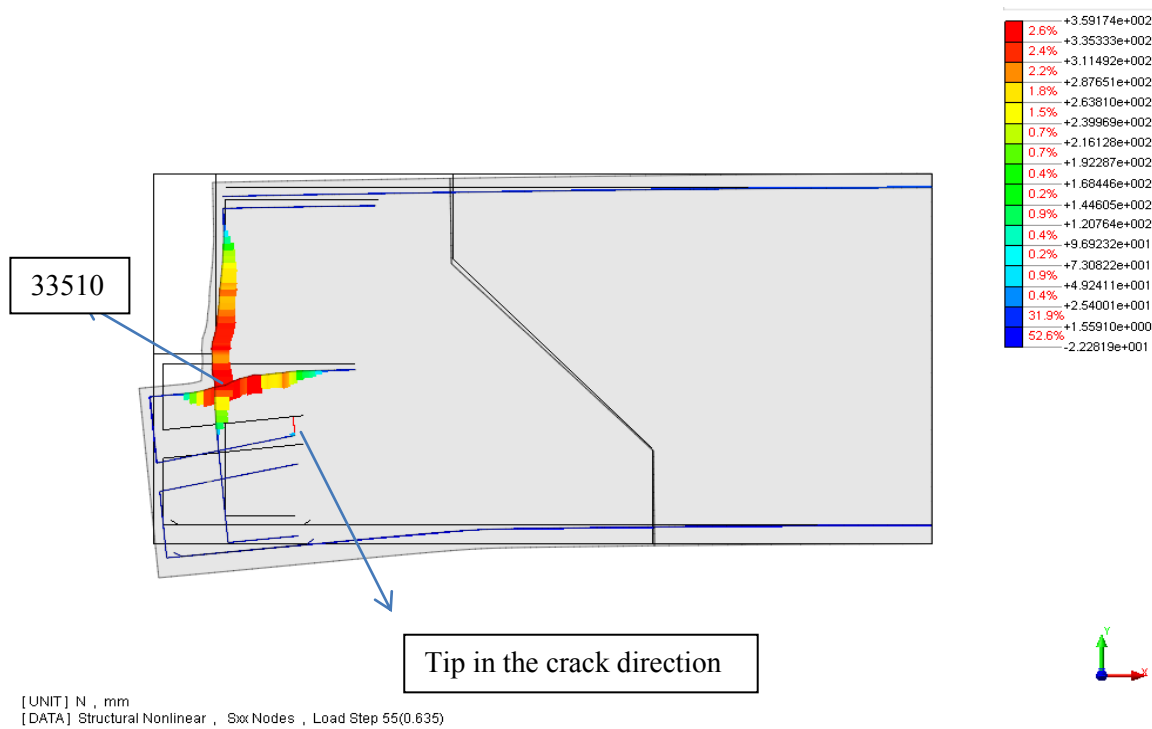
Figure 2.13- Reinforcement stresses for Analysis 1(rotating crack) at step 55

[UNIT] N , mm
[DATA] Structural Nonlinear , Principal Stress S1 Nodes(V) , Load Step 34(0.53)
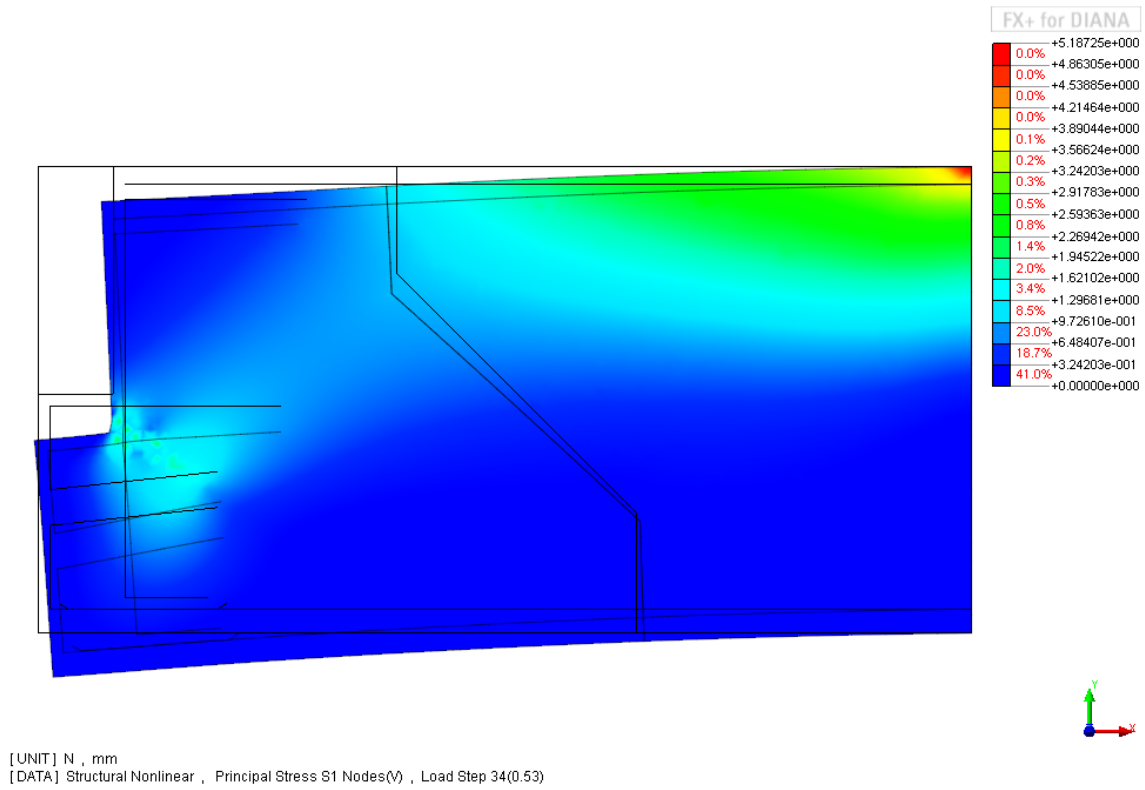
Figure 2.14 -Tensile stresses for Analysis 1(rotating crack) at step 34
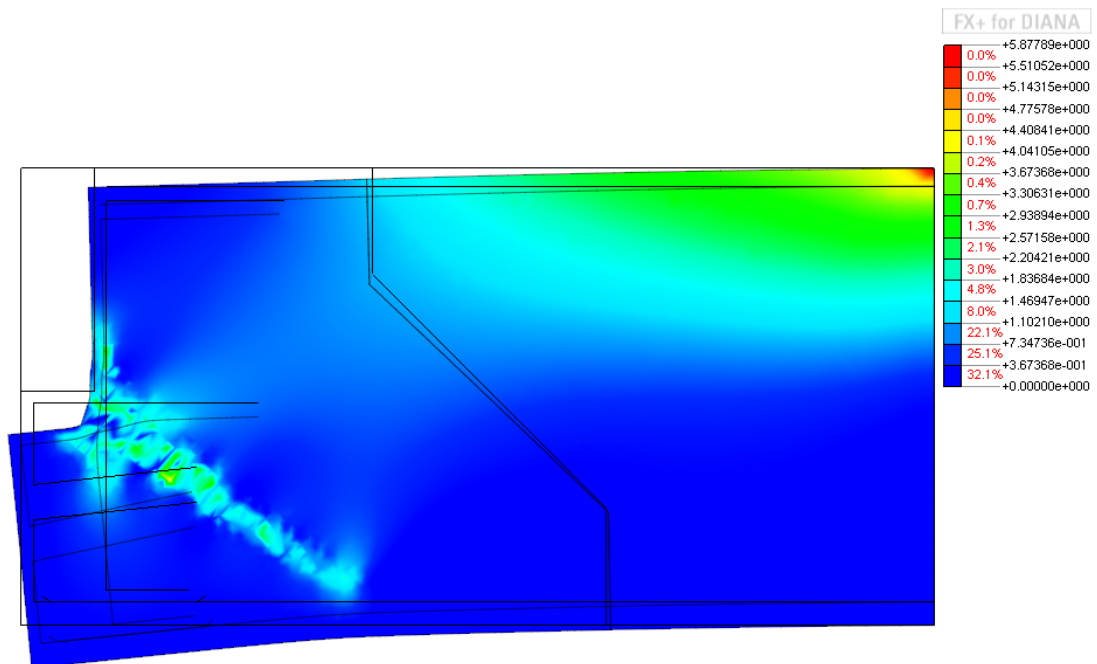
Figure 2.15 -Tensile stresses for Analysis 1(rotating crack) at step 48

The ultimate load capacity of the element can be estimated to about 500 N/mm. In comparison to the results which were obtained earlier [3], the element capacity is much lower. This differing result could be caused by:

36

- Material properties used are different
- The solver used is different (ATENA was used earlier)
- The element division is different
- The mesh is different

In the material properties, the value of Gf (fracture energy) used in the earlier analysis is not known. The crack model is another material parameter which could contribute. A fixed crack model gives a higher value in the load-displacement plot compared to a rotating crack model. The model used by Schols[3] was a fixed crack model. The solver ATENA is expected to be more robust than DIANA, which could be an important factor causing the difference. Also, element division plays a role in determining the load-displacement plot, as will be discussed later in this chapter.

2.6 Results of analysis 2

In the second analysis, all the factors were kept the same as in the previous analysis, except that the crack model chosen was fixed. The peak obtained with a fixed crack model was higher than that obtained in the rotating crack model of analysis 1(comparison shown in **Figure 2.16)**. It was expected that the peak will be higher, since the crack direction is fixed and the analysis tend to be more robust. This is why the element capacity is over-estimated. The steel stress was plotted for the same reinforcement element, 33510 (**Figure 2.13)**, and a very similar curve was obtained, shown in **Figure 2.17** . However, it was noticed that no flat plateau (localized constant stress) was formed in this case compared to analysis 1 for the element 33510. It was because there is no reinforcement coming in the direction of the crack as in analysis 1. This also gives the difference in the behavior of a fixed crack model and a rotating crack model.
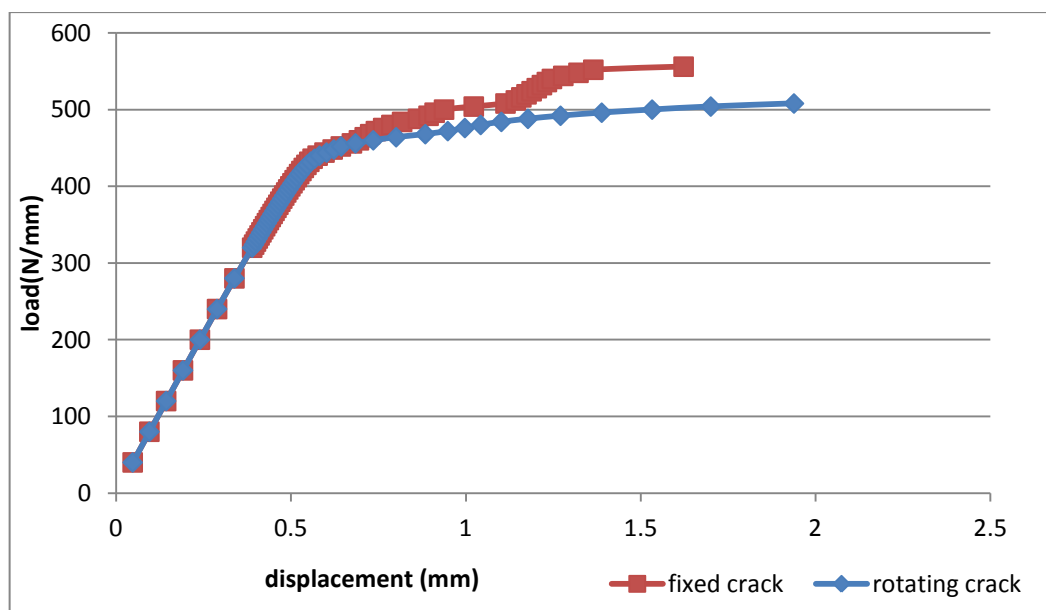
Figure 2.16- Load vs displacement plot for Analysis 1 (rotating crack) & Analysis 2 (fixed crack)
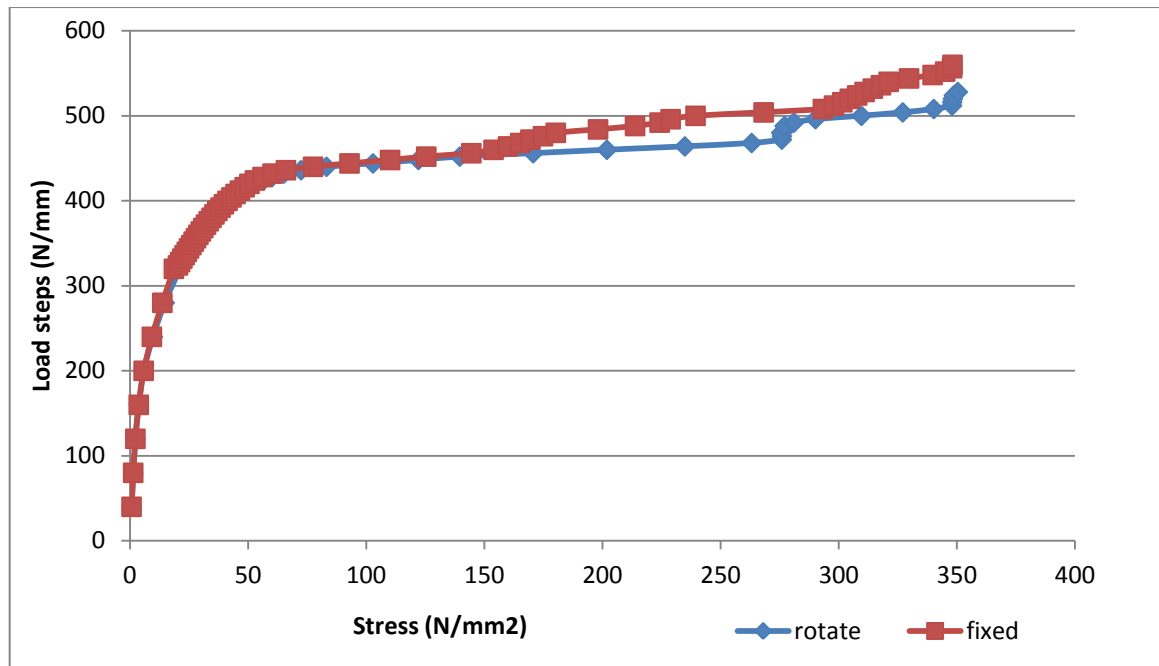
Figure 2.17- Steel stress vs load step for Analysis 1 (rotating crack) & Analysis 2 (fixed crack) for 33510

2.7 Results of analysis 3

In this analysis, the division of the element was changed. Instead of using three lines to divide the element **Figure 2.10**, one straight cut was made **Figure 2.18**. The top and bottom coordinates of this line were the same as the top and bottom coordinates of the previous division. A rotating crack model was chosen for the analysis. It was found that the peak obtained was comparatively higher than the rotating crack model of the 3 lined division. A comparison of the load displacement plot of these analyses is made in **Figure 2.19**. From the graph of load vs displacement it appears that this model achieves a higher peak than the case of 3-lined division (rotating crack).
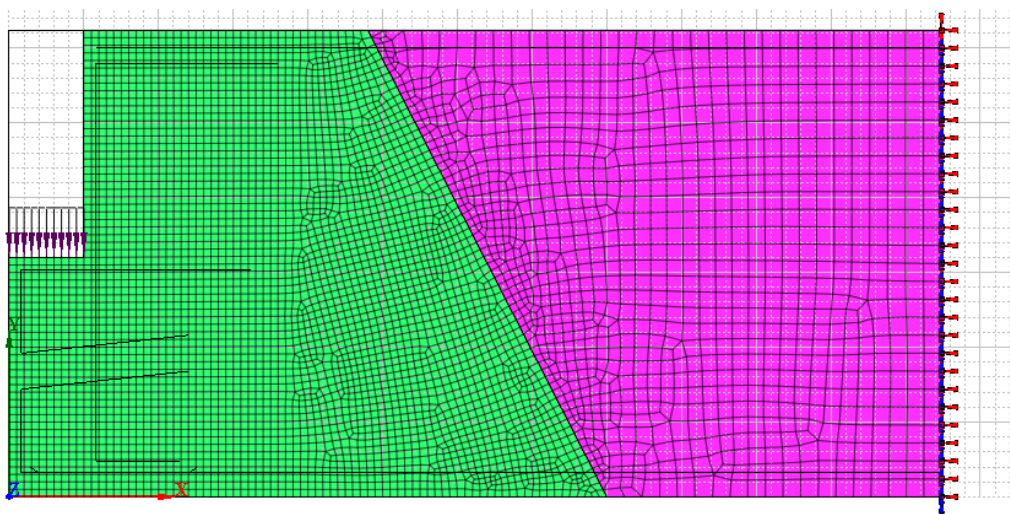
Figure 2.18- 2-D element with load on the left and support on the right
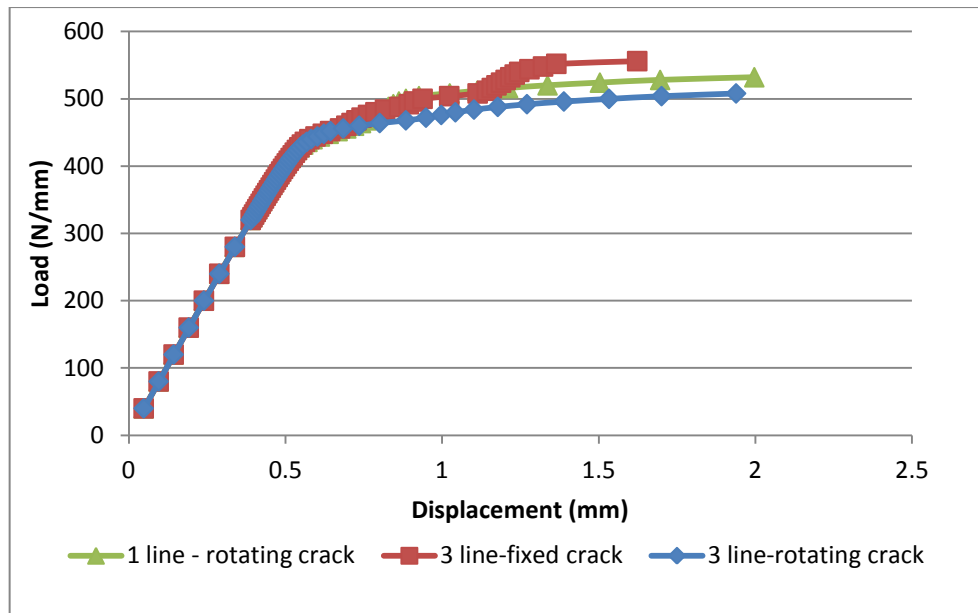
Figure 2.19- Load vs displacement plot - Analysis -1,2 and 3
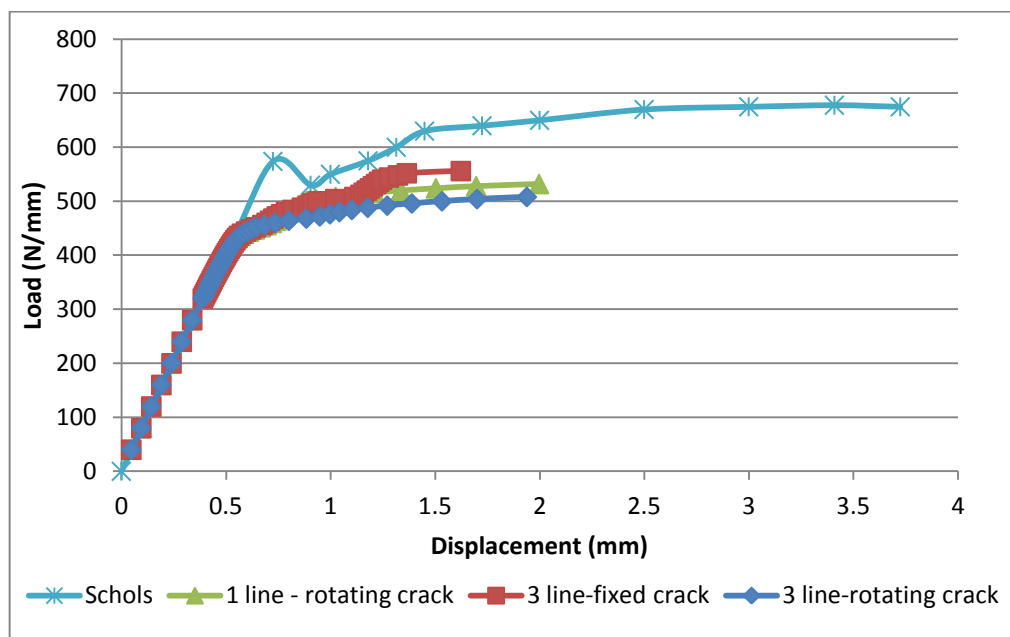
Figure 2.20- Final comparison with Schols' model [3]

2.8 Conclusions drawn from the 2-D analysis

It was found that the post peak behavior of the shear key was dependent on a variety of factors which are listed as follows

Type of division- There was a notable difference found in the behavior when the element was divided in two parts in a different manner. It was noticed in the analysis 1 and 3 shown in this chapter. The division also affected the way the crack propagates, as tipping of reinforcement was

39

noticed for the figure on the right (Analysis 1). However no such tipping was observed for the left figure (Analysis 3).
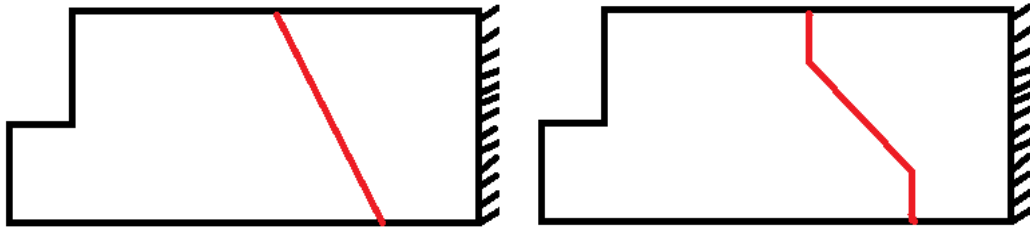
Figure 2.21 Use of different way of dividing the element

Crack model- The total strain crack model which was picked for this analysis had two main options of fixed and rotating crack width. If fixed crack model was picked, the peak was higher compared to the rotating crack model. It is recommended to use rotating crack model as the results are more conservative. In this case as well there was no tipping reinforcement.

2.9 Hand calculations of the strut and tie model

The behavior of the shear key has been analyzed with Non-linear Finite Element model and the factors leading to change in its behavior have been understood. However, it is also necessary to validate the analysis performed earlier by hand in order to confirm the results obtained. One of the ways of achieving this is through calculation by strut-tie model. Strut and tie model is a useful design method for shear critical structures **[18]**. This method, however assumes a linear strain distribution for all loading stages, which make them more conservative. The capacity of struts is determined by concrete strength. The capacity of ties is determined by steel reinforcement and node/connection also represents concrete. Since it is derived from equilibrium of forces, it should not violate any yield criteria and hence provides a lower bound estimate of the capacity of the member/element.

Here, the first assumption is to convert the distributed load of 800N/mm to a concentrated force as shown in **Figure 2.22**. Since the width of force application is 250 mm. Total force is equal to 200 kN. The color red in the **Figure 2.22** represents Tensile Tie and dashed line (blue) represents compressive struts.

The compatibility equations are:

$$F = C1\ sin\theta_1$$
$$T1 = C1\ cos\theta_1$$
$$C1\ sin\theta_1 = T2$$
$$C1\ cos\theta_1 = C2$$
$$C3\ cos\theta_2 = T2$$
$$C3\ sin\theta_2 = T4$$
$$C3cos\theta_3 = T3$$

$$F = T2 = T3$$
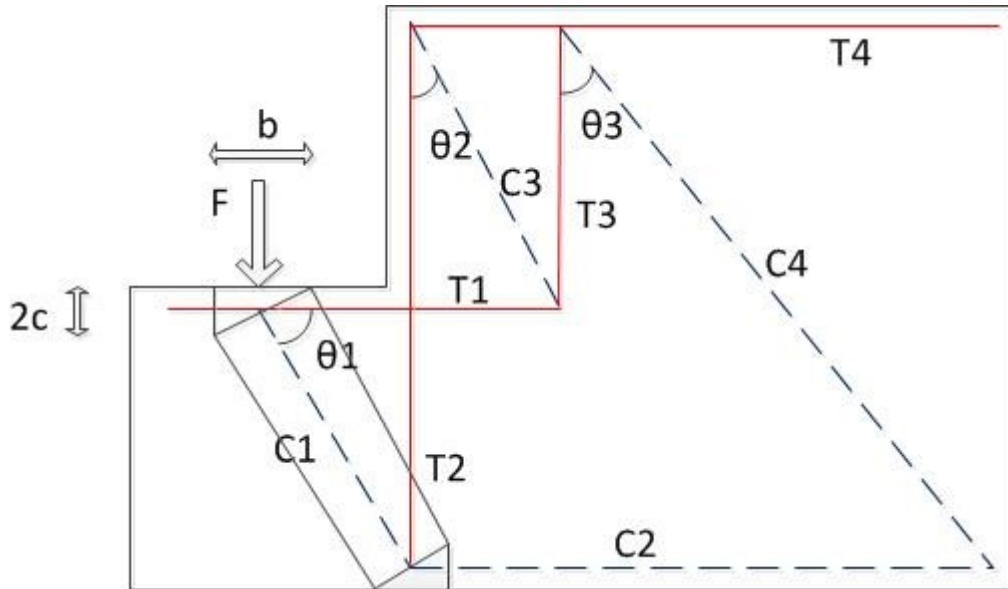
Figure 2.22 Strut and tie model- T represents Tension element, C represents Compression element

Since the coordinates of the reinforcement are already available with us, we can calculate the value of θ_1 and θ_2 (The hand drawing can be found in the **Appendix B2**).

$$\tan(\theta_1) = \frac{640}{165} => \theta_1 = 75°$$
$$\tan(\theta_2) = \frac{520}{690} => \theta_2 = 37°$$

The forces which are critical for the analysis are:
$$C1 = 207 \; kN$$
$$T1 = 53.57 \; kN$$
$$T2 = 200 \; kN$$
$$C2 = 53.57 \; kN$$
$$C3 = 250 \; kN$$

To know whether the element has sufficient capacity, we need to check the tensile ties, the compressive struts and the nodes. Since, we already know that the DIANA model fails by the yielding of the steel reinforcement, we will first check those.

The ultimate stress of steel is 435 N/mm². We find out the area of steel required for T1 & T2.

$$A_{T1} = \frac{53.57 * 10^3}{435} = 123 \; mm^2$$
$$A_{T2} = 200 * \frac{10^3}{435} = 459 \; mm^2$$

With 16 mm φ, the area available is 200 mm². So it can be concluded that T1 has sufficient strength while T2 does not. The ultimate capacity that can be carried by T2 is 435N/mm²*200 mm² = 87kN. However if we consider the yield capacity, which is 348 N/mm2, then load that can be carried is 70kN.

This implies load/mm= 70*1000 N/250mm = 280 N/mm   **Eq 2.1**

We notice that is much lower than the capacity of the element obtained through the analysis (500 N/mm).

Next we check the **nodes** and the **concrete strut.**

$tan\theta_1 = b/2c$
c= distance from the reinforcement =40 mm
b=300 mm
width of the concrete element, h = $\sqrt{(2c)^2 + b^2} = 310.5\ mm$

We notice that this value is higher than the width where force is applied (250 mm) and also the width of the element itself (200 mm). Hence, 200 mm is considered as the width of the concrete strut.

Stress=$207 * \frac{1000}{200*200} = 5.17\ N/mm2$

This is much lesser than the concrete strength of 23.3 N/mm². Hence, it can be said that the concrete element is safe in compression. The nodes also much be checked. According to the standards of fib **[19]**, for a CCT node, the maximum capacity is 0.75 f_c, which is equal to 17.47 N/mm². This value is much higher than the capacity required. Hence we are safe in the nodes.
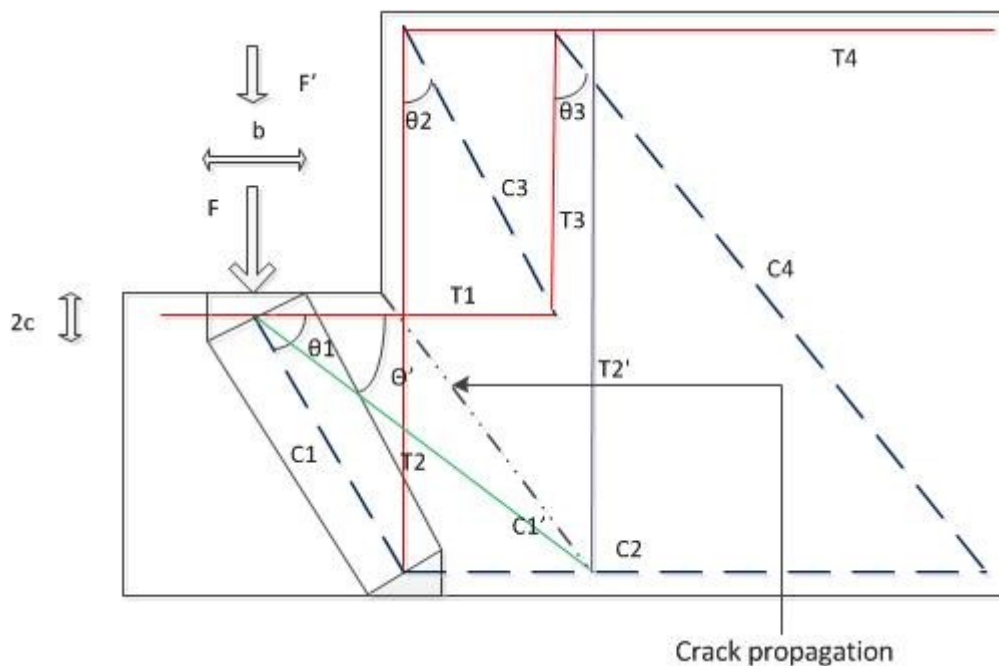
Figure 2.23 Strut and tie model-modified

Because of the differences observed in the capacity calculated by strut and tie model in comparison to the analysis carried out in DIANA, another strut and tie model was superimposed on the existing model. In the **Figure 2.23**, the colors green and purple represent the modified strut and tie model.

It is assumed that an additional force F' acts on the shear key. This force F' is taken by the T1 and C1'. Since, the capacity of T1 was determined by taking into account the vertical force of 800 N/mm, or 200 kN in the first step, we can conclude that it has enough capacity for the extra load.

It was understood that the crack propagates at the angle of 45˚ between T1 and T2, **Figure 2.23**. It was expected that the end of the crack acts as a node in the strut and tie model marked in **Figure 2.23** as 2. So the concrete strut C1' marked in green will end at that strut. By making the simple equilibrium equation, the force F' that can be additionally applied to the model can be calculated. Since, there is no reinforcement present, the tensile force represented by T2' in purple color, should be carried by concrete. The maximum load that can be carried by concrete determines the extra vertical force that can be taken by the strut and tie model (**Figure 2.24**).

The concrete tensile capacity is 1.5 N/mm2. So the load that can be carried =1.5*200*200 mm^2=60 kN

The load/meter=60*1000/250=240 N/mm   **Eq 2.2**

Hence the total load that can be carried =280+240 N/mm=520 N/mm (**Eq 2.1& Eq 2.2**)

This makes the capacity of the total strut and tie model comparable to the capacity predicted by DIANA. Although we have to take into account the tensile capacity of concrete.
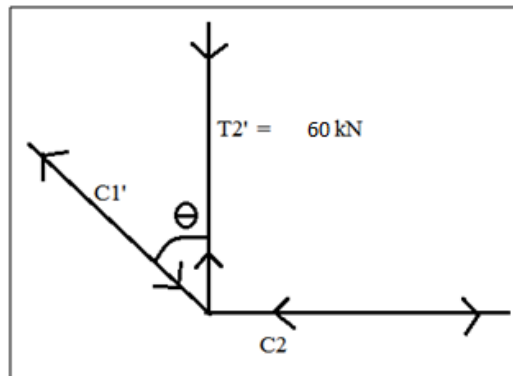
Figure 2.24 Point 2 in Strut and tie model

2.10 Summary

In this chapter, the analysis of the shear key of the tunnel was performed and the load displacement plot was obtained. A difference in the load capacity of the tooth was found when compared to the model used by Schols [3]. Next, hand calculations were performed to check the validity of a strut and tie model. By using the tensile capacity of concrete, it was proved that both the models gave similar values of the failure load.

Chapter 3

Shear key interaction

3.1 Introduction

In the previous chapter, a single shear key model was observed and its cause of failure was determined. In this chapter, modeling of the double tooth connection is done with the help of DIANA. The 2-D model of the tooth existing in the floor of the Tunnel was made, to understand the interaction between the two different segments of a tunnel. To generate a situation close to reality, it was decided to have the same value of rotation in the tunnel tooth as was observed in reality.

3.2 Interaction between shear key

A major aspect which needs to be addressed in the modeling is the interaction of the two segments of the concrete tunnel. In the actual structure, 2mm thick bitumen layer was provided in between the segments. However, with time it is expected that the bitumen layer would have lost its stiffness. Hence, it is expected that the interaction occurs between the concrete segments without any strength contribution from bitumen. To understand the interaction, in the **Figure 3.1**, the expected behavior when rotation and settlement are applied to the model is shown. Looking at the diagrams, it can be said that the properties of the interface elements such as compression, tension and shear resistance are of prime importance. In **Figure 3.1** (left), the shear and compression of the elements is critical. In **Figure 3.1** (right), the tension becomes critical. Also, another aspect that comes into play is the friction between the bitumen and the concrete elements and between concrete and concrete elements. A friction coefficient, μ of 0.3-0.9 is suggested to be used for this study **[3]**. The friction between two elements in DIANA is defined with the help of structural interface elements.

The 2-D model is mainly used to understand and observe the behavior of the interface (representing the bitumen layer) and the reinforcement in the concrete. A 3-D model is necessary to understand the crack propagation behavior. The 3-D model although advantageous is difficult to model due to its complexities. Hence, first the interface interaction will be studied in 2-D and later applied to the 3-D model.
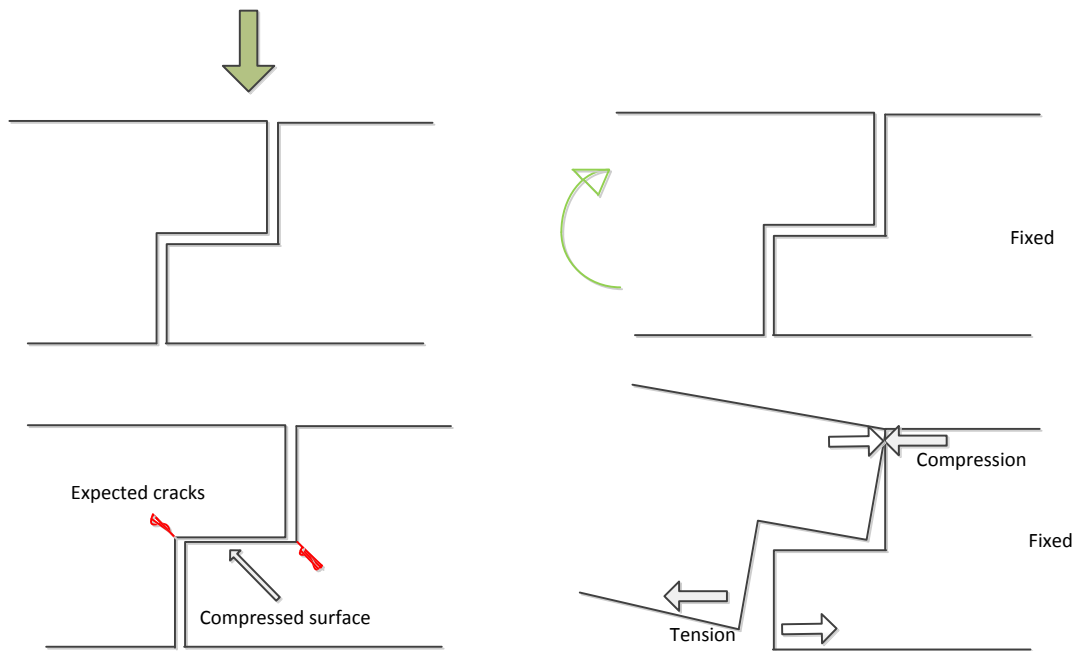
Figure 3.1 - Cracking behavior on application of Force on the shear key (left) and Behavior on application of Moment on the shear key (right)

3.3 Interface elements in DIANA

Interface elements are used to model discontinuities between the conventional elements. Typical examples of interface elements are elastic bedding, discrete cracking, friction between surfaces, joints in masonry etc. In our case, the interface elements will be used to model the friction between surfaces.

The interface elements in DIANA are defined with the elastic stiffness, D. Depending on the application; the stiffness can be specified per direction and can depend on the friction, temperature and maturity **[13]**. In one of the earlier works in the definition of interface elements in DIANA N61F interface elements were used. In this case for driven tunnels, N61F interface elements were oriented along the normal axis of the joint **[14]** (**Figure 3.2**). Three degrees of freedom were provided to the joint according to the three directions of forces present in the model which were normal force, shear force and moment. No interaction was assumed between the different degrees of freedom in the model which in reality was not true. The longitudinal joints in the tunnel have a complex non-linear behavior due to their incapacity to transfer tensile stresses. For a certain axial stress with increasing Bending moment, loss of contact occurs on one side of the joint which varies with the axial stresses **[15]**. In another study, the loss of contact in the longitudinal joint was specified by unilateral interface elements CL24I **[16]**. Nonlinear stiffness was assigned to them with a rigid behavior in compression and gapping is produced in tension. In the work, the behavior of the bituminous packer was tested and a non-linear stress-strain diagram for low-stresses and hardening process close to $10N/mm^2$ was observed as shown in **Figure 3.3**.

If we concentrate at the interface elements available from the point of view of DIANA, there are node interface elements like N4IF, N6IF where the interface surface and the directions are user

specified. Then there are the line interface elements, like L16IF, L8IF, L20IF, CL24I, CL32I which can be placed between edges of 2-dimensional elements. With these elements, the interface surface and directions are evaluated automatically from the geometry itself. However, the drawback with these elements is that they can-not be used in geometric nonlinear analysis. Finally there are plane interface elements like Q24IF, CQ48I which are placed between faces of three dimensional elements. Here also the interface surface and the directions are evaluated automatically from the geometry **[17]**.

In this work, in the 2-D analysis, the interface elements used are L8IF. The bitumen is not expected to have retained any stiffness; hence its contribution is not considered. In the 3-D model, Q24IF is used for the analysis. These elements were defined automatically in FX+, using the convert element option.

Rotation under shear force

Pure rotation
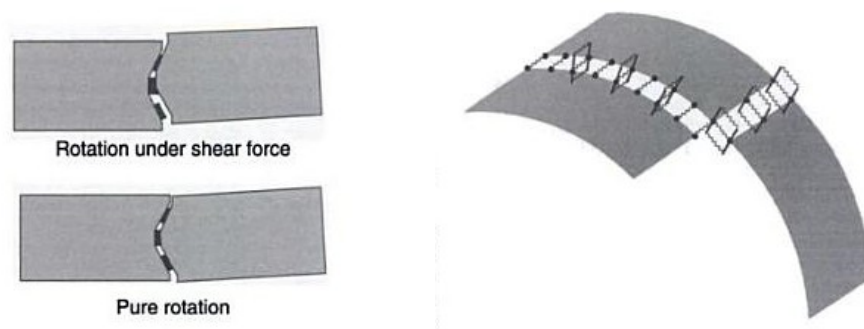
Figure 3.2 - Rotation with and without shear force in driven tunnels (left) and 3-D view at joint model (right) **[14]**
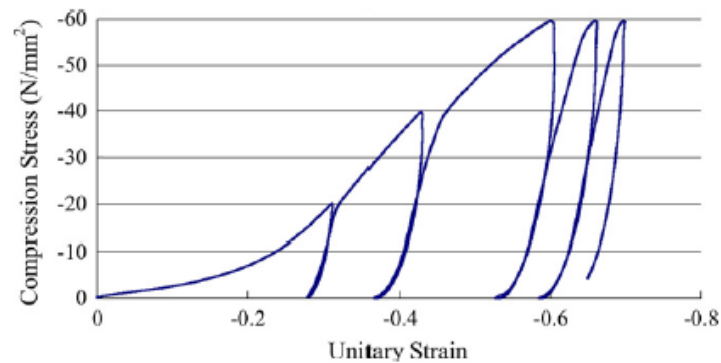
Figure 3.3 - Stress strain for bituminous packer L9 under cyclic loading **[16]**

3.4 Support condition

The model definition here was similar to the model definition for the 1-tooth analysis. It consisted of geometry, supports and loads in FX+ and of material and interface property definition in DIANA.

The most significant part of the model definition was the application of forces and supports. The tunnel element had to be loaded globally in order to produce the same rotations, **Figure 3.4 (right)**. The tunnel element must not be loaded locally near the tooth to produce the required rotation, because it will produce a bias result of the real situation. **Figure 3.4 (left)** explains the situation which was avoided in the research. Since, the settlement of the tunnel elements is relative to each other, it cannot be imitated with a model of a part of the tunnel. Hence, rotation in the lateral direction only will be the parameter used for study.
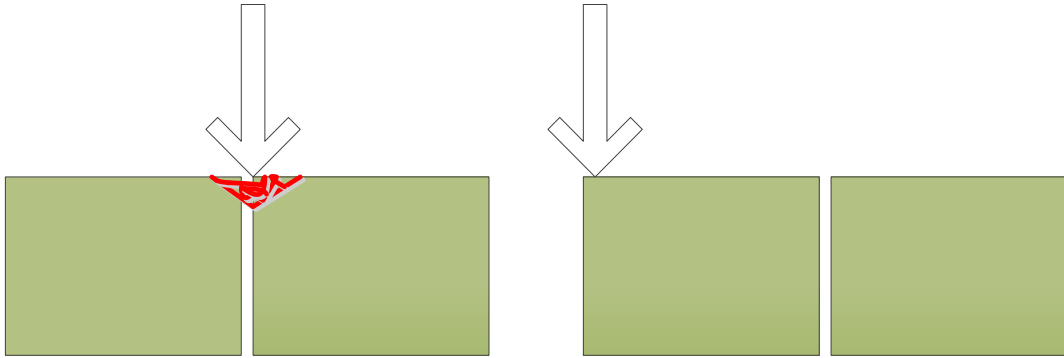
Figure 3.4- Left- Loading at the connection of the segments (local), Right- Loading at the end of one segment (global)

The tooth model was continued on the existing shear key model which was made for the 1st analysis described in Chapter 2. Same concrete model as earlier used was applied for the analysis of interaction as well. If the loading stages in the tunnel are considered, it is noticed that first, there is compression in the tunnel segment/segments (1 in **Figure 3.5**) followed by rotation of both the tunnel segments, **Figure 3.5, left**. During the compression phase, one of the segments should be fixed on the side, so that there is uniform compression through the tunnel cross-section. In the next step, the tunnel elements should rotate with respect to each other. Since, one side of the tunnel is fixed; moment forces are applied on the left side of the tunnel to produce the desired rotation.
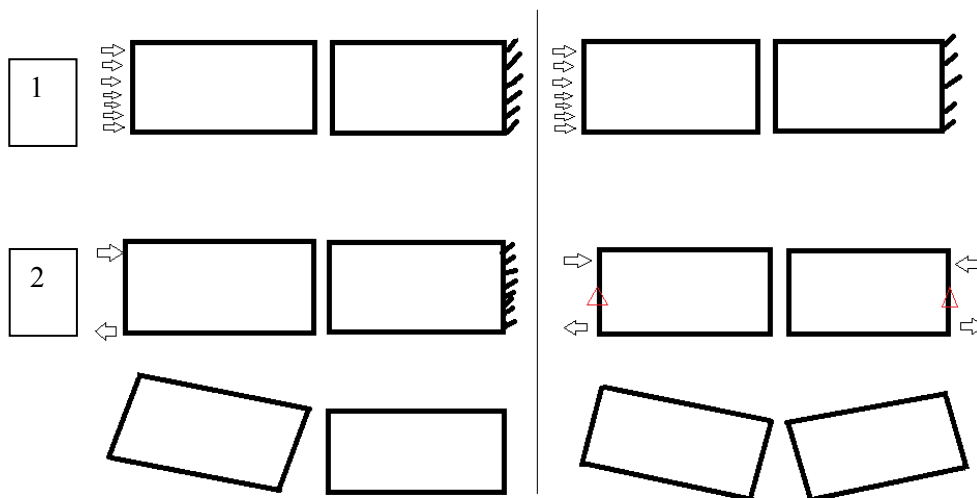
Figure 3.5- Left- Method 1-Non-linear analysis and Right- Method 2- Phased analysis

This process can also be approached in a different method by using phased analysis. In phased analysis, the supports on the tunnel can be varied in steps to produce the desired situation. In phased analysis, in first step, the right segment can be fixed and compression force due to water is applied. In the second step, hinged supports are provided on both segments and moment forces are applied, **Figure 3.5, right**. Although phased analysis is aesthetically more appealing, it gives no other advantage over the other method. Since, the second method (phased) is more complex and hence it was decided to go ahead with the first process.
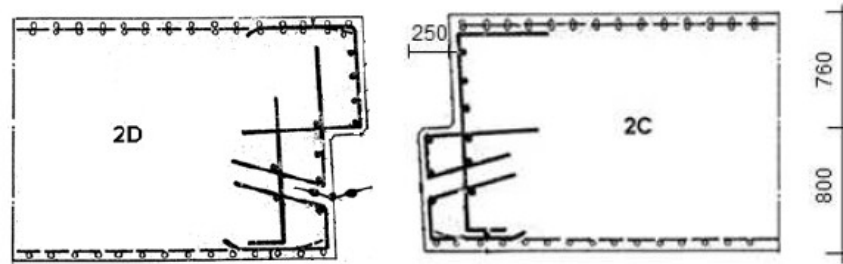
Figure 3.6- Tooth structure in the bottom of the tunnel [3]

3.5 Loads applied on the structure

Two types of loads were used in the current analysis. The first load was compression due to the water pressure, where 60% of the total compression was applied. The value was reduced to 60%, in order to account for the losses due to shrinkage and creep in concrete. The value of pressure at the bottom of the tunnel is found to be 121.3 kN/m^2 **[3].** In this 2-D analysis, only the tooth in the bottom of the tunnel is being considered, the pressure force is assumed to be constant over the tooth height, **Figure 3.7**. The 2-D model has a thickness of 200 mm, hence, the pressure becomes:

p = 121.3*0.2 = 24.26 N/mm

Second type of load applied was moment forces causing the rotation of the element. It was not known what moment will cause the required amount of rotation. So, an arbitrary moment was applied in the form of force couple at the top and bottom of the left segment. The forces were applied at the end edges of the element with a magnitude of 200 N/mm over 300 mm (both at top and bottom), **Figure 3.8**.
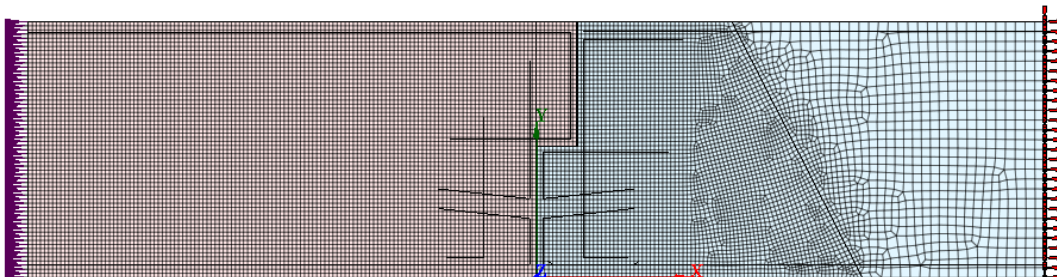
Figure 3.7- Step 1: Fixed on right and compression on the left
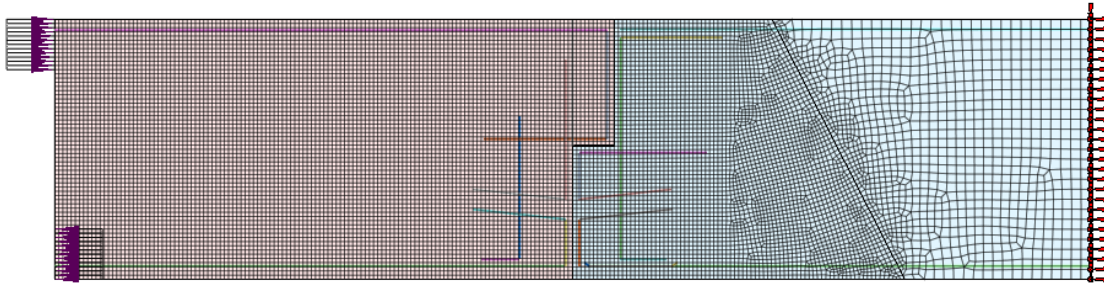
Figure 3.8- Step 2: Equal and opposite forces causing moment

3.6 Interface element definition

The definition of the interface element was important from the point of view of interaction of the two shear keys. In reality, while casting, 2mm bitumen layer was present between the concrete segments. However, with time, it is expected that the bitumen has completely worn out. Hence, it was decided to not include the properties of bitumen for the interface between the keys. Hence, the interface should represent the behavior of concrete to concrete interaction, transferring forces in compression but not in tension. While modeling the interface element in DIANA, a 2mm gap was modeled, but it has no real significance as the interface elements have zero thickness irrespective of the model. This 2 mm gap was modeled for ease of differentiating between the two different segments of the tunnel and has no implications.

The interface element properties are defined with Coulomb criteria (**Figure 3.11-** Mohr-Coulomb criteria and GAP properties were provided. The GAP criterion in DIANA ensures that in case of occurrence of tension, there is no transfer of forces over the interface element, but separation of the adjacent elements is obtained. The friction coefficient, η= 0.3 was chosen, as it is the lowest possible value that can occur in between the concrete segments. The value of friction coefficient generally varies from 0.3-0.5.

Another important property is the stiffness of the interface elements, which should be sufficient, so that there is smooth transfer of forces. Otherwise in compression it might result in concrete elements going into each other (which is not practical). The value of stiffness is calculated by dividing the Young's modulus of concrete by thickness. A value of 17000N/mm^3 was used in this case and it was found to be sufficient to ensure no deformation occurs in the interface. **Table 3.1** summarizes the properties of interface element used in the analysis.

$D = E/t$

Where D is the stiffness in N/mm^3

E is the Young's modulus of concrete = 34000 N/mm^2

t=thickness of the interface = 2 mm

$D = 34000/2 = 17000$N/mm^3

Stiffness in the normal direction = **17000 N/mm^3**

Stiffness in the shear direction/ shear stiffness= 17000*0.3= **5100 N/mm^3**
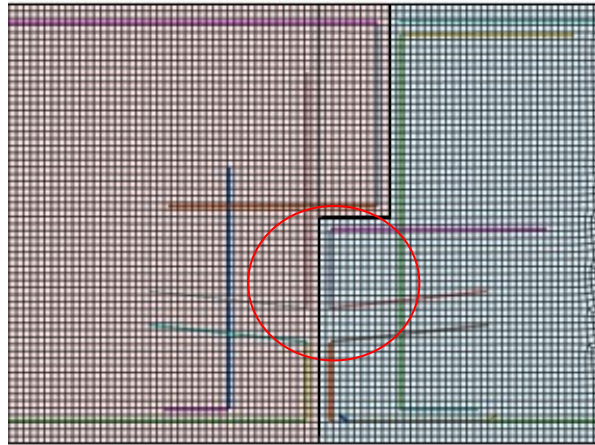
Figure 3.9- Interface element- in centre (black-line)
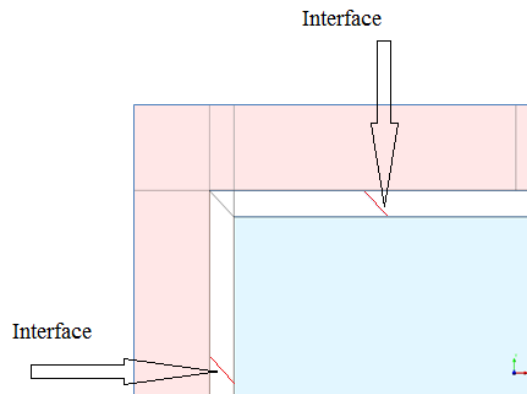
Figure 3.10- Magnified Interface element, as circled in red in **Figure 3.9**
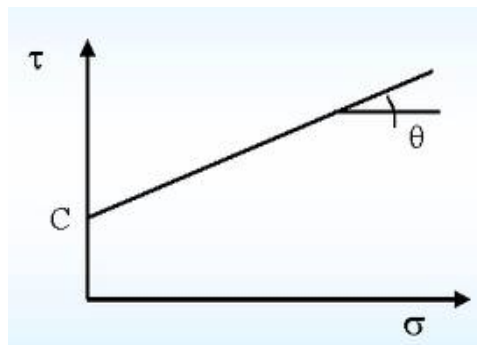
Figure 3.11- Mohr-Coulomb criteria

Property	Property value	
Interface	L8IF	
Failure criteria	Coulomb (FRICTI)	
Stiffness (DSTIF)	Normal = 17000 N/mm3	Shear = 5100 N/mm3
GAP	Tensile strength = 0 N/mm2	
FRCVAL	tanφ= 0.3	

Table 3.1 Interface element properties

Force direction	Transfer through interface
Compression-perpendicular direction	Yes
Tension-perpendicular direction	No
Shear in parallel direction	Yes (limited-depends on friction coefficient)

Table 3.2 Interface element force transfer

3.7 Expected Model behavior

The moment forces are applied in steps such that at one instant, the shear key is able to reach the same value of lateral rotation as found in the tunnel. In **Figure 3.12,** it can be observed that the value of rotation between the two elements is represented by θ. In this work we focus on a particular connection between two segments, where the rotation was found to be $2*10^{-3}$ rad. This point lies in element 2 and segment connection C-D.
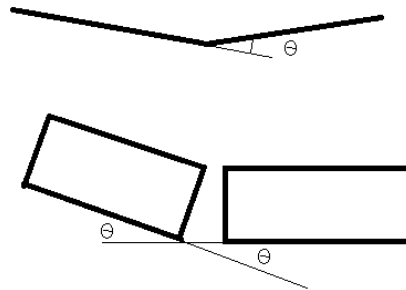
Figure 3.12- Rotation between the segments

3.8 Results of the analysis

A non-linear analysis was performed with compression as the first load and moment forces as the second load. The compression force was applied as 1 load step. It was observed that around 90% of the elements had a compression value of 0.12 N/mm^2. Since, 0.121 N/mm^2 was the actual value of the compression force due to water pressure, this was expected. In the right end of the element, it was noted that there was slight deviation in the values of compression. However, since we are concerned with the connection and not with the supports, it can be ignored. **Figure 3.13**, shows the result of the 1st load step. The principle compressive stress plot (S3) is depicted in the figure.

The compression force was applied all at once while the moment force, 200N/mm was applied in 20 load steps, each 5% of 200 N/mm. The result is denoted as 0.05(20). The compressive stress plots of the load steps 6 and 8 are shown in the **Figure 3.14 and Figure 3.15.** It was found that, on increasing the moment forces, the gap between the elements became evident. After load step

8, no convergence was obtained as the gap between the two elements became very large. The stresses in the concrete and steel were found to be very small at load step 8, **Figure 3.16**. The value of Ө in the last load step 8 was found to be 10 times smaller than the one observed in reality. Since we cannot proceed further than load step 8, not much can be predicted about the actual behavior. A plot of moment vs rotation was made, and a flat plateau was obtained at load step 8, **Figure 3.17.**
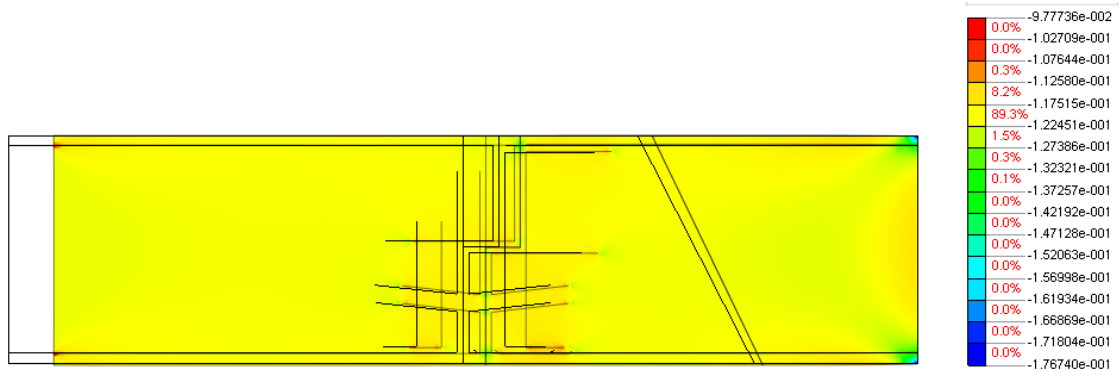
Figure 3.13- Load step 1, Compressive stress, S3
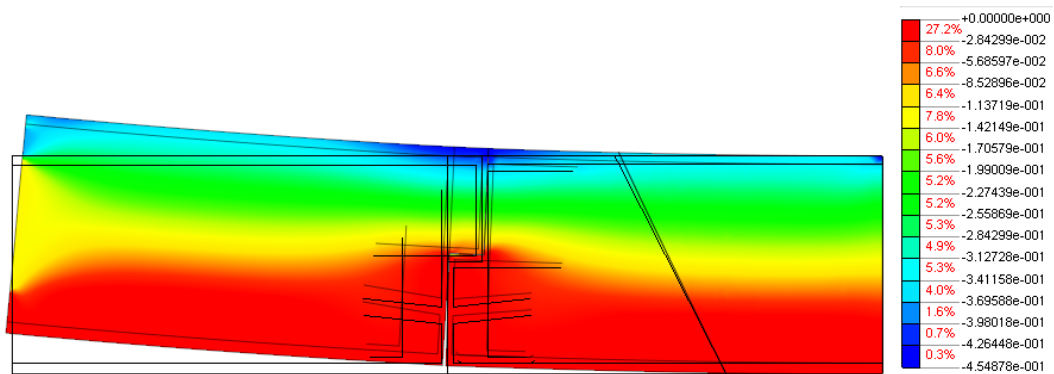
Figure 3.14- Load step 6- 50 N/mm, Compressive stress, S3
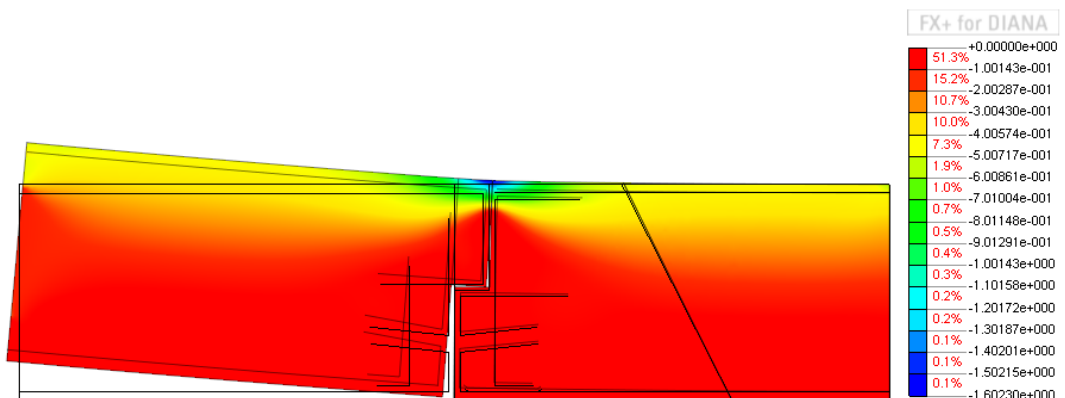
Figure 3.15- Load step 8-70 N/mm, Compressive stress, S3
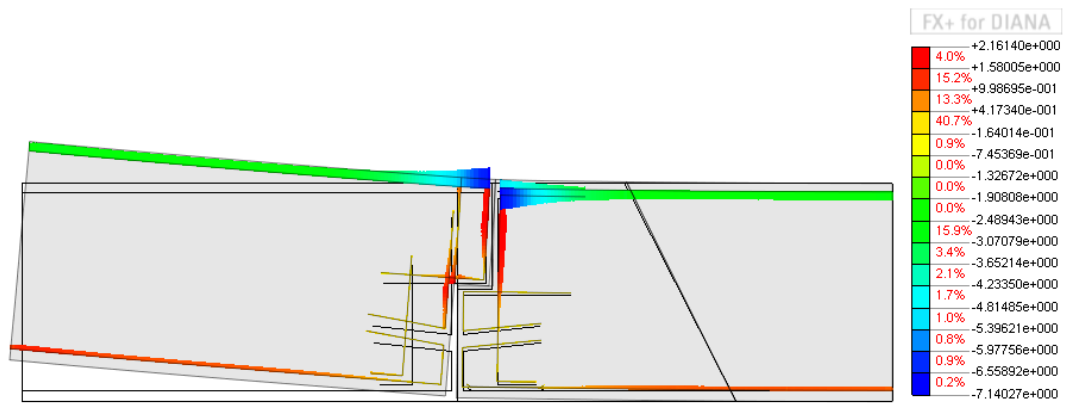
Figure 3.16- Load step 8- Reinforcement stresses, Sxx
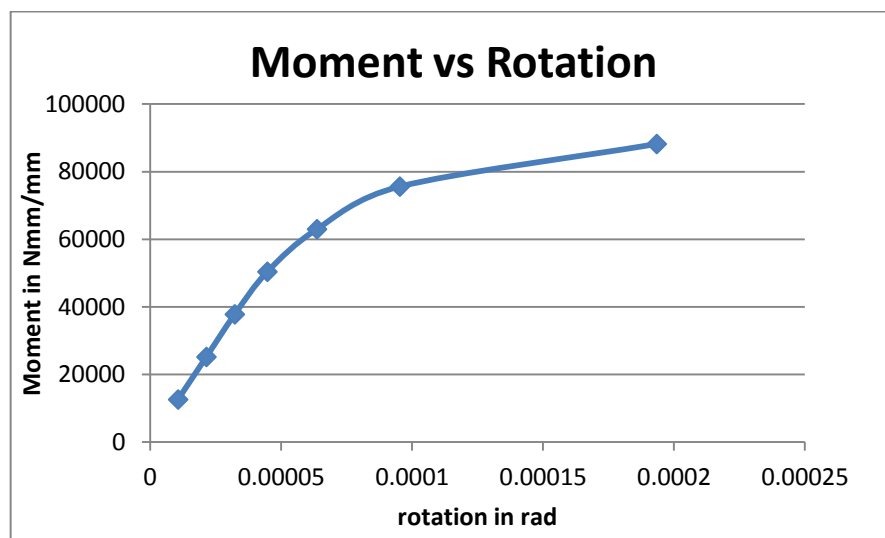
Figure 3.17- Moment vs Rotation for the segment

3.9 Summary

In this 2-D analysis, it was found that the tooth had started to develop a gap and after a few load steps divergence was obtained. However, no stress value exceeded the limits for concrete or steel. Since the actual value of Θ could not be reached, prediction of the behavior cannot be made. Hence, this model is not sufficient to conclude on the tunnel serviceability condition, as only a part of the floor of the tunnel was studied. Hence it can be established that a full size model of the tunnel should be studied in order to come to any conclusion on the structure's serviceability.

Also, after discussion with experts, it was concluded that the value of friction coefficient used should be much higher. Hence, for further calculations it is recommended to use a value of **η = 0.5-0.9**.

Also, in this 2-D model, the effect of the shear force in the tooth has been ignored. The cracking as a result of a shear force is expected to be one of the main causes of leakage. Hence, in the 3-D model which will be discussed in the following chapters, a shear force will precede the moment forces causing rotation.

Chapter 4

Macro behavior of the tunnel

4.1 Introduction

In the previous chapter, the behavior of the interaction was modeled, when the two parts of the tunnel were subjected to a couple causing a moment. In order to have an idea about the amount of force (force-couple) which will be required to cause the required rotation in the full tunnel segments, this part of the study was done. Hand calculations were performed to calculate the forces which cause the rotation of $2*10^{-3}$ rad. This was done to have an idea about the tunnel condition.

4.2 Calculation

Let us consider the **Figure 4.1**: A normal force, N and a moment, M have been applied to both the left and the right segments. Let us consider the left segment. The force, N gets transferred to the other segment as N_c.
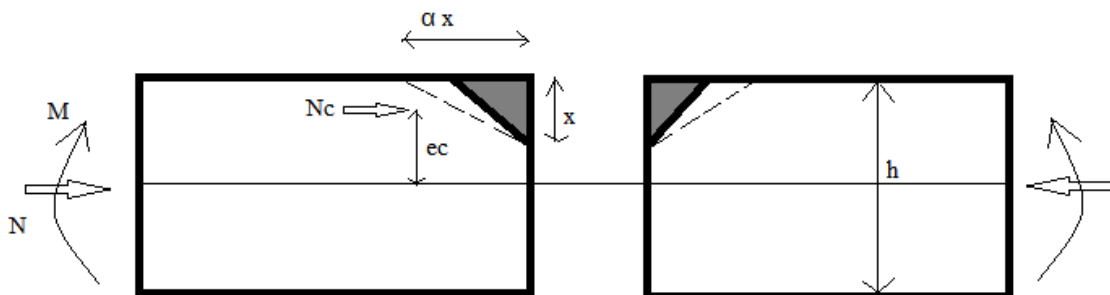
Figure 4.1- Moment vs Rotation for the segment

First, we solve this problem by force and moment equilibrium and thereafter we back calculate from the value of rotation to get the value of the moment that should be applied to the tunnel segment.

$$\sum H = 0 \ and \ \sum M = 0$$

$$N = N_c$$

$$N = \frac{1}{2} * \sigma_c * x * B$$

$$B = width$$

$$M = Nc * e_c$$

$$e_c = \frac{h}{2} - \frac{x}{3}$$

$$assume, \alpha = 2$$

$$strain, \in = \frac{\sigma_c}{E_c}$$

$$\Delta l_{top \ fiber} = \alpha x * \frac{\sigma_c}{E_c}$$

$$rotation \ \varphi = \frac{\Delta l_{top \ fiber}}{x}$$

We will start from the last equation, as we know the rotation and work our way backwards to the top. However, we first need to determine the normal force acting on the tunnel segment. The force due to water pressure varies over the height of the tunnel. Over here for easy calculation, we take the average value of the force due to water pressure.

The pressure varies from 0.068 to 0.121 N/mm^2 from top to bottom [3].

$$Average \ pr = \frac{0.068 + 0.121}{2} = 0.0945 \ N/mm^2$$

Note: It has been assumed here that 0.095 N/mm^2 is the pressure due to water in the tunnel cross-section. This means that it is not the actual pressure due to water outside the tunnel. But this is the pressure which the tunnel cross-section experiences.

We also need to find out the area on which this pressure acts to find out the value of force, N. For this purpose, we calculate the area approximately, as it would take a lot of time to do so accurately (**Figure 4.2**).
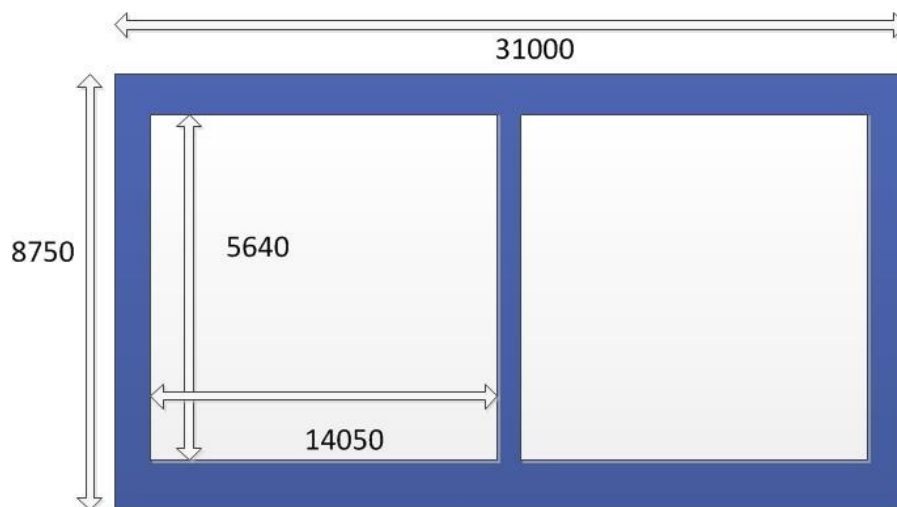
Figure 4.2- Cross-section considered (all dimensions are in [mm])

$$Area = (8750 * 31000) - (2 * 14050 * 5640) = 112.7 * 10^6 \text{mm}^2$$
$$N = 0.0945 * 112.7 * 10^6 = \mathbf{10.65 * 10^6 N}$$

We know that the rotation between the segments is $2*10^{-3}$. However, it needs to be translated into the rotation of each segment. From the **Figure 4.3**, we conclude that $\emptyset = \theta/2$.
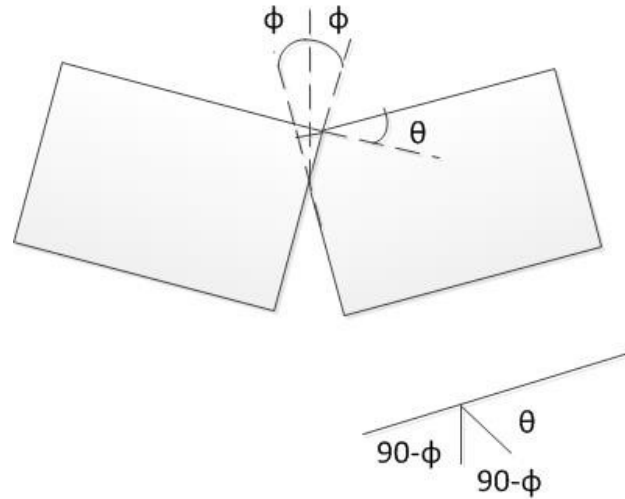
Figure 4.3- Calculation of angle between two segments

Now we have all the variable to back calculate from the rotation to the moment applied.

$$\emptyset = 2 * \frac{10^{-3}}{2} = 10^{-3}$$
$$\emptyset x = \Delta l_{top \ fiber}$$
$$\Delta l_{top \ fiber} = \emptyset x = \alpha x * \frac{\sigma_c}{E_c}$$
$$10^{-3} = 2 * \frac{\sigma_c}{34000}$$
$$\sigma_c = 17 \frac{N}{mm^2}$$
$$N = \frac{1}{2} * \sigma_c * x * B$$

Assuming that compression occurs only in the top flange (tunnel roof)

$$10656.4 * 10^3 = \frac{1}{2} * 17 * x * 13990$$
$$x = 42.31 \ mm$$
$$e_c = \frac{8750}{2} - \frac{42.31}{3} = 4360 \ mm$$
$$M = N * e_c = 10656 * 10^3 * 4360 \ Nmm = 46471.3 \ kNm$$

Note: For simplicity the roof and floor are asuumed to be of equal thickness during the calculation of e_c. There is a slight difference, but it has been ignored here.

Hence, it can be concluded that a moment of 46.5 $*10^3$ kNm will cause a rotation of 2$*10^{-3}$ rad between the segments. However, the concrete compression zone is only 42 mm, and it has a minor impact on the internal lever arm.

Now, we look at the shear capacity of the joint by assuming the friction coefficient 0.5.

$$V = \mu * N_c = 0.5 * 10656.4 * 10^3 N = 5300 * 10^3 \; N = 5300 \; kN$$

According to the calculations performed by Schols **[3]**, the shear force on the joint = 2481 kN (see **Figure 1.19**), which is less than the capacity of the joint. Hence, we can say that the vertical contact areas of the joint should be capable of transferring all the shear force (without loading the tooth). But, we also note that the contact length is very small, merely 42 mm. This value is not possible practically. So we might expect the FEM model to diverge before reaching this point.

We need to perform the same analysis by FEM in order to verify these calculations and come to any conclusions about the behaviour of the segment connection.

4.3 Summary

The purpose of this calculation was to calculate the amount of force which will be required to cause the rotation of 2$*10^{-3}$ rad between the segments. This was important for the 3-D analysis as the effect of both shear and bending moment is expected to be studied. Since the shear force values are already avalable to us from the earlier calculations, the bending moment was determined by hand calculations and was found to be 46000 kNm for the entire tunnel. These values might be slightly different from those occuring in reality but they give the best possible approximations.

Chapter 5

3D model of the tunnel

5.1 Introduction

The 3-D model of the tunnel is made in order to come to a conclusion about the behavior of the tunnel connection. In the previous chapters it has been established that a 2-D model is not sufficient for this purpose. A 3-D model is necessary to understand the crack propagation behavior. The 3-D model although advantageous is difficult to model due to its complexities. In the 3-D model, one of the major difficulties is to access the proportion of the half joint that is effective in transferring shear. Because of shear lag effects, for wide spans of up to and in excess of 10 m, large parts of half joint are likely to be ineffective as shear transfer is concentrated in the stiffer zones close to the walls of the section. This restricts the capacity of the joint. First part of the chapter is focused on calculating the effective parts in the 3-D model which transfer shear. The second part will be focused on the schemes of loading which are expected to occur in the actual tunnel.

The 3-D model of the tunnel was built in a similar manner as the 2-D model. The main features of this model consisted of the geometry of the model, the reinforcement details, the interface elements and the forces which were defined in the preprocessor. For the ease of understanding the behavior of the model, initially linear analysis is carried out. Once the model is confirmed to be performing well, non-linear analyses are carried out.

5.2 Geometry

For the geometry, it was decided to include the full cross-section of the tunnel connection to the best possible accuracy. The total length of the tunnel considered for the research work was 2*H, where H represents the total height of the tunnel **[2]**. It is expected that the forces in any structure distribute themselves uniformly after a distance H, and that is why a length of H on both sides of the connection was selected for the analysis. The reason why a bigger length was not picked for this work was because of the time that is required for the analysis, and hence, lesser the elements, the better. The details of the geometry were obtained from the drawing in the repository of TNO for Kiltunnel (**Appendix C1**) (**Figure 5.1**).
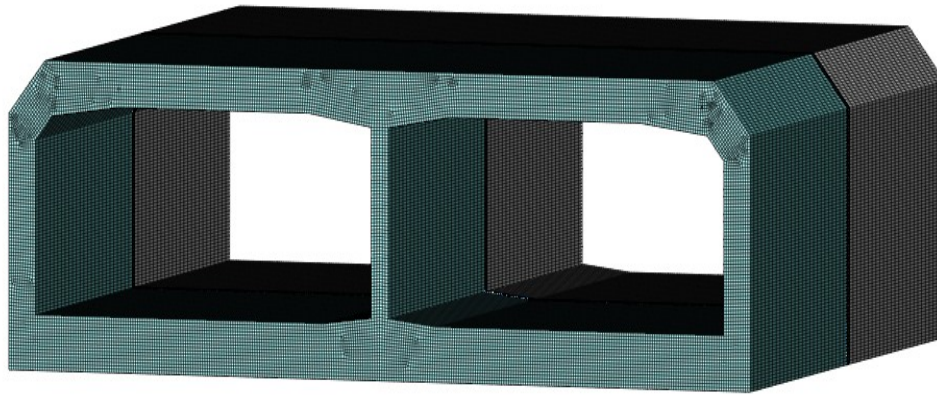
Figure 5.1- 3-D geometry of the two segments- cross-sectional view

5.3 Reinforcement

The reinforcement of the tunnel was similarly obtained from the drawings and fed in FX+. The reinforcement was also kept as accurate as possible except for some places where assumptions were made. For the tooth reinforcement at the deck, the height of the reinforcement varied from the outer wall to the middle wall in the actual structure. However in this model, for saving time, the reinforcement height for the tooth was kept constant. The reinforcement was fed as discrete reinforcement, which allows for any local modifications in the structure if necessary later. (**Figure 5.2**)
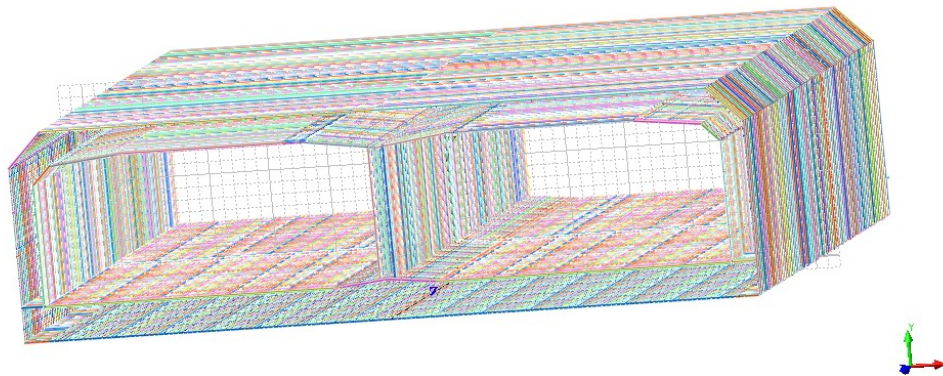
Figure 5.2- Reinforcements of the two segments
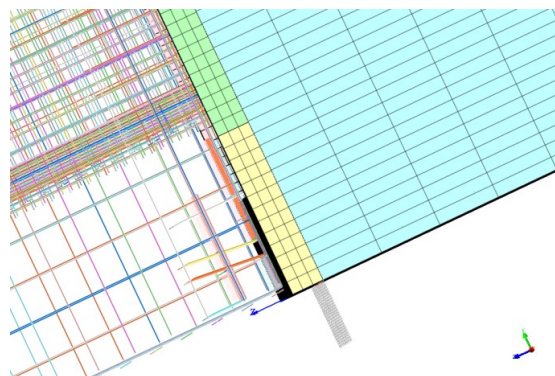
Figure 5.3- Reinforcements in the tooth

5.4 Basic model-modifications

After the first basic model was made ready, a linear analysis was performed in order to check the model. However, on testing it was found that the model was taking more than 24 hours to perform 1-iteration. Because of this reason it was proposed to cut the model into half and perform the analysis. Since the cross-section of the tunnel is symmetric, the tunnel was cut into half at the middle wall. This reduced the number of elements by half and the analysis time became much lesser for each step.

In the **Figure 5.4**, the half cross-section on which further calculations were performed is shown. In **Figure 5.5**, the tooth of the tunnel can be seen. The protruding outside periphery is a part of the loaded first segment. The next segment that comes in will have a protruding inner periphery. This will form the tooth of the tunnel around the entire circumference. Since the cross-section was divided into half, the boundary conditions of the tunnel were changed accordingly. The translation of the middle wall in x-direction (**Figure 5.4**) was constrained. The total tunnel should not translate in the x-direction; otherwise the inner protruding segment can completely slip out of the outer protruding segment and cause instability in the system. Also, one end of the tunnel was fixed. In this structure, the length of the tunnel was also reduced to H on both sides, making it total of 2H. This was done due to two reasons, 1- the effect of stresses on any structure of height, H is expected to become even after a length = H, 2- this way, the number of elements were also reduced, making the simulations faster.
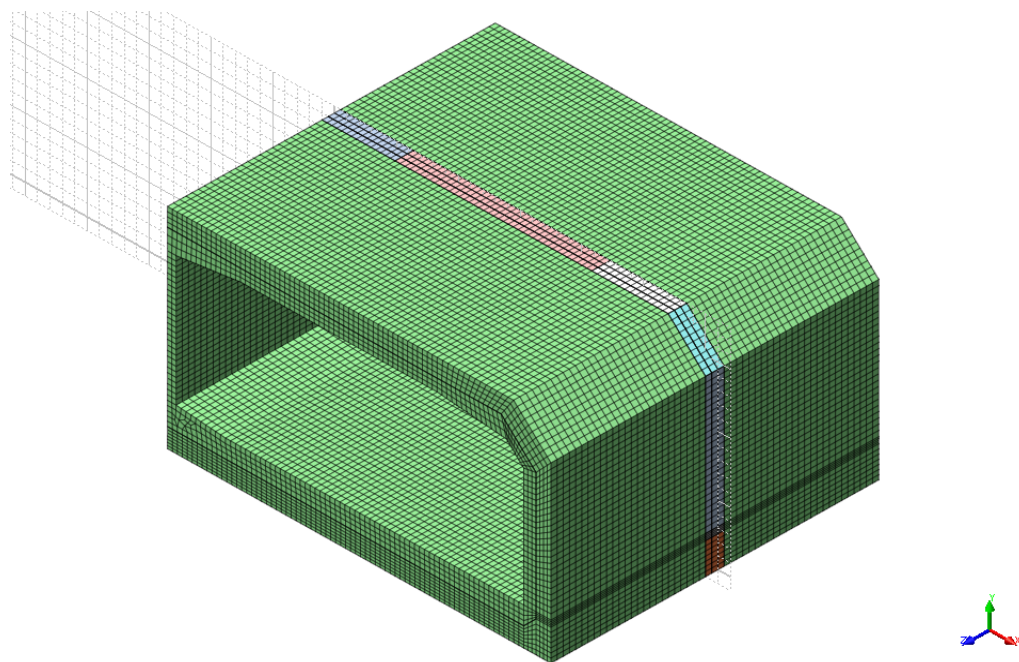
Figure 5.4- Half cross-section of the immersed tunnel

Loaded end

Outside-protruding
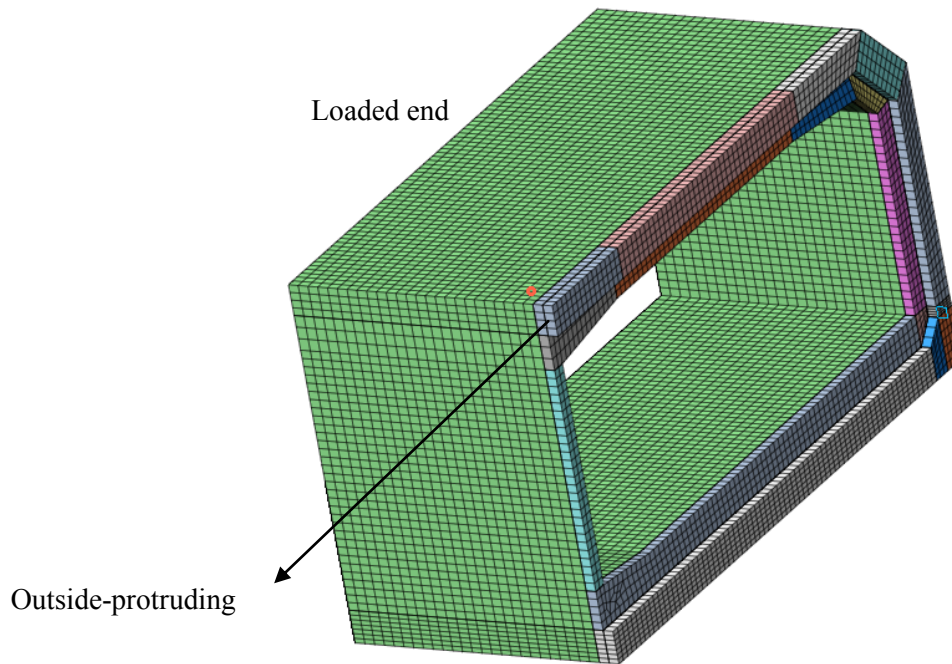
Figure 5.5- Tooth of the tunnel

5.5 Element type

One of the biggest challenges in the 3-D modeling of immersed tunnel lies in the selection of right element type with a good aspect ratio. There are many ways in which the 3-D model could be made. First procedure which was used in this research was to make 2-D meshes and protrude them to obtain a 3-D structure. However, since the geometry of the tunnel is complicated, there were problems in obtaining node-compatibility in this procedure.

Second procedure which was used for modeling was to make 3-D solids and then mesh them. This procedure helped in removing the earlier problem of node compatibility. Once, the decision on the making of model was done, next question was to pick the element type which should be used. The Auto-mesh feature of FX+ generates triad element, shown in **Figure 5.6**, which have the advantage of small computational time. But they often tend to be stiffer. This stiffness can sometimes lead to wrong results can hence it is recommended to use cubic elements only for the model. Hence, it was decided to use brick elements with 8 Nodes for the problem. Generally for FEM analysis in 3-D, it is recommended to use Mid-sized nodes for the analysis. However, again due to limited computational capacity, it was not used in this research. Another problem which was faced during the meshing was that the element sizes could not be increased over the length of the element as it was leading to problems in the node-compatibility. Hence the same size of elements is used throughout the entire tunnel as in the tooth. The size of the brick elements of the mesh were around 250X250X250 mm^3 for major part of the tunnel. However, near the corners, the size variations were very high
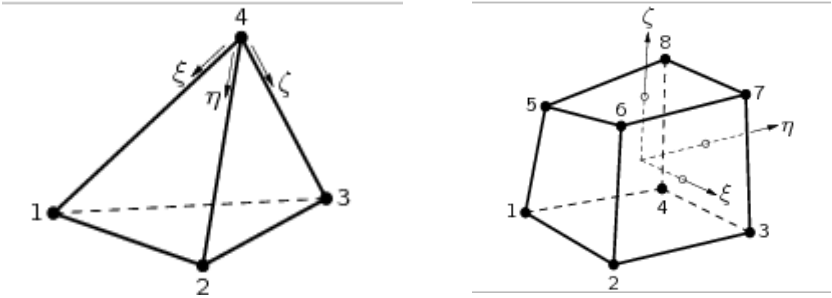
Figure 5.6- Triads-on the left and brick elements-on the right

5.6 Support

The 3-D model was fully fixed on one end in all three directions (x, y and z), and it was horizontally supported at the centre throughout the length of the segments. Horizontal support was required to be provided in the centre because the tunnel was divided into half and it should not translate in the horizontal direction due to minute eccentricities in the loads. The scheme is shown in **Figure 5.7** and the supports in FEM model are shown in **Figure 5.8**.

Side Support
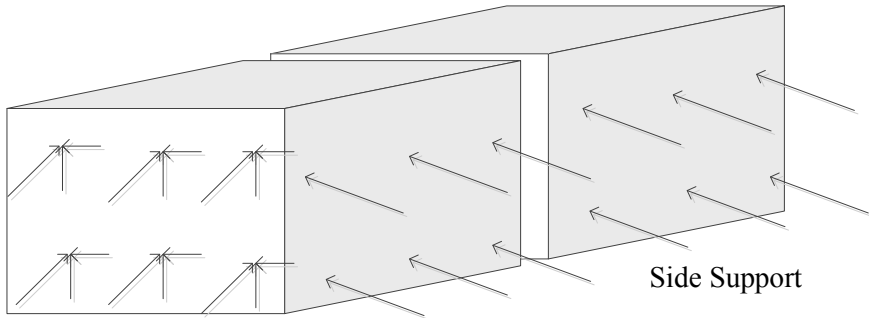
End Support **Figure 5.7-** Support- scheme

Side Support

Tunnel tooth

End Support
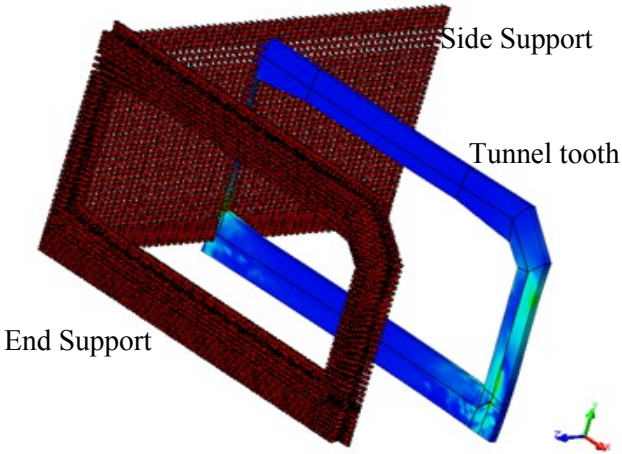
Figure 5.8- Support

5.7 Interface

The interface between the two segments of the immersed tunnel was the most important part of the model. The transfer of forces between the segments takes place through the interface. The horizontal interface is responsible for transferring of shear forces through contact pressure while the vertical interface transfers the forces by friction. The thickness of the interface was kept at 2 mm both in the horizontal and vertical direction. This distance was also helpful in differentiating the two parts of the tunnel from each other.

The interface consisted of three types:

- Between the vertical outer surfaces of the two segments, shown in **Figure 5.10**
- Between the vertical inner surfaces of the two segments, shown in **Figure 5.9**
- Between the flat horizontal-vertical surfaces of the two segments, shown in **Figure 5.10**

The interface was made by first making solids of 2 mm thickness between the two segments of the tunnel and then converting these solids into interface elements. Node-compatibility here also is an important factor without which the analysis may not run correctly. The interface was modeled by Mohr-Coulomb criterion, **Figure 3.11**. The value of tanθ, or friction coefficient was taken as 0.5-0.9. Cohesion, c was assumed as 0. Mode 2 is for making the behavior brittle after the appearance of gap in the model. as discussed in **Table 5.1**.

Property	Property value	
Failure criteria	Coulomb (FRICTI)	
Stiffness (DSTIF)	Normal = 17000 N/mm^3	Shear = 9000-15000 N/mm^3
GAP	Tensile-strength 0 N/mm^2	
FRCVAL	tanφ = 0.5-0.9	
MODE 2	Brittle (0)	
Cohesion	0	

Table 5.1- Interface element properties
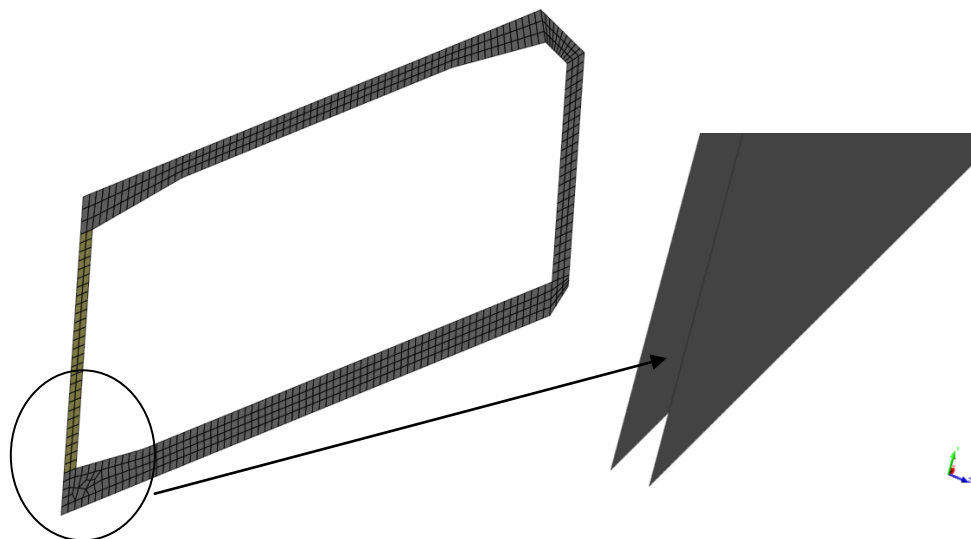
Figure 5.9- Vertical Inner Interface (left), magnified view (right)
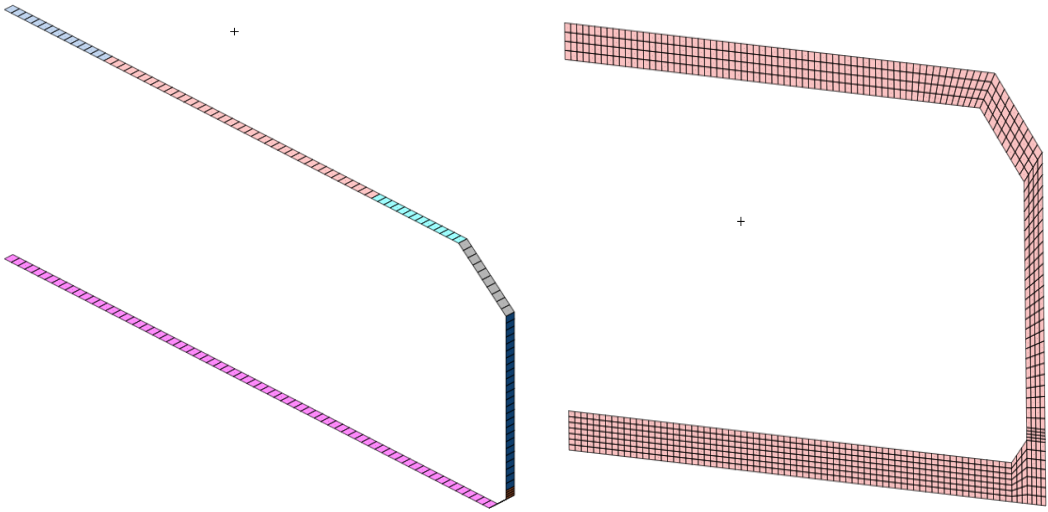
Figure 5.10- Horizontal Interface (left) and Outer vertical interface (right)
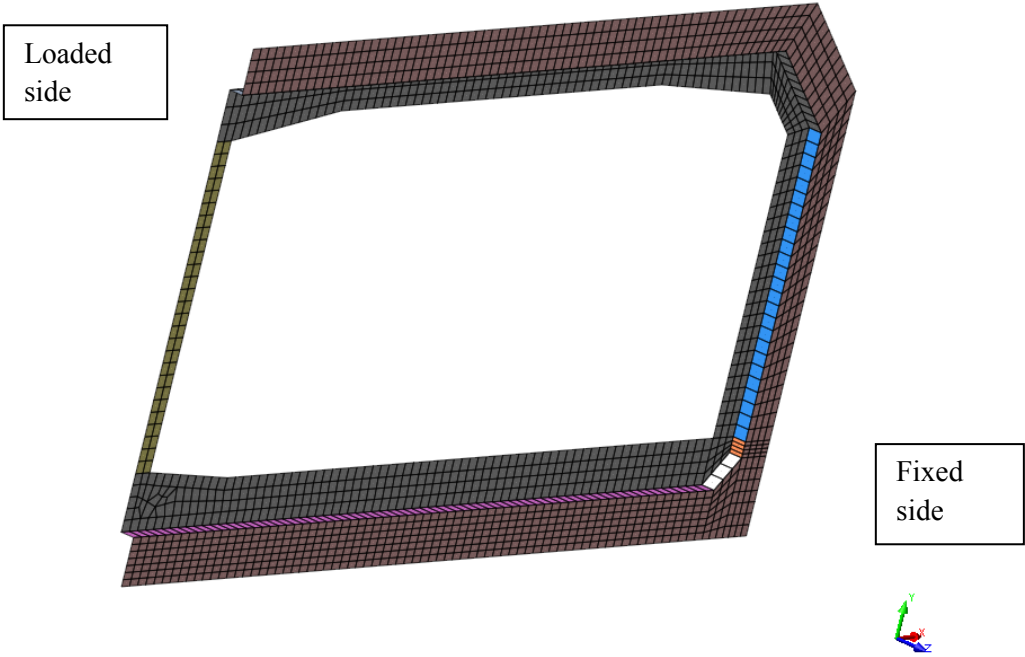
Figure 5.11- Full interface model

5.8 Application of loads

The concept of the application of loads remains the same as discussed in the earlier chapters. There are two parts of the tunnel segments which come together at the tooth. One segment is

fixed at the end. On the other segment end, the load is applied. The part which is loaded and the fixed part are depicted in **Figure 5.12**.

- Pressure due to water

The pressure due to water results in compressive force across the cross-section of the tunnel. As explained in chapter 1, the water pressure taken is 60% of the actual pressure present at the time of sinking of tunnels. This reduction comes from the creep due to rubber and concrete. The 60% pressure due to water varies from 0.068N/mm^2 at the top to 0.121 N/mm^2 at the bottom, **Figure 5.13**.

- Shear force

It is expected that the shear force is the cause of the leakage/tooth fracture in the actual tunnel. The shear-force estimated in the structure has a value of 2481 kN which is expected to be on the connection for the full tunnel cross-section. This value was found from the setting line of the immersed tunnel **[3],** also discussed in chapter 1, (**Figure 1.19**).

To apply the shear-force, a stiff plate was designed at the end cross-section of tunnel, **Figure 5.14**. It was done, so that the shear force applied can be equally distributed to all parts of the tunnel and there is no local accumulation of forces. The stiff plate was hence modeled across the entire cross-section of the tunnel. It closes the end of the tunnel in the model as seen in the **Figure 5.14**. This stiff plate does not exist in the structure but was used for the analysis only. The shear-force is applied to the stiff plate at the center of gravity of the entire tunnel cross-section. Hence it was applied at the middle wall of the half-cross section at a distance of 4 meters from the bottom (COG in y-direction = 4 m).The thickness of the stiff plate was chosen to be 100 mm. The stiffness (Young's Modulus) of the plate was kept at $2*10^{11}$ N/mm^2. The high value of the stiffness of the plate was arrived at by carrying out trial simulations ensuring that no local deformation of the plate occurred.

- Moment

As described in chapter 4, with the help of available rotation, the moment required for the tunnel segments to rotate was calculated and found to be 46000 kNm for the entire cross-section of the tunnel. This force was applied as a moment couple with a lever arm distance of 8000 mm.

$$M = f * z$$
$$M = moment$$
$$F = force$$
$$z = lever\ arm$$
$$F = \frac{46000 * 10^6}{8000} = 5.75 * 10^6 N$$

So the force of 5750 kN or approx 6000 kN is applied at the top and bottom as shown in **Figure 5.15**. This value of force was found for the full cross-section.

*__Note:__ In many diagrams, the side view is used to depict the fixed side and loaded side. The side views are sometimes switched for convenience (meaning the fixed side may come to the left or right side). However, the side view change does not represent any change in loaded side and the supported side. The loading scheme remains the same as shown in **Figure 5.12**.*

a = 6.7 meters
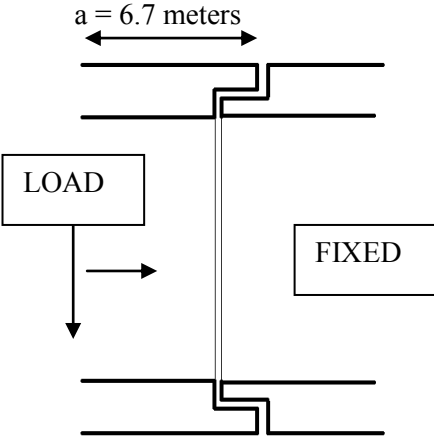
Figure 5.12- Loaded and fixed part of tunnel segment
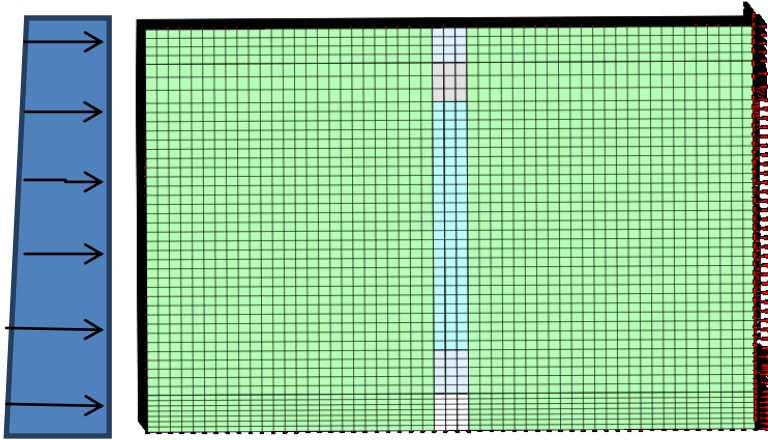
Figure 5.13- Water pressure, tunnel is fixed on right, load applied on left

Stiff plate

a = 6.7 meters

F
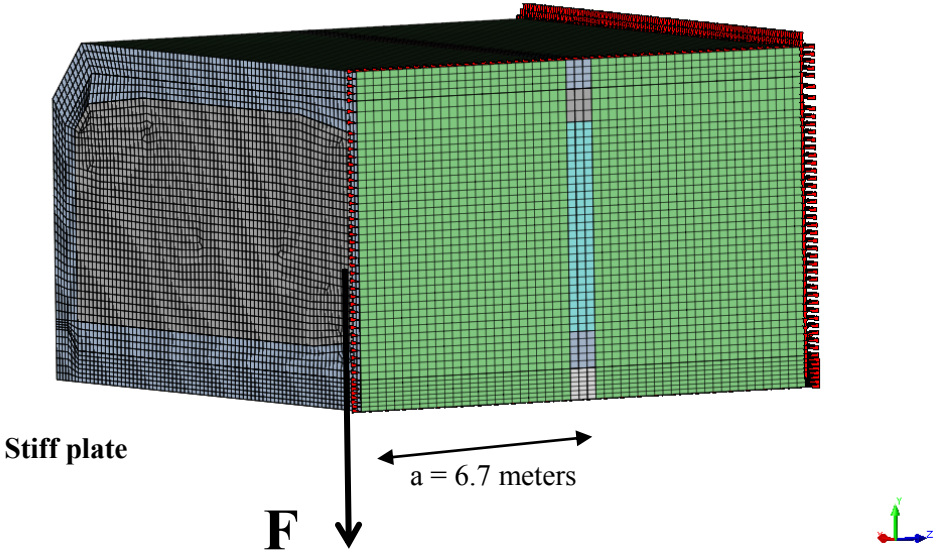
Figure 5.14- Shear force, load applied on the left side, the right side is fixed
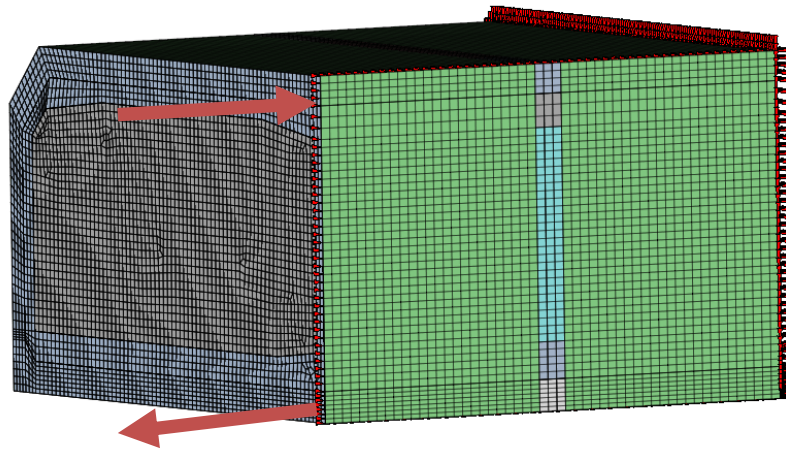
Figure 5.15- Moment couple force, load applied on the left side, the right side is fixed

5.9 Summary of element type, convergence criterion and loads

The properties of the concrete and steel used were the same as described in **Table 2.1**. **Table 5.2**, summarizes the type of elements used in the model. **Table 5.3** describes the convergence criterion used. **Table 5.4** summarizes the loads used and why a certain value was chosen. Whenever a capacity analysis is being carried out, the load applied is generally higher than the expected load occurring on site. This is done because the element/structure capacity is expected to be more than the calculated values. For all the analysis for shear force and bending moment, a higher value was required to be chosen. Hence for convenience, a value double the occurring values (expected shear is 2481 kN, **Figure 1.19** and expected moment 46000 kNm, **Figure 4.2**, both for full cross-section) was used. This means that if the analysis reaches 0.5 in load step, the expected values are reached.

Element	Type	Description
3-D solid elements	HX24L	8-noded brick elements
Interface elements	Q24IF	8-noded brick elements
Reinforcement	BAR	Discrete
Stiff-element	HX24L	8-noded brick elements

Table 5.2- Element type used

Convergence criterion	Method used
Control	Force control
Displacement norm	No
Force norm	Yes(0.01)
Energy norm	Yes(0.001)
Procedure	Newton –Raphson (modified)
Number of iterations	5

Table 5.3- Convergence criterion used

Load	Value for full cross-section	Value applied to half cross-section	Reason
Water pressure (Normal force)	$10.6 * 10^6$ N	$5.3 * 10^6$ N	As only half the cross-section is modelled, the corresponding water pressure is used
Water pressure (Moment, anticlockwise)	Approx.32000 kNm	Approx.16000 kNm	As only half the cross-section is modelled, the corresponding water pressure is used
Shear force	2481 kN	2481 kN	Cross-section has more capacity than the value found on site/calculations
Bending moment (clockwise)	46000 kNm	46000 kNm	Cross-section has more capacity than the value found on site/calculations

Table 5.4- Loads and explanation of their values

5.10 Results of the linear analysis -A

- *Only Compression*

When the load due to water pressure was applied all at once, the analysis produced the expected outcome. The result of the load due to water pressure is shown in **Figure 5.16**. The value of the compressive stresses increased from top to bottom linearly, indicating the linear increase in force. These results are important as they serve as a check for the accuracy of the 3-D FEM model.

Load steps used- 1(1)

5.11 Results of the analysis- B

- *Compression + Shear Force*

The shear force analysis was performed for the structure. Here, first the pressure due to water was applied, and next the shear force as depicted in **Figure 5.14** was applied. The water pressure was applied in one load step whereas shear was applied in 10 load steps. This means that each step was 10% of the total shear of 2481 kN. Since it is half the cross-section, aim is to reach only 50% of the total applied force. Gapping was produced at the top of the structure after a few load steps. This gapping was expected, as the shear force was applied at the end, **Figure 5.17**. Load steps are described in **Table 5.5**.

A point which should be remarked here is the presence of an implicit moment in the structure due to the presence of the shear force at the end. This shear force comes to the tooth as a combination of force and moment. Because of this reason, it is expected that the divergence will occur earlier than expected. To counteract this problem, a compensating moment was required such that the tooth was subjected to only a shear force, see **Figure 5.18**.

[UNIT] N , mm
[DATA] Structural Nonlinear , Principal Stress S3 Nodes(V) , Load Step 1(1)
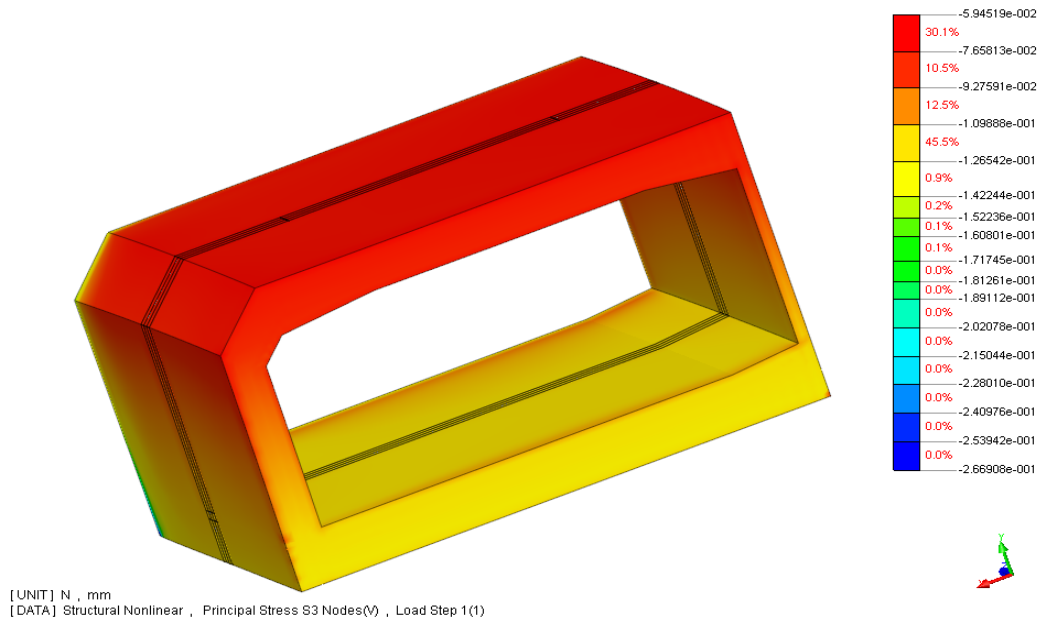
Figure 5.16- Compressive stresses in the tunnel cross-section due to water pressure- (In view - the section where forces were applied)

[UNIT] N , mm
[DATA] Structural Nonlinear , Principal Stress S3 Nodes(V) , Load Step 8(0.7)
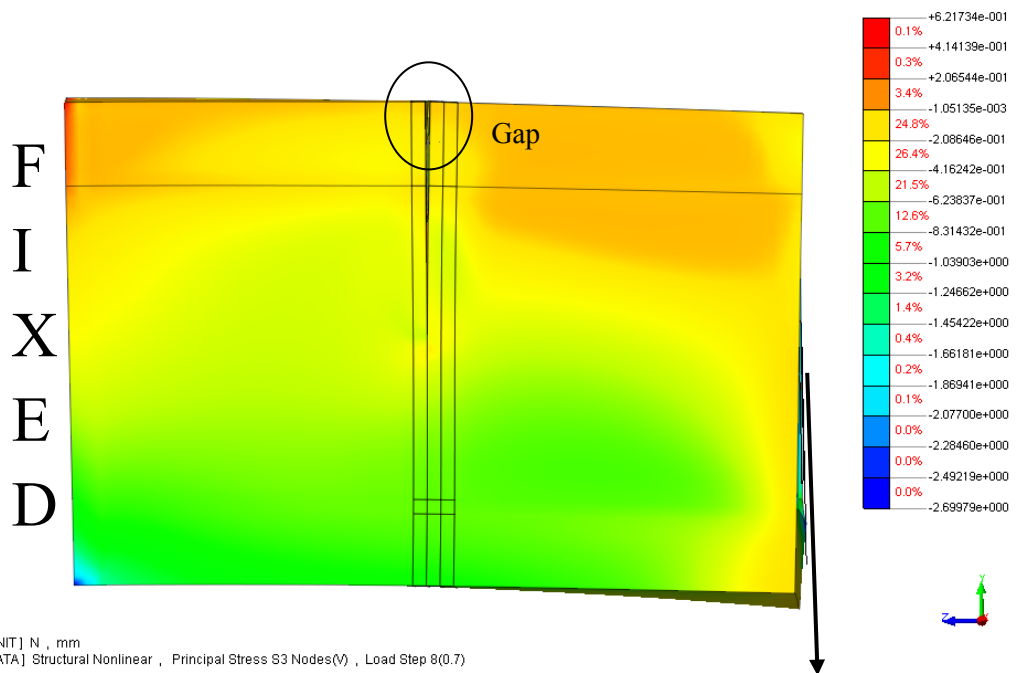
Figure 5.17- Side view -Compressive stresses, with gapping at the top of tooth (no Mohr-Coulomb)

Load steps	Force type
1	Compression due to water
0.1(10)	Shear-force

Table 5.5- Load steps for Analysis B

72

5.12 Results of the analysis- C

- *Compression + Shear Force + Compensating Bending Moment*
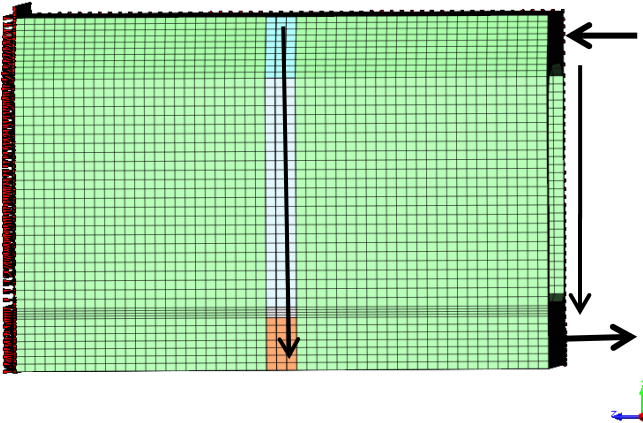
Figure 5.18- Side view- Shear force-with compensating moment (at tooth-only shear force)

Since the above discussed model cannot be used to arrive at conclusions about the behavior of a 3-D tunnel, a compensating moment was provided. In the **Figure 5.19** , the shear force was applied at the center of gravity of the entire tunnel, and the moment forces were also applied in the same manner. In this load combination, the effective moment is almost negligible and only a shear force is seen at the tooth. It should be noted here that the compensating bending moment is provided for the shear force only. There is a bending moment due to the water pressure as well, but it has not been compensated for in this case as it is expected to always stay in the tunnel. Load steps applied are given in **Table 5.6**.

Load steps	Force type
1	Compression due to water
0.1(10)	Shear-force+ Compensating BM

Table 5.6- Load steps for Analysis C
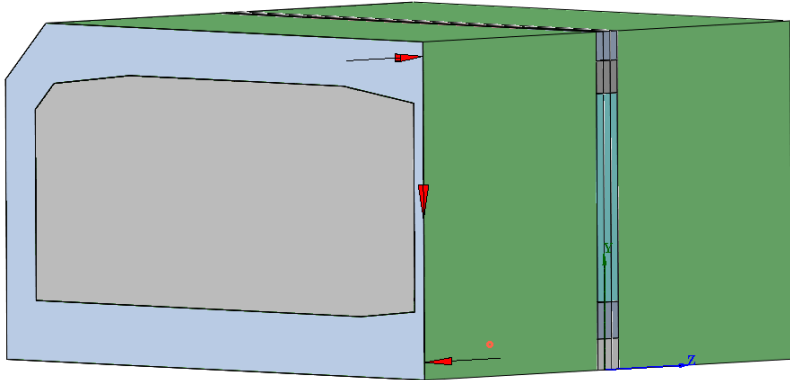
Figure 5.19- Shear force-with compensating moment applied at cog of the full tunnel

When this load was applied in steps, the shear stresses were noted in the structure, **Figure 5.20**. A plot of the shear stress values along the width of the tunnel was plotted; the elements were selected in the section next to the tooth, **Figure 5.21**. The section selected was on the side of the support. So the loads pass through the tooth of the tunnel and interface and the measurements are taken in the section right next to the tooth. It was decided not to pursue the tooth because of the complications involved in the measurement of the interface stresses. The shear stress of the element nodes selected was plotted along the width of the tunnel (**Figure 5.22**). Once the stresses in the nodes were obtained, the average area per node was calculated. It was done by calculating the total cross-sectional area of the tunnel and dividing it by the number of nodes. The total shear force at the cross-section was calculated by multiplying the stress at each node by the average area calculated. It was found to be close to the value of the shear force which was applied at that load step. Further, to calculate the contribution of each part of the tunnel cross-section, the shear force in parts from 0-3000 mm (from the centre wall) was calculated and divided by the total force. It was found that 34% of the force is passing through the middle wall. Similarly, the % for the area between 3000 mm and 12000 mm was calculated and found to be 9%. The highest amount of force was found to be acting at the corner wall with a 57% contribution, **Figure 5.23**.

Shear force calculation at load step-0.3
Total Load = 0.3*2481 = 744.3 kN

$$Total\ area = 112766 * 10^3 mm^2$$
$$Area\ of\ Half tunnel = 56383 * 10^3\ mm^2$$
$$Number\ of\ nodes = 1840$$
$$Average\ area\ per\ node = \frac{56383 * 10^3}{1840} = 30642\ mm^2 \approx 30000 mm^2$$
$$F, force\ occuring\ totally = \sum Stress\ at\ each\ node * average\ area$$
$$F = 696\ kN$$

This value is close to the applied value of 744 kN. The difference is occurring because of the approximation made in the calculation of the average area. The size of the elements is not exactly the same throughout the cross-section and hence there is a difference in the shear-force.

A very important point which should be remarked here is that the shear force for the entire tunnel cross-section is found to be 2481 kN. So for half the tunnel segment it is 0.5 times 2481kN, 1240 kN. During the analysis a high force was applied to see how farther the calculations can proceed. In simple words, it was aimed at applying double the expected shear force in the tunnel cross-section modeled (which is half the cross-section). So, the aim is to reach a load step value of 0.5 (0.5*2481 kN). Over here, the maximum which could be numerically reached is 0.3.

Load	Applied (for full-tunnel) Aim-0.5 (half-cross-section)	Final load step 0.3
Shear Force	2481 *10³ N	744*10³N
Compensating Bending Moment for Shear Force	2*10⁶ N	0.6*10⁶ N
Distance	8000 mm	8000 mm
Bending Moment	16*10⁹ Nmm	4.8*10⁹ Nmm

Table 5.7- Loads applied for analysis C

[UNIT] N , mm
[DATA] Structural Nonlinear , SYZ Nodes , Load Step 4(0.3)
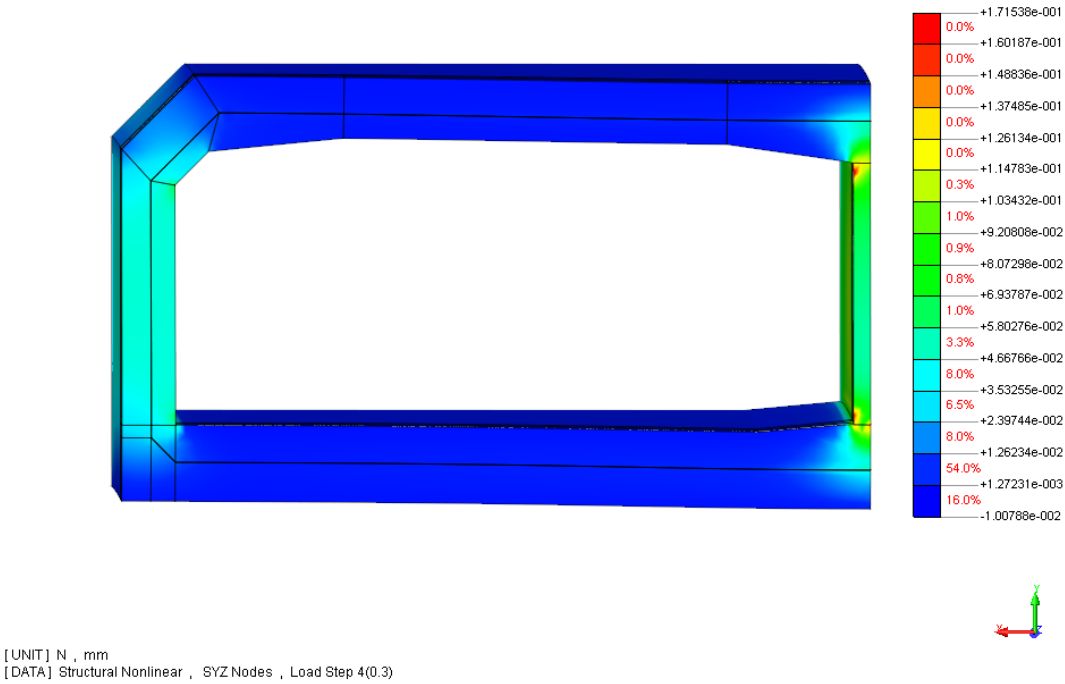
Figure 5.20- Shear stresses- with compensating bending moment at tooth
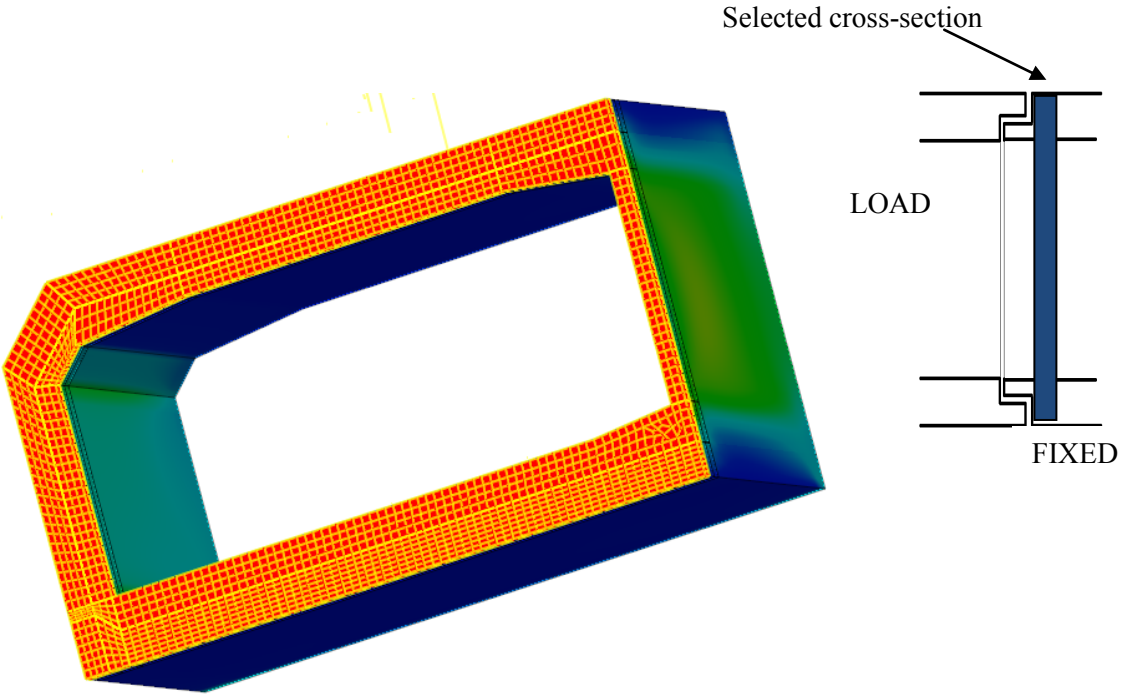
Figure 5.21- Elements selected for obtaining the shear stresses (next to the tooth-closer to support)
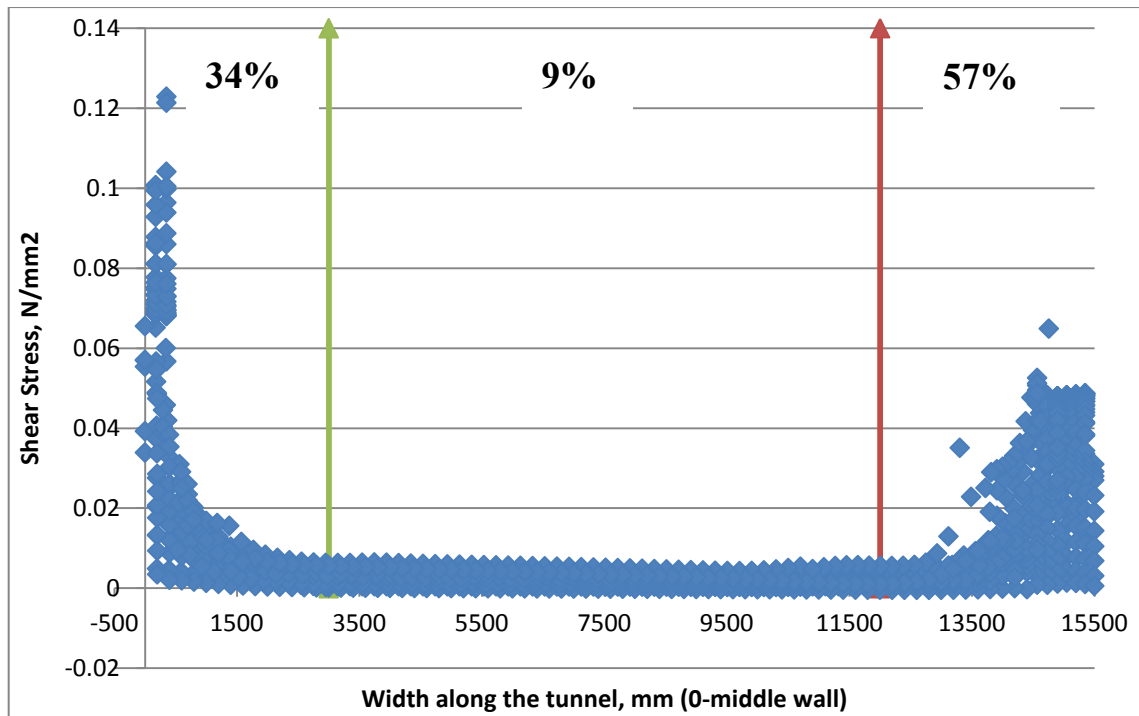
Figure 5.22- Shear stresses at a section next to the tooth

	Schols	46%	0%	54%
	Parwani	34%	9%	57%
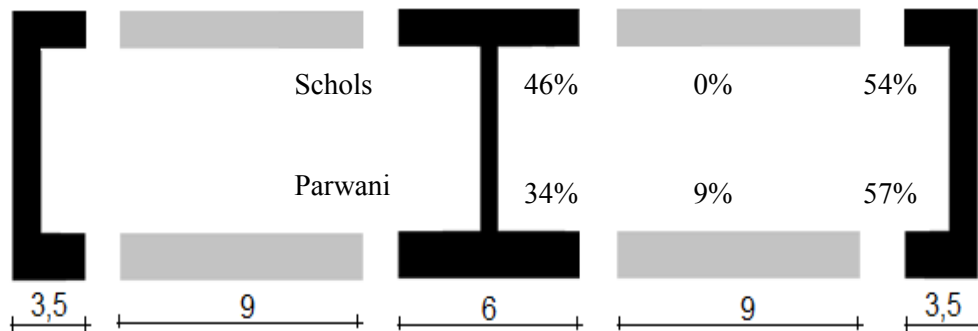
Figure 5.23- Percentage of shear force that passes through half of the cross-section (Comparison of results with the effective width concept of Schols [3]), Dimensions [m]

According to this analysis, it can be concluded that the outer wall is the most heavily loaded by the shear force, **Figure 5.22**. However, if the shear stresses are observed in **Figure 5.22**, then the highest values occur at the middle wall.

An interesting point is that this distribution is for half the cross-section. If we translate the same percentages to the entire cross-section, it appears that the middle wall takes up the highest amount of load (in absolute terms) according to both Schols' analysis and the current analysis. In the current analysis, there is not a huge difference in the shear force (absolute values) between the outer and the inner wall. But according to the Schols [3] analysis, there is a large difference. The thickness of the middle wall is 700 mm and the thickness of the outer wall is 1100 mm. Clearly, a high amount of force passing through the middle (thin) wall is more critical than a relatively less amount of force passing through the outer wall (thick). Since this analysis is linear;

it is possible that there is redistribution of forces in the walls after the inner wall might start to crack in a non-linear analysis.

Schols

27%   46%   27%

3,5   9   6   9   3,5

Parwani

28.5%   4.5%   34%   4.5%   28.5%
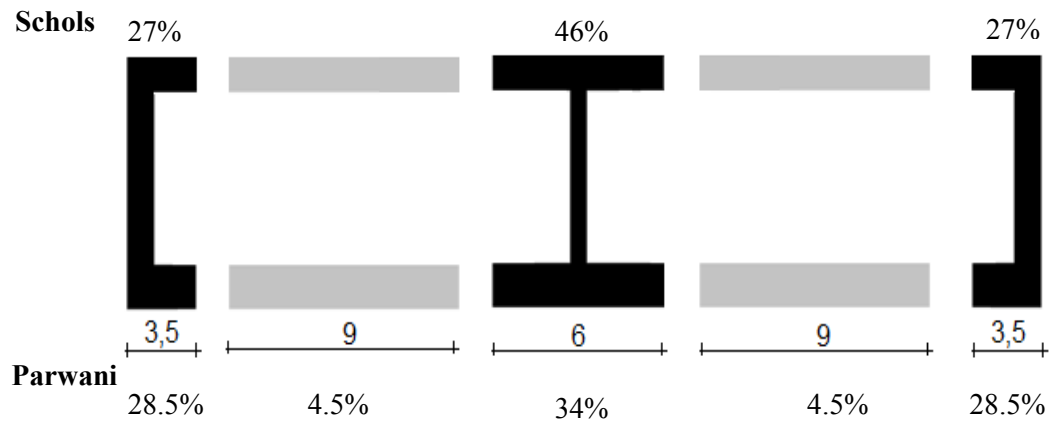
Figure 5.24- Percentage of shear force that passes through the entire cross-section **(**Comparison with the entire cross-section of the percentage contribution with Schols [3]), Dimensions [m]

This analysis, although non-linear, does not show high stresses in the concrete and hence we need to go further in terms of load steps to calculate the failure mode.

The premature halt of the analysis is contributed to the fact that the walls are not capable of handling more forces in shear through friction. The friction coefficient used in the analysis was 0.5. If the friction coefficient (η) was increased to 0.9, the analysis goes further to load step 0.4. Hence the coefficient of friction is an important factor affecting the analysis. Next reason for the premature stop of analysis is the load application. Although the moment due to the shear force was compensated by a bending moment, there is still bending due to the water pressure itself. This could be one of the causes why the horizontal part of the interface is not taking up the load in the further load steps. In order to take this analysis a few steps ahead, an extra bending moment is required. Finally, it is also important to apply a bending moment which causes the rotation of $2*10^{-3}$ rad which was aimed at the beginning of the 3-D analysis.

5.13 Scheme of the segment connection

It has been discussed in the previous chapters that the connection of the segments of the tunnel resembles a socket-spigot joint, where one part fits in the other as shown in **Figure 5.25**. In the 3-D analysis, a critical aspect is the part of the segment which is loaded and the part of the segment which is fixed. Another aspect is the direction of the shear-force applied at the end of the tunnel. A final aspect is the moment causing the rotation of the tunnel.

The data which is available with Rijkswaterstaat was collected for certain points shown in the **Figure 5.26**. Hence, nothing can be said about the relative displacements/rotations of the two segments at the joint location. This also implies that an estimate has to be made about the possible loading schemes that might occur on site in the tunnel cross-section.
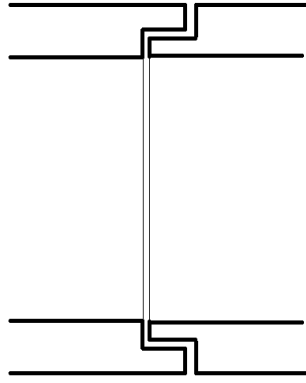
Figure 5.25- Tunnel tooth at the joint
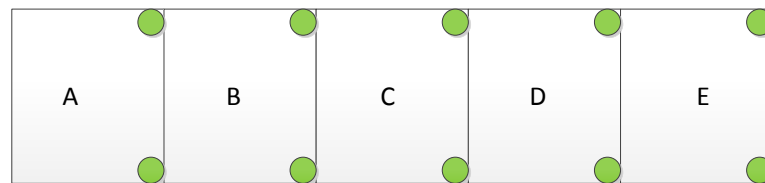
Figure 5.26- Monitoring points

It is already known that the pressure due to water force creates axial compression in the tunnel. Also, the water pressure increases from top to bottom, resulting in a bending moment. This is depicted in **Figure 5.27**. Here Nw represents the normal force due to water and (-)Mw represents the moment caused by the water force (anti-clockwise). Since this is the first load which is applied to the structure, it is denoted as step 1. Next, we have to apply a shear force with bending moment. There are two main loading schemes denoted by *a* and *b*. First is when the shear force is applied upwards (step 2-a), **Figure 5.28**. By applying an upwards shear force, we are loading the bottom tooth of the tunnel. Second is when the shear force is applied downwards. We now load the top tooth (Step 2-b), **Figure 5.29**. Other factors which are considered include the bending moment which should be applied to compensate for the effect of the shear force at the end. This value is calculated by multiplying the shear force by the lever arm from the point of rotation. The bending moment applied to compensate for the effect of the uniformly increasing water pressure (shown in **Figure 5.27** as -Mw) was applied as Mw. Finally Mrot, which was calculated in Chapter 4, causes the rotation of the tunnel.

Important: All these forces, calculated for full cross-section were applied to half the tunnel. This implies that all the forces applied were double of what is needed for half the cross-section (capacity). A higher value was applied as it is expected that the tunnel has more capacity than the calculated value of forces.

In the **Figure 5.28** and **Figure 5.29**,
V = Shear force (2481 kN)
V.a = Compensating bending moment due to shear force (2481 kN * 6.7 m)
Mw = Compensating moment due to water
Mrot = Moment causing rotation of $2*10^{-3}$ rad
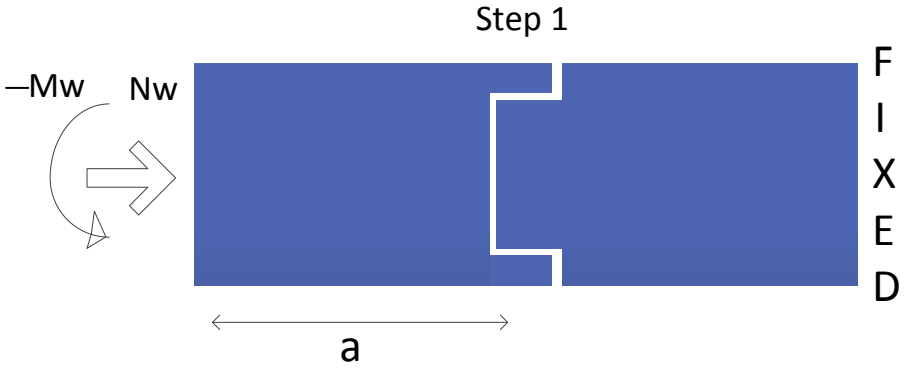
Step 1

Figure 5.27- Step 1- Application of water pressure-resultant (moment + normal force)
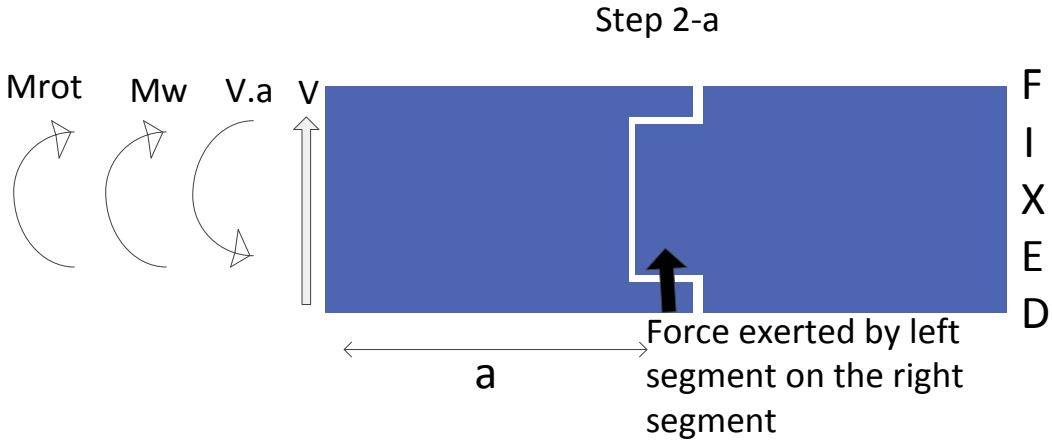
Step 2-a

Figure 5.28- Step 2-a, A shear force loading the bottom tooth
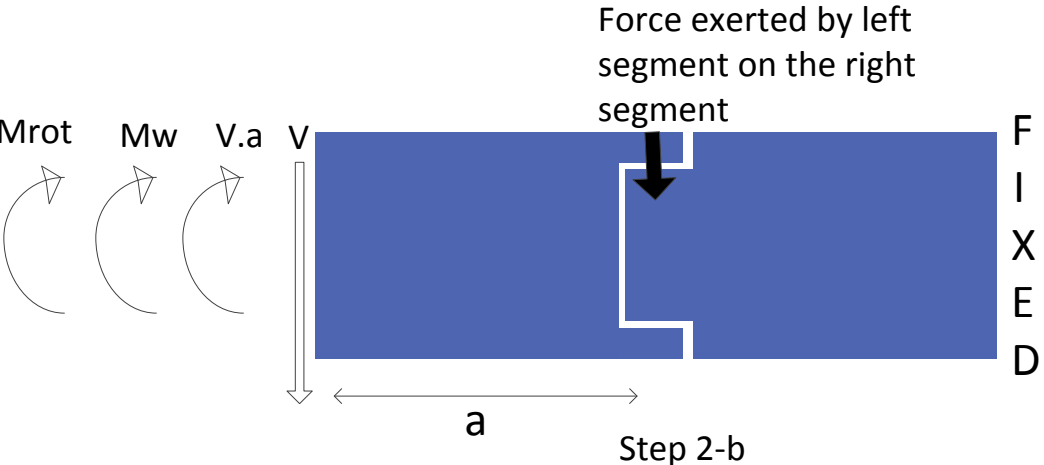
Figure 5.29- Step 2-, A shear force loading the top tooth

The tunnel cross-section in the Finite Element 3-D model has been designed such that the part which protrudes outside is the loaded side. The other one is the fixed side. There are mainly two possibilities that should be taken into account. One, when the shear force applied faces

downwards. Two, when the shear force faces upwards. A series of analysis were thereafter performed to see the tunnel tooth behavior which will be discussed in the coming section. A comparison will be drawn between the analyses. It will be mentioned in the coming sections. Certain values of the properties were fixed to avoid ambiguities. The value of the friction coefficient was fixed at 0.9, the stiffness in normal direction is $17000 N/mm^3$, in shear is 15300 N/mm^3. So, the only variables in the analysis are the values of forces and their directions. In the **Appendix D1**, part of the .dat file and the .dcf file used for the analysis is provided. The properties of concrete and steel used were the same as used in the 2-D analysis (**Table 2.1**). In all the coming analysis, the first step is the application of the water pressure which causes compression and a bending moment. In the next step, the load which is applied is discussed in types-I, II, III, IV and V in the next five sections.

Property	Value used
Friction coefficient	0.9
Stiffness in normal direction	$17000 N/mm^3$
Stiffness in shear direction	$153000 N/mm^3$

Table 5.8- Values fixed for all analysis (Type I to Type V)

5.14 Type I- Top tooth loading - Pure shear

5.14.1 Aim

To obtain the effect of pure shear loading on the top tooth at load step 0.5 (which is 0.5 * 2481 kN). Further load steps would indicate the extra capacity of the tooth.

5.14.2 Loads applied (Figure 5.30)

Step 1: Apply axial force from water. This also includes a bending moment.

Normal force due to water = $5.3 * 10^3$ kN (**Table 5.4**)
Bending moment due to water (approx.) = 16000 kNm (anti-clockwise)
Note: these values are for half the tunnel

Step 2: Apply a high shear force. Apply a corresponding bending moment which compensates the moment generated due to that shear force. Also, apply double the bending moment that compensates the moment generated due to water. See also **Table 5.11**.

Shear force applied = 2481kN. The required capacity for half the cross section is only 1240 kN. But we apply a higher value as we expect the tooth to have more capacity than the value occurring at site. We can arbitrarily pick a very high value; hence we choose to pick a value double its capacity, hence 2481 kN. So if the analysis reaches 0.5 load steps, the structure is safe. This shear force (2481 kN) at the end generates a bending moment of approx. ***16000kNm at the tooth (anti -clockwise). V.a = 2481 kN *6.7m=16000 kNm*** (**Table 5.11**).

Compensating Bending moment= 16000kNm (clockwise). By applying this, it has been assured that at the tooth, there is no bending moment generated due to shear at any load step.

Compensating bending moment due to water=2*16000=32000kNm (clockwise). The required compensating moment is only 16000 kNm. But double that value has been applied because by 0.5 shear load step, all the moment is compensated for and only pure shear at the top tooth exists.

Hence, total clockwise moment applied = 32000+16000 = 48000 kNm (for step 2 only)
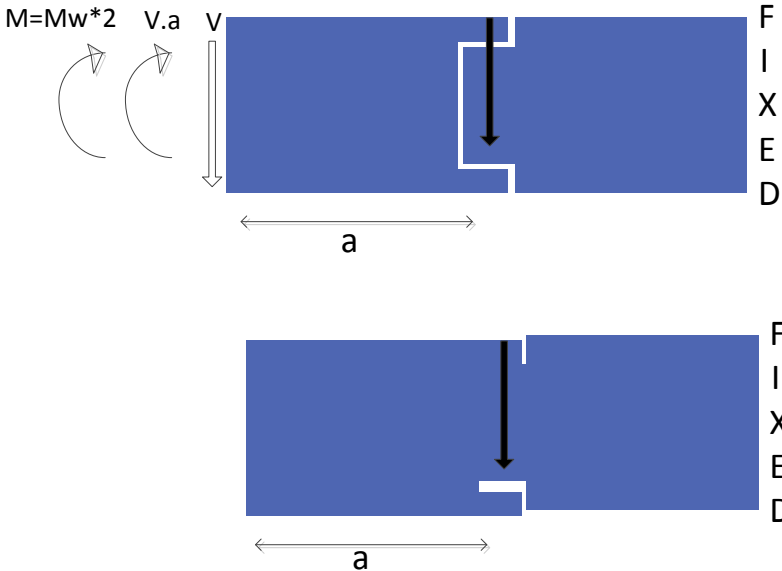
Figure 5.30- Top **:** Loading of the top tooth; Bottom: Expected behavior

5.14.3 Description

In the first analysis, the shear force was applied in the downward direction. Step 1 is the same as described in **Figure 5.27**. The second step is discussed in this section. The load steps are described in **Table 5.9**. The aim is to load the top tooth in pure shear at load step 0.5. This is possible only if all the bending moment is compensated for. The top tooth is loaded as shown in **Figure 5.30**. As it has already been explained in the previous section, V.a is the compensating moment which is provided to compensate for the effects of V at the tooth.

Load steps	Force type
1	Compression due to water (half cross section)
0.1(3) 0.02(35)	Shear-force+ Compensating BM due to shear+compensating BM due to water (full cross section)

Table 5.9- Load steps for Type I analysis

Mw is the compensating moment due to water. The applied value of Mw is twice as high (**Table 5.10**). This is because the existing Mw due to water, applied at the first load step is for half the cross-section. We aim to reach the value of 0.5 in the shear load steps to be safe. Hence, by load step 0.5, we fully compensate for the bending moment due to water $(0.5*(2*Mw) = Mw)$.

Therefore we have pure shear at 0.5 load step. Beyond that, the extra moment due to water pressure is increasing, which means that beyond 0.5, the situation is no longer that of pure shear. The moment is continuously increasing and may cause opening of the bottom tooth.

Load type	Load applied at load step (1.0)	Load value at end for last converged step (**0.58**)
Shear	2481 kN	1439 kN
Bending Moment (at end)	6000 kN*8 m= 48000 kNm	$27.84*10^3$ kNm

Table 5.10- Loads applied for type I analysis

5.14.4 Result

The displacement behavior of the tunnel followed the expected behavior which was drawn. The stresses however at the last load step are not very high. A plot of tensile stresses was obtained and the maximum tensile stress in concrete reached was 0.6 N/mm^2. A side view of the concrete tunnel is shown (**Figure 5.31** and **Figure 5.32**), where the right side is fixed and the load is applied on the left.

When the shear stress in the cross-section at the tooth was noticed, it was confirmed that the forces are concentrated near the walls. It also showed that gapping was produced more near the walls and hardly in the other parts of the tunnel. A view of the tunnel tooth, closer to the load is shown in the **Figure 5.33**. The supports are represented by a red color and they were included to clarify the loading position in the tunnel. The highest shear forces were found near the vertical interface between the two parts of the tunnel segments, showing resistance to the vertical movement of one with respect to other (marked with a circle). Magnified views of both the outer and inner wall are shown in the **Figure 5.34** and **Figure 5.35**. The peak stresses are concentrated at the wall to slab connection in the inner wall. For the outer wall, the peaks are not just at wall to slab connection, but also near the connection between the outer walls, **Figure 5.35**.

[UNIT] N , mm
[DATA] Structural Nonlinear , Principal Stress S1 Nodes(V) , Load Step 18(0.58)
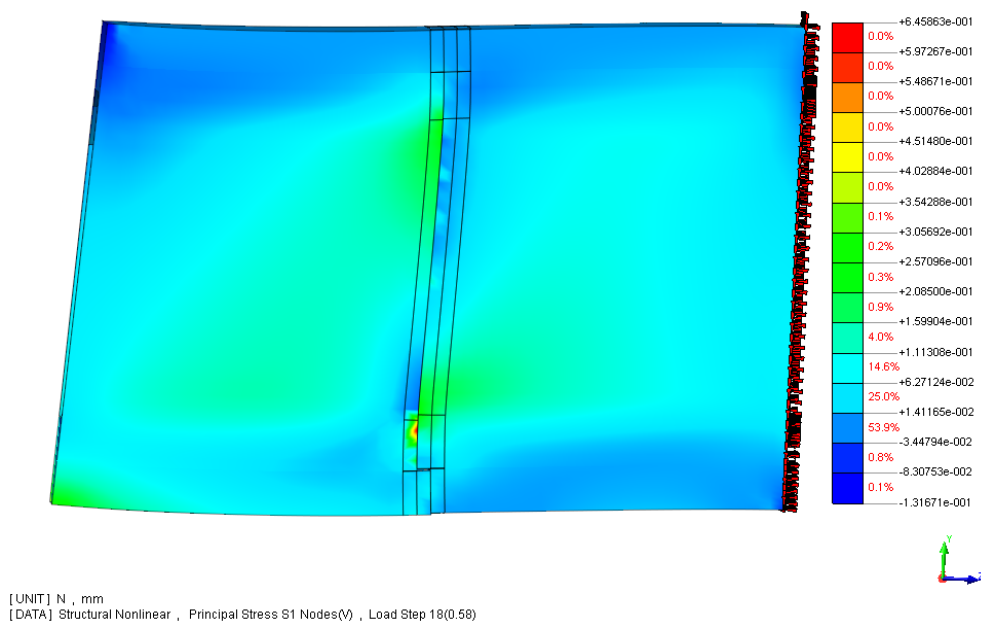
Figure 5.31- Side view of tunnel- Principle tensile stresses S1, fixed on the right side

[UNIT] N , mm
[DATA] Structural Nonlinear , Principal Stress S1 Nodes(V) , Load Step 18(0.58)
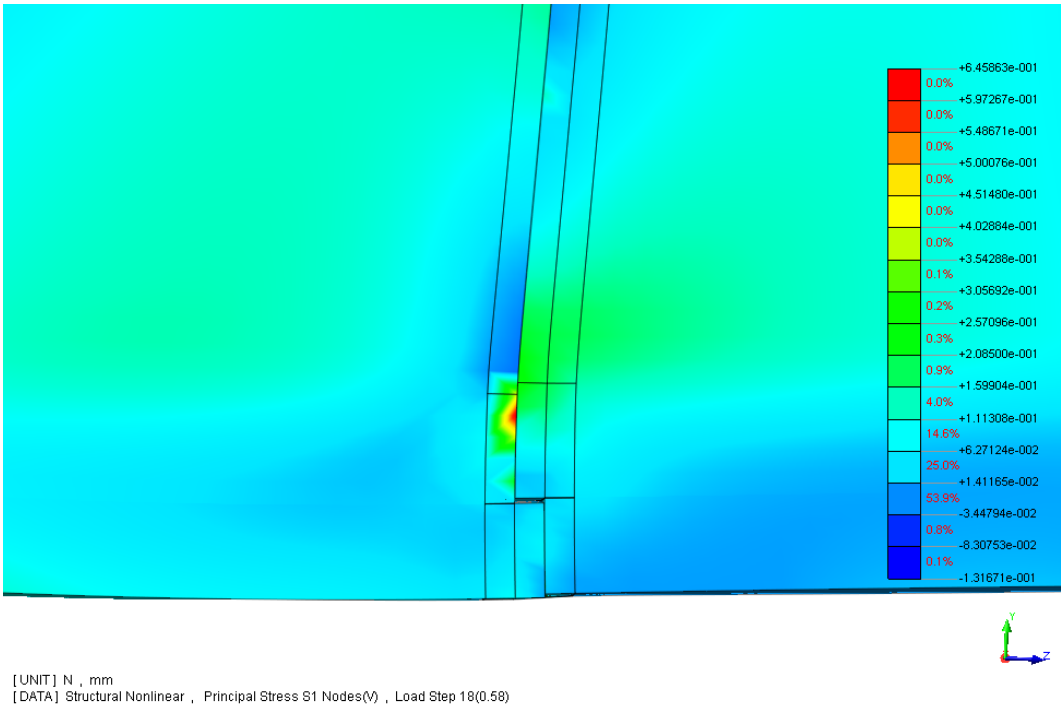
Figure 5.32- Magnified side view of tunnel-displacement in bottom tooth- Principle tensile stresses S1

[UNIT] N , mm
[DATA] Structural Nonlinear , SYZ Nodes , Load Step 18(0.58)
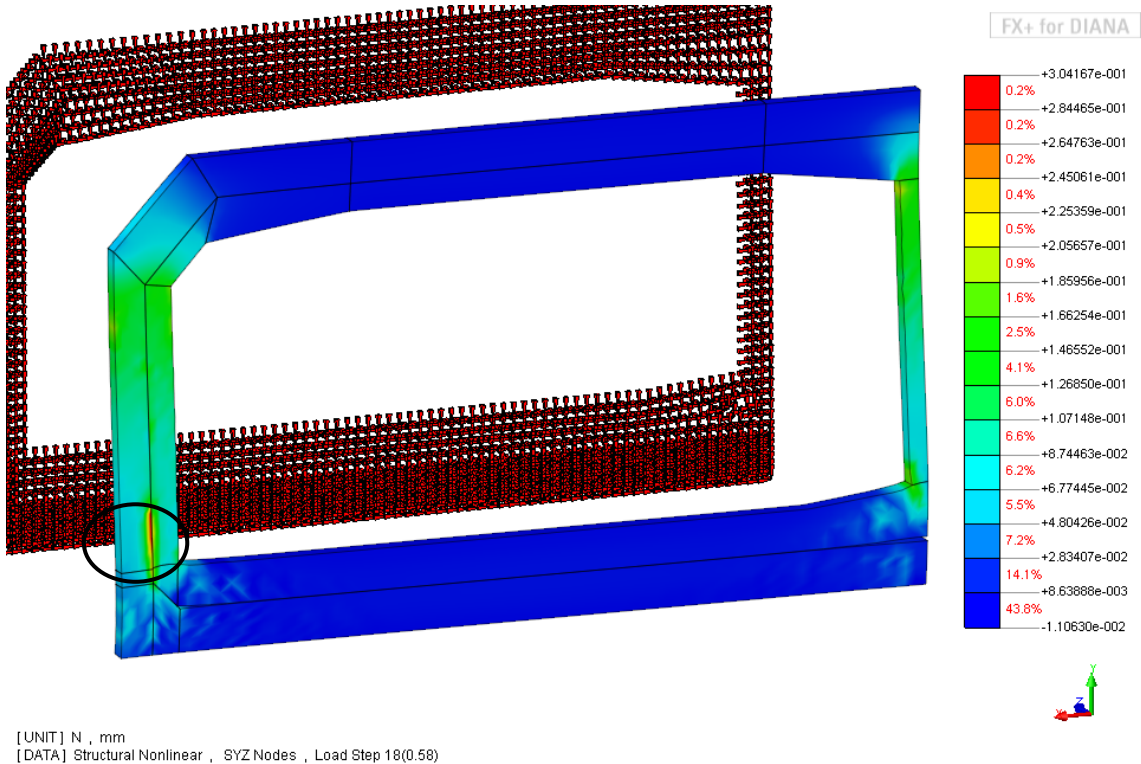
Figure 5.33- Shear forces at the tooth (view from loaded side) and behind, in red is the support. The circled part shows the location of highest shear stresses
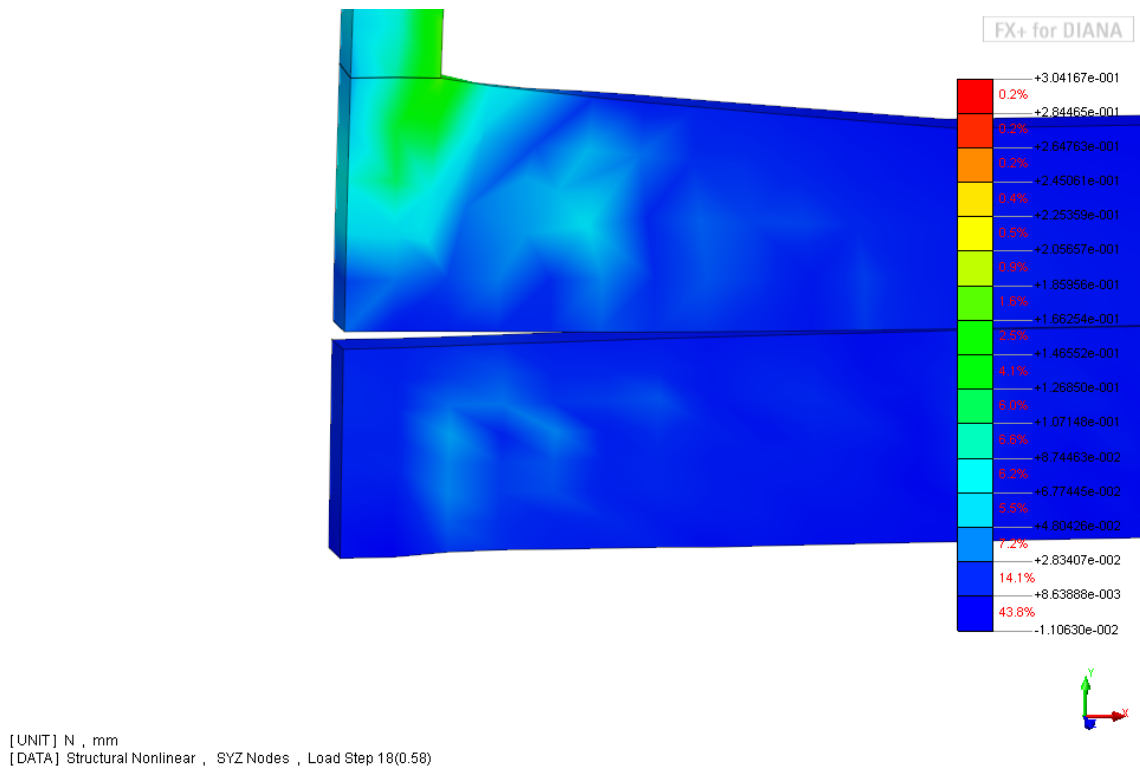
Figure 5.34- Magnified view of shear stresses near the middle wall, also noticed is the gapping present which disappears away from the wall
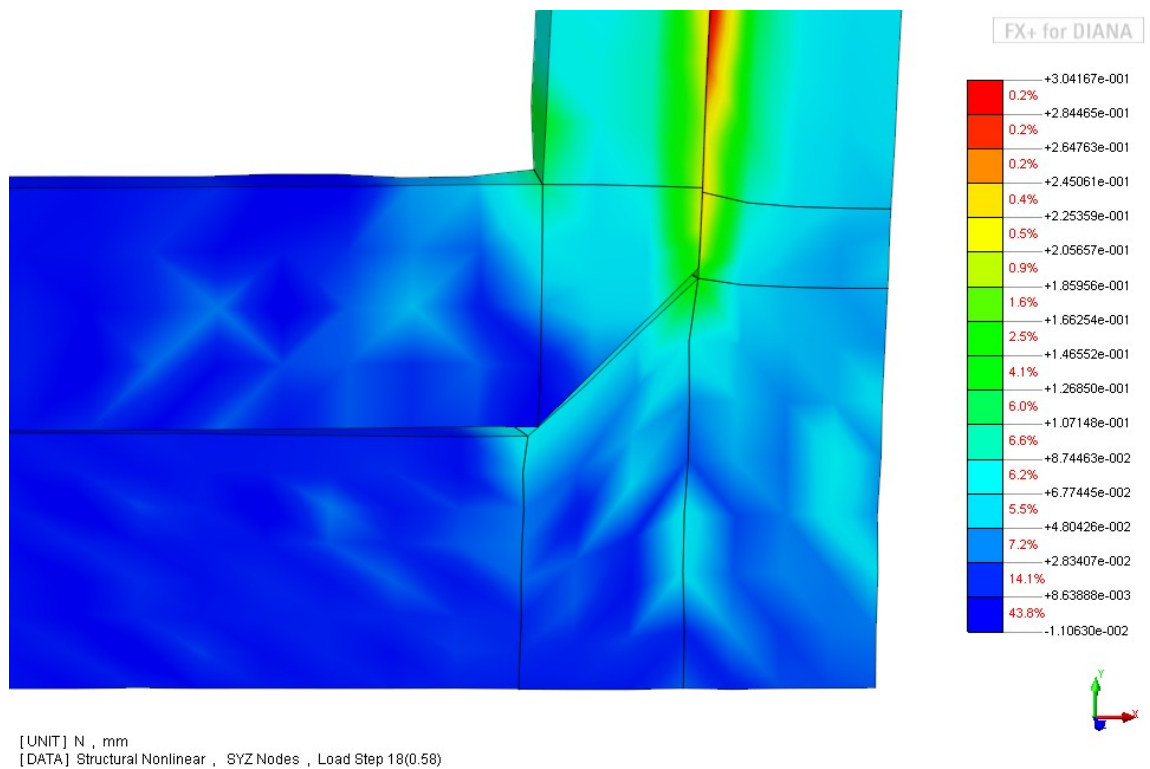
Figure 5.35- Magnified view of shear stresses near the outer wall, also noticed is the gapping present which disappears away from the wall

5.14.5 Rotation

The rotation of the segment was important to see if the value lies close to the observed rotation of $2*10^{-3}$ rad. The maximum displacement in the y direction was recorded.

$$\theta = \frac{displacement\ in\ y\ direction}{length\ of\ 1\ segment} = \frac{0.076\ mm}{6750\ mm} = 1.1 * 10^{-5}\ rad$$

This value of rotation is 200 times lesser than the measured value. However, this analysis was carried out to study pure shear effects and not rotation effects.

5.14.6 Cause of divergence

The stresses found are lower than the maximum concrete tensile capacity. Therefore, the reinforcement is not activated. The expected reason for the structural failure is the loss of equilibrium. When the interface stresses were studied, it was noted that the interface had developed tensile stresses in the horizontal contact surface. This means that the force is being transferred through friction in the vertical direction. Hence, it is expected that once the shear force exceeds the force that can be transferred via friction, the analysis diverges. The approximate bending moment that occurs in the tooth was also calculated for these load steps. The bending moment at the tooth effects from the applied bending moment, the bending moment due to water (in opposite direction) and the bending moment resulting from the force itself as shown in **Table 5.11**.

It should be noted that in the real structure, there is an elastic foundation, which will redistribute the forces. In this case, the tunnels are hanging in air, and loss of contact leads to the halt of simulation.

Load step	Bending moment applied at end (-)	Bending moment due to water (+)	Bending moment due to force-2481kN (+)	Total moment at the tooth (-)
0.5	$48*0.5*10^3$ kNm = $24*10^3$ kNm	$16*10^3$ kNm	(V.a)*0.5 = 2481*6.7*0.5 =$8*10^3$ kNm	$0*10^3$ kNm
0.58	$27.84*10^3$ kNm	$16*10^3$ kNm	$9.6*10^3$ kNm	$2.2*10^3$ kNm

Table 5.11- Bending moment applied and bending moment present at the tooth for the type I analysis

5.14.7 Interpretation

This analysis shows that the structure can successfully carry more shear force than the value occurring on site (analysis crossed load step 0.5). It is a linear analysis, which means that without cracking, the structure can carry this shear force.

5.15 Type II- Top tooth loading- Shear + bending moment
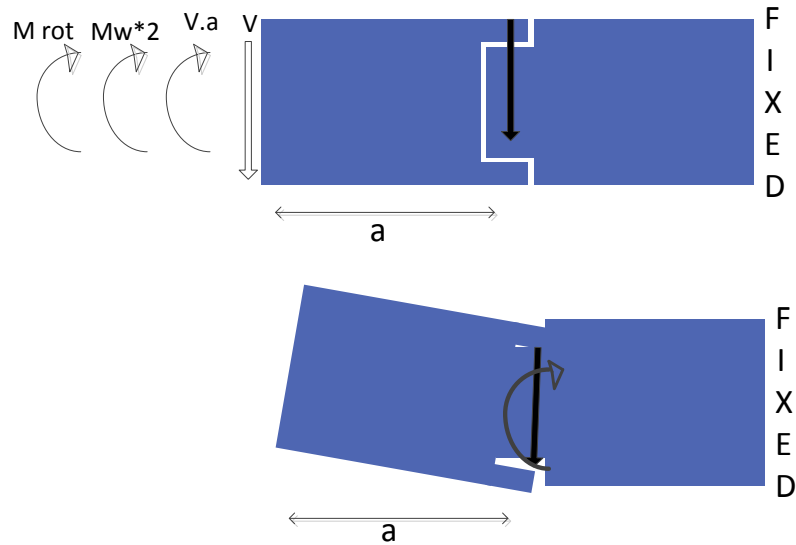
Figure 5.36- Top **:** Loading (shear +bending moment); Bottom: Expected behavior

5.15.1   Aim

To obtain the effect of shear + moment loading the top tooth at load step 0.5. Further load steps would indicate the extra capacity of the tooth. The moment comes from the rotation of $2*10^{-3}$ rad.

5.15.2   Load applied (Figure 5.36)

Step 1: Apply axial force from water. This also includes a bending moment.

Normal force due to water=$5.3 * 10^3$ kN (half tunnel)
Bending moment due to water (approx.) = 16000 kNm (anti-clockwise)

Step 2: Apply a high shear force and apply a high bending moment (clockwise). Apply a corresponding bending moment which compensates the moment generated due to that shear force. Also, apply double the bending moment that compensates the moment generated due to water.

Shear force applied =2481kN. The required capacity for half the cross section is only 1240 kN. But we apply a higher value as we expect the tooth to have more capacity than the value occurring at site. We can arbitrarily pick a very high value; hence we choose to pick a value double its capacity, hence 2481 kN. So if the analysis reaches 0.5 load steps, the structure is safe. This shear force (2481 kN) at the end generates a bending moment of approx. ***16000 kNm at the tooth (anti -clockwise).*** *V.a = 2481 kN *6.7m=16000 kNm*

Compensating Bending moment = 16000kNm (clockwise). By applying this, it has been assured that at the tooth, there is no bending moment generated due to shear at any load step.

Compensating bending moment due to water =2*16000 = 32000kNm (clockwise). The required compensating moment is only 16000 kNm. But double that value has been applied because by 0.5 load step, all the moment is compensated and only pure shear at top tooth exists.

Bending moment = 46000 kNm (clockwise). A bending moment of 23000 kNm is required to produce a rotation of $2*10^{-3}$ rad for half the cross section. We apply however a bigger bending moment, as we expect that connection has more capacity. So if the analysis reaches 0.5 load steps, the structure is safe.

Total clockwise moment at 1.0 load step = 32000+16000+46000 = 94000 kNm (Actually applied was around 96000 kNm, **Table 5.13**)

5.15.3 Description

In this analysis as well, the top tooth is loaded as shown in **Figure 5.36**. The aim is to have rotation along with a shear force in the tunnel connection. In the similar way as described in 5.14.3, the aim is to reach 0.5 load steps. The load steps are described in **Table 5.12**. The forces applied are shown in the **Table 5.13**. The expected behavior of the connection is shown in **Figure 5.36**. The extra force which is added to this analysis is that of M_{rot}. This M_{rot} is applied to produce the rotation of $0.2*10^{-3}$ rad.

Load steps	Force type
1	Compression due to water (half-cross section)
0.1(3) 0.02(35)	Shear-force+ Compensating BM due to shear+Compensating BM due to water+BM causing rotation (full cross section)

Table 5.12- Load steps for Type II analysis

Load type	Load applied at 1.0 load step	Last converged load step **0.3**
Shear	2481 k N	744 kN
Bending Moment (at end)	12000kN *8 m =96000kNm	$28.8*10^3$ kNm

Table 5.13- Loads applied for Type-II analysis

5.15.4 Result

Load step	Bending moment applied at end (-)	Bending moment due to water (+)	Bending moment due to force at tooth -2481kN (+)	Total moment at the tooth (-) at 0.3 step
0.3	$28.8*10^3$ kNm	$16*10^3$ kNm	2481*6.7*0.3 $=5*10^3$ kNm	$7.8*10^3$ kNm

Table 5.14- Bending moment applied and bending moment present at the tooth for type II analysis

In this analysis, it was noticed that the analysis stopped much earlier than the previous analysis, namely at load step of 0.3. The maximum displacement in y-direction was found to be lower than

in the previous analysis. The tensile stresses were also very low as shown in **Figure 5.37**. The highest stresses were again found in the wall-base connection of the tunnel both for the inner and the outer wall. In **Table 5.14**, the total bending moment at the last step is 7800 kNm (This is part of 46000 kNm moment applied). To obtain a rotation of $2*10^{-3}$ rad for half cross-section, we need 23000 kNm. Hence this bending moment is very low to produce rotation. This was also confirmed from the low displacement found in y-direction.

5.15.5 Cause of divergence

Loss of equilibrium is the expected cause of divergence. The shear force value reached is lower than the previous analysis. Hence moment is a bigger contributing factor in the equilibrium of the structure**.**

[UNIT] N , mm
[DATA] Structural Nonlinear , Principal Stress S1 Nodes(V) , Load Step 4(0.3)
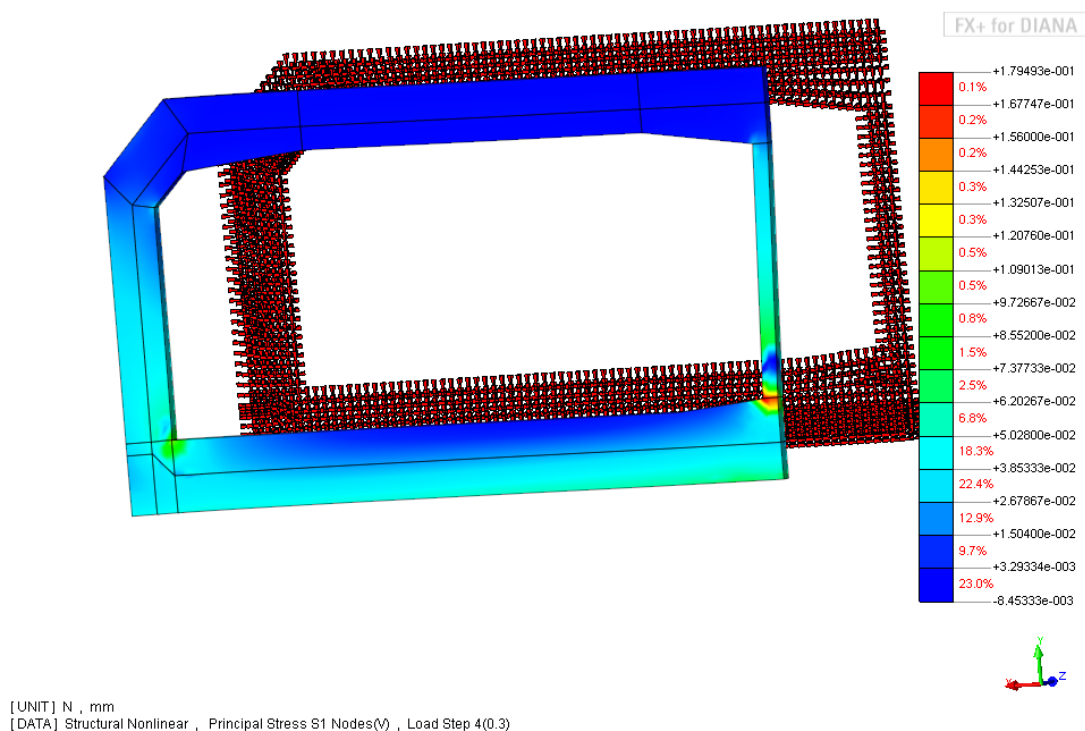
Figure 5.37- Principle tensile stresses- higher at wall to base connection for type II analysis (view from the loaded side)

5.16 Type III- Bottom tooth loading–pure shear

5.16.1 Aim

To obtain the effect of pure shear loading on bottom tooth at load step 0.5. Further load steps would indicate the extra capacity of the tooth.

5.16.2 Load applied (Figure 5.38)

Step 1: Apply axial force from water. This also includes a bending moment.

Normal force due to water = $5.3 * 10^3$ kN (half cross-section)
Bending moment due to water (approx.) = 16000 kNm (anti-clockwise)

Step 2: Apply a high shear force. Apply a corresponding bending moment which compensates the moment generated due to that shear force. Also, apply double the bending moment that compensates the moment generated due to water.

Shear force applied =2481kN. The required capacity for half cross section is only 1240 kN. But we apply a higher value as we expect the tooth to have more capacity than the value occurring at site. We can arbitrarily pick a very high value; hence we choose to pick a value double its capacity, hence 2481 kN. So if the analysis reaches 0.5 load steps, the structure is safe. This shear force (2481 kN) at the end generates a bending moment of approx. *16000 kNm at the tooth (clockwise). V.a = 2481 kN *6.7m=16000 kNm*

Compensating Bending moment = 16000 kNm (anti-clockwise). By applying this, it has been assured that at the tooth, there is no bending moment generated due to shear at any load step.

*Compensating bending moment due to water =2*16000 = 32000 kNm (clockwise)*. The required compensating moment is only 16000 kNm. But double that value has been applied because by 0.5 load step, all the moment is compensated and only pure shear at bottom tooth exists.

Hence, total clockwise moment applied at 1.0 load step = 32000(water)-16000(shear) = 16000 kNm (Table 5.16)
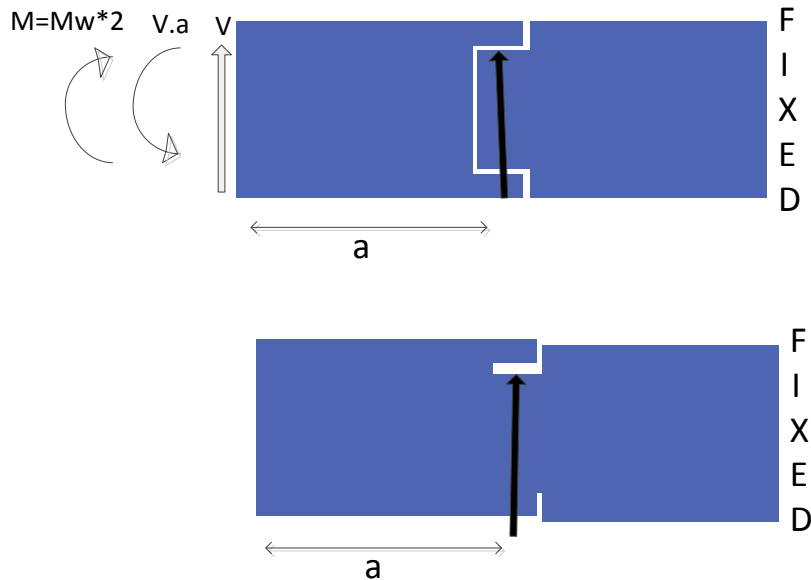
Figure 5.38- Top**:** Loading of the bottom tooth (shear); Bottom: Expected behavior

5.16.3 Description

In this analysis, the bottom tooth is loaded as shown in **Figure 5.38**. It is aimed to have a situation of pure shear in the bottom tooth of the connection. This case is very similar to type 1 analysis, except that the direction of shear force is reversed. In this analysis also, the first step is application of water pressure which causes compression and bending moment. The next step is discussed in **Figure 5.38**. The main difference which should be noted is that the direction of shear force is reversed. This causes reverse direction of compensating bending moment.

Load steps	Force type
1	Compression due to water (Half-cross section)
0.1(3) 0.02(35)	Shear-force+ Compensating BM due to shear+Compensating BM due to water (Full-cross section)

Table 5.15- Load steps for Type III analysis

Load type	Load applied at 1.0 load step	Last converged load step **0.36**
Shear	2481 k N	893 kN
Bending Moment (at end)	2000*8 kNm=16000 kNm	$5.76*10^3$ kNm

Table 5.16- Loads applied in type III analysis

5.16.4 Result

The last converged load step was 0.36. The details of the loads at the last step can be followed in **Table 5.15** and **Table 5.16**. In the last converged step, the tensile stresses in concrete were found to be very low **Figure 5.39**. Bending moment at the tooth is shown in **Table 5.17**.

[UNIT] N , mm
[DATA] Structural Nonlinear , Principal Stress S1 Nodes(V) , Load Step 7(0.36)
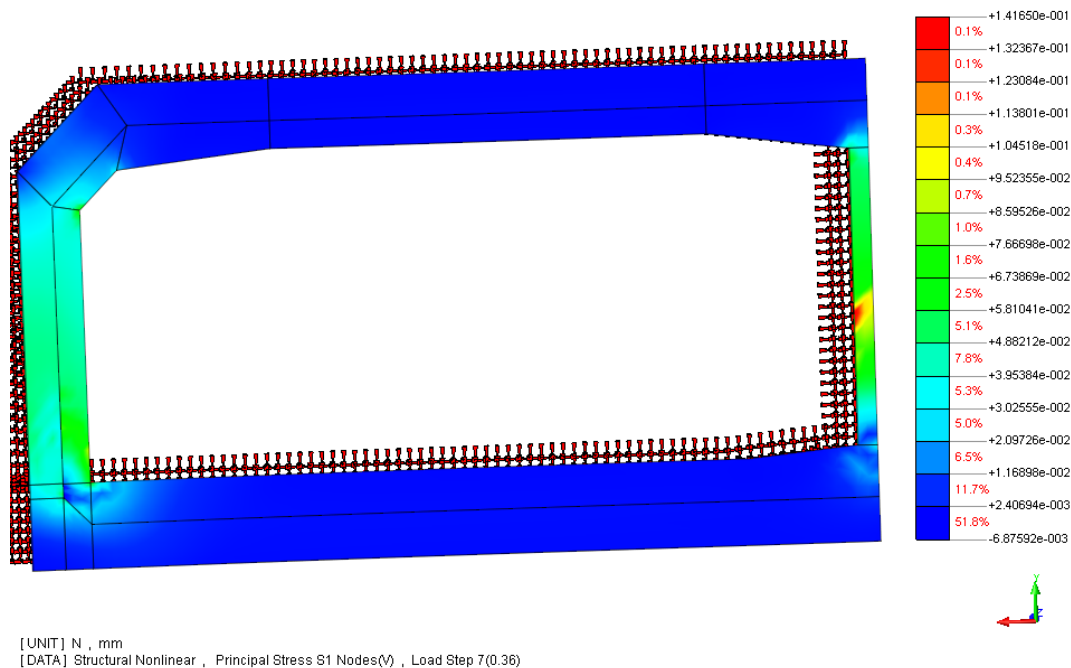
Figure 5.39- Principle tensile stresses for type III analysis, behind-support indicated by red

Load step	Bending moment applied at end (-)	Bending moment due to water (+)	Bending moment due to force at tooth -2481kN (-)	Total moment at the tooth (+)
0.36	$5.76*10^3$ kNm	$16*10^3$ kNm	$2481*6.7*0.36$ $= 6*10^3$ kNm	$4.3*10^3$ kNm

Table 5.17- Bending moment applied and bending moment present at tooth for type III analysis

5.16.5 Cause of divergence

In the step 0.38, huge cracks developed and caused the program to diverge. These cracks were located in the outer wall of the connection between tunnel segments (tooth), **Figure 5.40**. This could be caused because the load steps are higher than what should be applied to this structure. Another possible explanation to this behavior could be because the mesh is not very good.
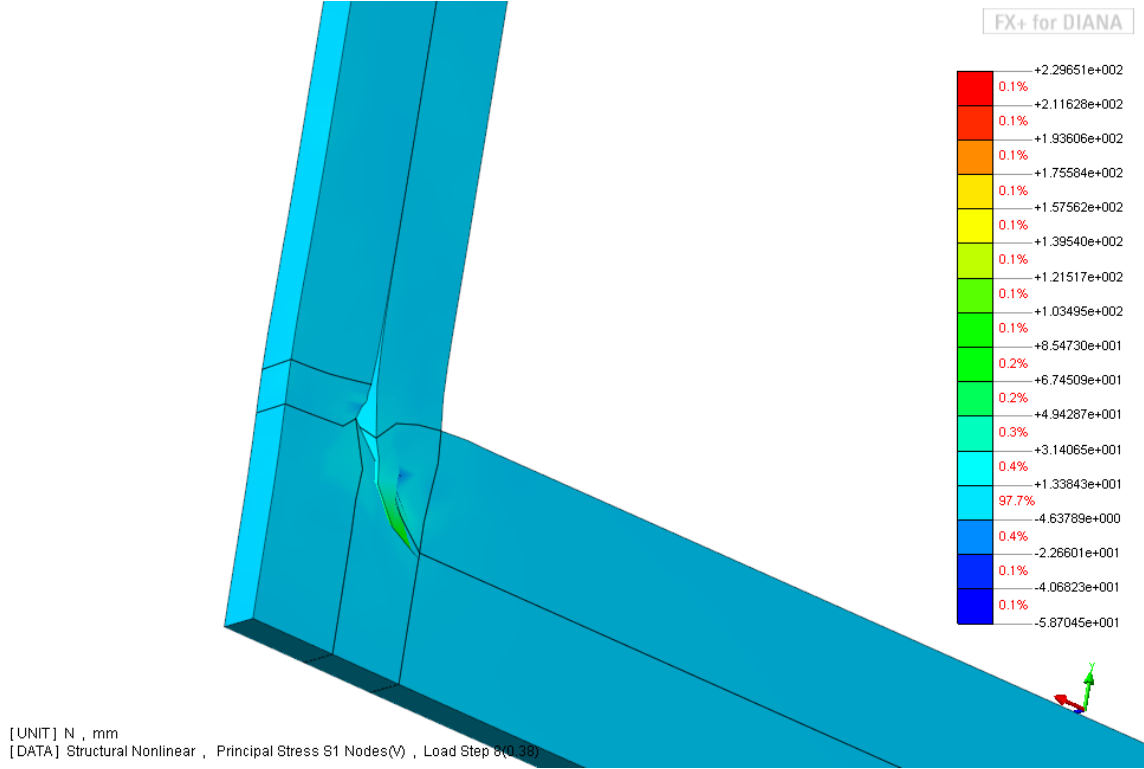
Figure 5.40- Cause of early divergence- Type III analysis

5.17 Type IV- Bottom tooth loading- shear + bending moment

5.17.1 Aim

To obtain the effect of shear + bending moment loading on bottom tooth at load step 0.5. Further load steps would indicate the extra capacity of the tooth. The bending moment comes from the rotation of $2*10^{-3}$ rad.

5.17.2 Load applied (Figure 5.41)

Step 1: Apply axial force from water. This also includes a bending moment.

Normal force due to water = $5.3 * 10^3$ kN (half cross-section)
Bending moment due to water (approx.) = 16000 kNm (anti-clockwise)

Step 2: Apply a high shear force and a high bending moment. Apply a corresponding bending moment which compensates the moment generated due to that shear force. Also, apply double the bending moment that compensates the moment generated due to water.

Shear force applied = 2481 kN. The required capacity for half cross section is only 1240 kN. But we apply a higher value as we expect the tooth to have more capacity than the value occurring at site. We can arbitrarily pick a very high value; hence we choose to pick a value double its capacity, hence 2481 kN. So if the analysis reaches 0.5 load steps, the structure is safe. This shear force at the end generates a bending moment of approx. ***16000 kNm at the tooth (clockwise). V.a = 2481 kN *6.7m =16000 kNm***

Compensating Bending moment = 16000 kNm (anti-clockwise). By applying this, it has been assured that at the tooth, there is no bending moment generated due to shear at any load step.

Compensating bending moment due to water =2*16000 = 32000 kNm (clockwise). The required compensating moment is only 16000 kNm. But double that value has been applied because by 0.5 load step, all the moment is compensated and only pure shear at bottom tooth exists.

Bending moment = 46000 kNm (clockwise). A bending moment of 23000 kNm is required to produce a rotation of $2*10^{-3}$ rad for half cross section. We apply however a bigger bending moment, as we expect that connection has more capacity. So if the analysis reaches 0.5 load steps, the structure is safe.

Total clockwise bending moment at 1.0 load step = 32000(water) - 16000(shear) + 46000 = 62000kNm (applied is 64000 kNm, Table 5.19)

5.17.3 Description

In this analysis also, the bottom tooth is loaded as shown in **Figure 5.41**. The aim is to obtain the effect of shear force with rotation on the tunnel tooth. Here, the interesting point is that, the shear force tries to close the bottom tooth, while the bending moment tries to open the bottom tooth and close the top. Since, both shear and bending moment are applied together and increased in load steps. It is expected that once the compression due to water pressure is gone, the calculations should stop. The load steps and their values are described in **Table 5.18** and **Table 5.19**.

Load steps	Force type
1	Compression due to water (Half-cross section)
0.1(2) 0.02(40)	Shear-force+ Compensating BM due to shear+Compensating BM due to water+Moment causing rotation (Full-cross section)

Table 5.18- Load steps for Type IV analysis

Load applied	Load applied at 1.0 load step	Last converged load step **0.22**
Shear	2481 k N	545 kN
Bending Moment (at end)	8*8000 kNm= 64000kNm	$14*10^3$ kNm

Table 5.19- Loads applied for type IV analysis
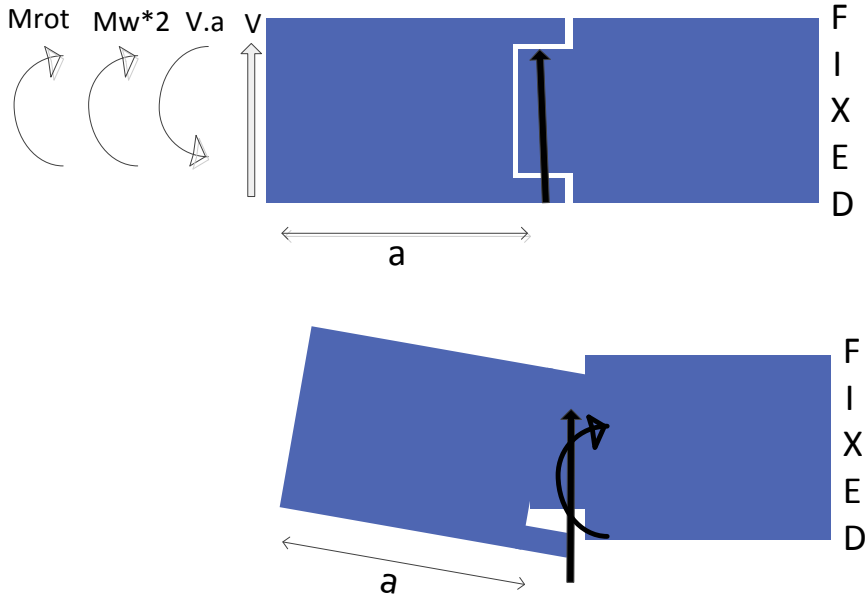
Figure 5.41- Top**:** Loading of the bottom tooth (shear); Bottom: Expected behavior

5.17.4 Result

In the last converged step (0.22), the tensile stresses in concrete were found to be very low **Figure 5.42**. The maximum displacement in the y-direction was 0.138 mm. This leads to a rotation value about 100 times lesser than calculated on site. Bending moment is shown in **Table 5.20**.

Load step	Bending moment applied at end (-)	Bending moment due to water (+)	Bending moment due to force at tooth -2481kN (-)	Total moment at the tooth (-)
0.22	$14*10^3$ kNm	$16*10^3$ kNm	2481*6.7*0.22 = $3.6*10^3$ kNm	$1.6*10^3$ kNm

Table 5.20- Bending moment applied and bending moment present at the tooth for type IV analysis

93

5.17.5 Cause of divergence

It is expected that there was loss of equilibrium which led to the divergence. Absence of compression in the interface leads to the calculation to stop. Also, the presence of opposite directions of bending moment leads to an early halt. This shows that the bending moment is the more critical of the two forces. Both in the bottom tooth and the top tooth analysis, type II and type IV, the final load step reached was smaller.
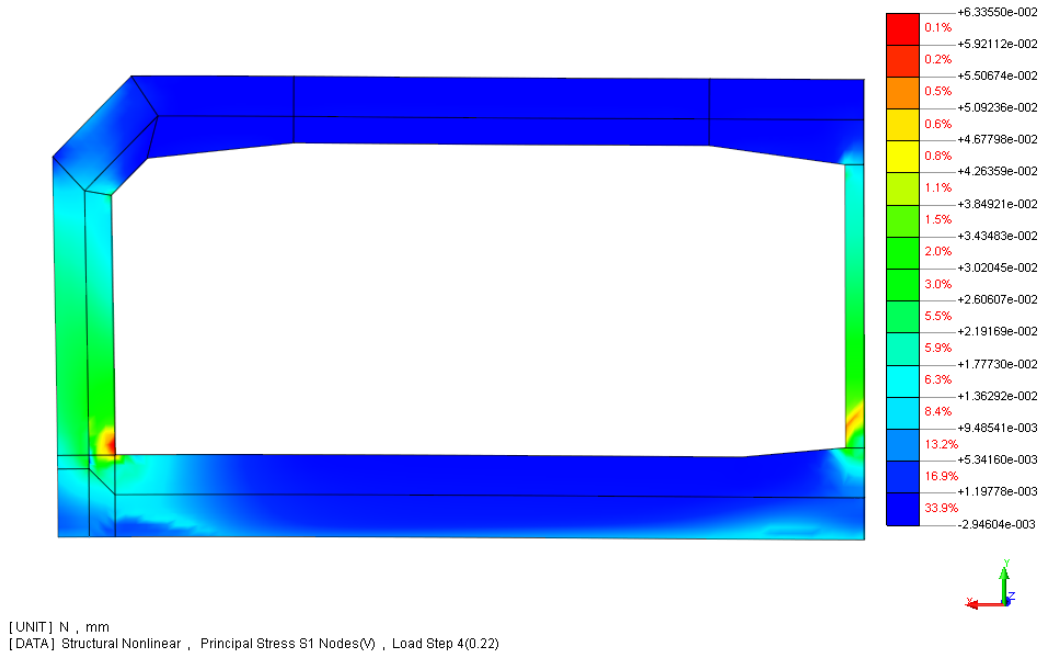

Figure 5.42- Principle tensile stresses near the loaded direction

.

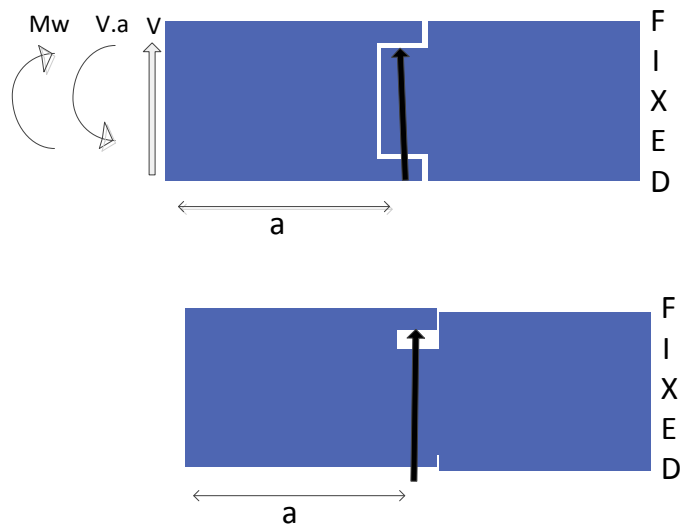## 5.18 Type V- Bottom tooth loading- shear

Figure 5.43- Top**:** Loading of the bottom tooth; Bottom: Expected behavior

5.18.1 Aim

To obtain the effect of pure shear loading on the bottom tooth at load step 0.5. Further load steps would indicate the extra capacity of the tooth. The main difference from the Type III analysis is the presence of half of the compensating bending moment due to water.

5.18.2 Load applied (Figure 5.43)

Step 1: Apply axial force from water. This also includes a bending moment.

Normal force due to water = $5.3 * 10^3$ kN
Bending moment due to water (approx.) = 16000 kNm (anti-clockwise)

Step 2: Apply a high shear force. Apply a corresponding bending moment which compensates for the moment generated due to that shear force. Also, apply a bending moment that compensates for the moment generated due to water.

Shear force applied = 2481 kN. The required capacity for half the cross section is only 1240 kN. But we apply a higher value as we expect the tooth to have more capacity than the value occurring at site. We can arbitrarily pick a very high value; hence we choose to pick a value double its capacity, hence 2481 kN. So if the analysis reaches 0.5 load steps, the structure is safe. This shear force (2481 kN) at the end generates a bending moment of approx. *16000kNm at the tooth (clockwise). V.a = 2481 kN *6.7m=16000 kNm*

Compensating Bending moment = 16000 kNm (anti-clockwise). By applying this, it has been assured that at the tooth, there is no bending moment generated due to shear at any load step.

Compensating bending moment due to water = 16000kNm (clockwise). The required compensating moment is only 16000 kNm.

Hence, total clockwise moment applied =16000-16000= 0 kNm

5.18.3 Description

The final case discussed in the schemes of analysis, is similar to the type III analysis except the compensating bending moment due to water. Earlier used was 2*Mw and now only Mw. Hence, the current bending moment favors the loading of the bottom tooth, **Figure 5.43**. In the **Table 5.21** and **Table 5.22**, the description of loads steps and loads is provided.

Load steps	Force type
1	Compression due to water (Half-cross section)
0.1(3) 0.02(35)	Shear-force+ Compensating BM due to shear (Full-cross section)+Compensating BM due to water (half-cross section)

Table 5.21- Load steps for Type V analysis

Load applied	Load applied at 1.0 load step	Last converged load step **0.54**
Shear	2481 k N	1340 kN
Bending Moment (at end)	0 kNm	0 kNm

Table 5.22- Loads applied for type V analysis

5.18.4 Result

In the last converged step, the tensile stresses in concrete were found to be very low. **Table 5.23** describes the bending moment present in the last load step.

Load step	Bending moment applied at end (-)	Bending moment due to water (+)	Bending moment due to force at tooth -2481kN (-)	Total moment at the tooth (+)
0.54	0 kNm	$16*10^3$ kNm	2481*6.7*0.54 = $8.9*10^3$ kNm	$7.1 *10^3$ kNm

Table 5.23- Bending moment applied and bending moment present at the tooth for type V analysis

5.18.5 Cause of divergence

In the step 0.56, the concrete tensile stresses became high. It leads to crack formation near both the inner and the outer walls. Near the inner wall, both the top and bottom of the tooth were affected. Near the outer wall only the bottom of the tooth was majorly affected by cracks. The tensile stresses were very high in this load step, **Figure 5.44**.

5.18.6 Interpretation

The slow increase of concrete stresses could not be seen in this analysis. The cracks in the structure show that the failure is expected near the tunnel walls. There is also a possibility that if the steps are very small, we are able to see the slow development of the cracking pattern. But due to time constraint, this was not studied in this thesis.

At the last load step which converged, we can say that the bottom tooth of the tunnel is capable of carrying the shear force which is expected (expected-0.5, resisted-0.54), along with some extra bending moment ($8.9*10^3$ kNm).

Now, we compare these results with the results of the type-I analysis where shear force was in downward direction. In the type 1 analysis, the tunnel could take upto 0.58 of the applied load and the aim again was to reach 0.5. In that case the bending moment in the opposite direction (opening of bottom tooth) favored the analysis. Here, the bending moment due to water favors the analysis. The direction of force in upward direction already causes the reduction of the bending moment present due to water. No extra bending moment (which causes opening) was applied. Hence, in both these analysis, the connection can take up the expected shear force in linear analysis. It means that with these values of shear forces, there should be no cracks in the structure (in a linear analysis).
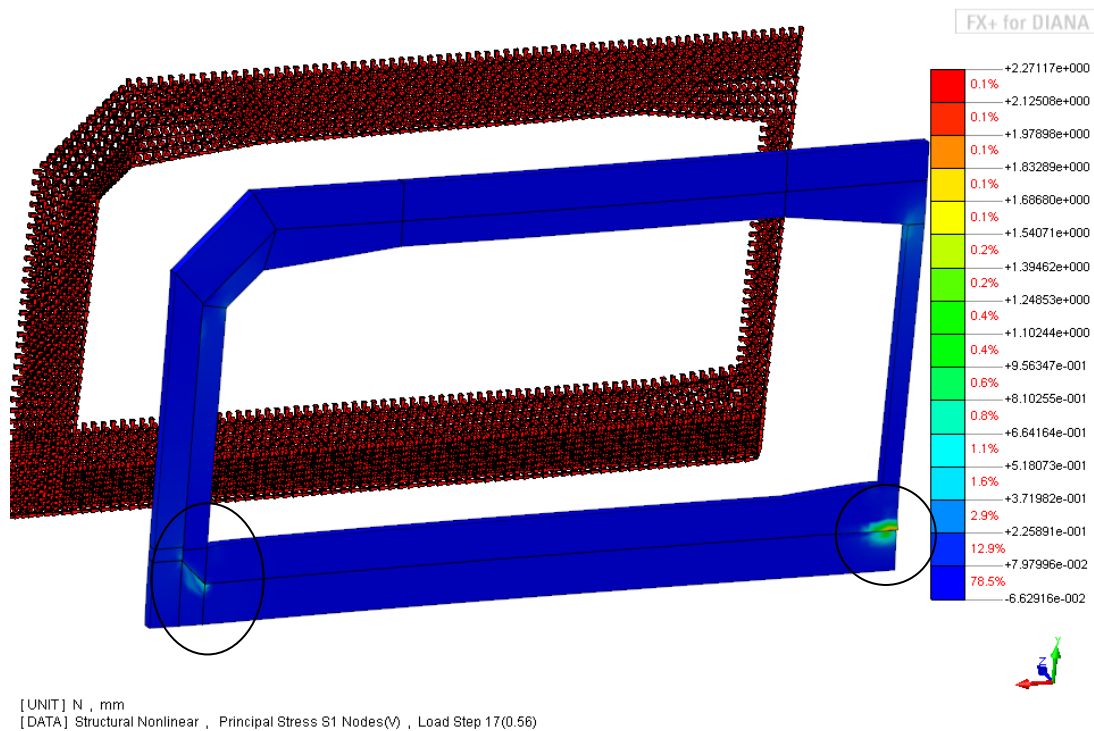
[UNIT] N , mm
[DATA] Structural Nonlinear , Principal Stress S1 Nodes(V) , Load Step 17(0.56)

Figure 5.44- Principle tensile stress for the last load step- highest at the bottom, near the walls

5.19 Summary

In this chapter, the 3-D analysis of tunnels was performed. In the first part, the types of loads acting on the tunnel were discussed. First, a linear analysis was performed and the validity of the effective width model was checked. It was found that the walls indeed take the majority of the shear force as analyzed earlier.

In the next part of this chapter, various schemes of tunnel loading were studied. This was done because of the lack of clear data about the relative behavior of the two segments at the tooth. The aim was to obtain the failure load and cracking of the tunnel in a non-linear analysis. However, the analyses stopped before showing detailed cracking of the tunnels.

Each analysis showed a different reason of failure. However, it was noticed in most of the analysis that the highest stresses were found in the wall to slab connection in their last converged steps. Another point of interest in the analysis result was the interaction between the two segments (at the tooth) near the interface. There were cracks formed near the walls, where interaction occurs.

By looking at Type 1 and Type 5 analysis, it can be said that when the bending moment is zero or if it causes compression in the loaded tooth (top/bottom), the tunnel can easily take the expected amount of shear force. However, when there is excessive pulling from the bending moment, the analysis stops early. It has been noticed that the bending moment is a very critical factor in these simulations as the divergence always occurred much earlier when the bending moment was added to the shear force analysis. The rotation of $2*10^{-3}$ rad which was found on

site could not be achieved in the analyses which were carried out. The rotations found were 50-100 times lesser, or rather negligible.

Chapter 6

Computational analysis of large 3-D models

6.1 Introduction

In the previous chapter, the results of the 3-D analysis were discussed. However to obtain these results a lot of time and efforts went into making the model. This chapter reflects on all the challenges faced during the 3-D modeling and analysis of this tunnel. It also reflects on the lesson learnt while carrying out these analyses. The chapter is written with the aim that it will help the readers to understand FE modeling and also guide them if they are faced with similar challenges with their models.

6.2 Speed vs Time

In order to study the behavior of structures, Finite Element analyses offer a promising solution. Over the past few decades, many Finite Element softwares have been developed by industry and academia. Each newer package aims to be faster and better. In the early stages of the FE package development, input for the structural nodes had to be provided manually. Today, the graphic user interface (GUI) available with most packages already comes with predefined shapes and geometries. The user-friendly features of the softwares save a lot of time and therefore money.

When the model and its properties are defined manually, it takes more time. But at the same time, the user is well-accustomed to all the features of his/her model. In the GUI, the user follows the computer, which tends to create a gap in the user's knowledge of the model properties/behavior. The debate on whether to opt for better GUI and speed up the calculations or go for manual input which consumes more time will continue to exist. DIANA package, which was used for the analysis in this thesis, comes with two types of user interfaces, iDIANA and FX+. While FX+ is certainly more user friendly and helpful for first time users, experts prefer for iDIANA because it serves less like a black-box. For this thesis, FX+ was used as it is much faster in making the model and easy to learn.

6.3 Challenges faced while making the model

The making of the 3-D model apart from being time consuming was also very challenging. The tunnel geometry comprising of concrete was first made and then reinforcements were defined.

- First, work was done on the geometry of the tooth of the tunnel. The tunnel tooth was divided into many small solids such that an even mesh could be obtained. These steps are described in detail in the **Appendix E1**.

- Once the solids were defined, they were meshed with the Auto-Mesh command. The Auto-mesh command in 3-D generates triads as also discussed in Chapter 5. The generated mesh is shown in **Figure 6.1**.In general in FX+, the command Auto-Mesh generates a mesh such that the analysis takes minimum amount of time possible.

Similarly solids for the entire tunnel were made. Aim was to increase the size of the mesh gradually from the tooth towards the end of the tunnel. This way the computation time would be faster. However, the generated result was not the desired result as shown in **Figure 6.2**. Here some parts of the tunnel produced the desired result in meshing, while the other parts did not. Hence, the mesh was extruded in both directions along the length to get the desired result. This resulted in the formation of elements shown in **Figure 6.3**. Another major change that was adopted in the tunnel model was that it was made into half to speed up the calculations, as seen in **Figure 6.4**.
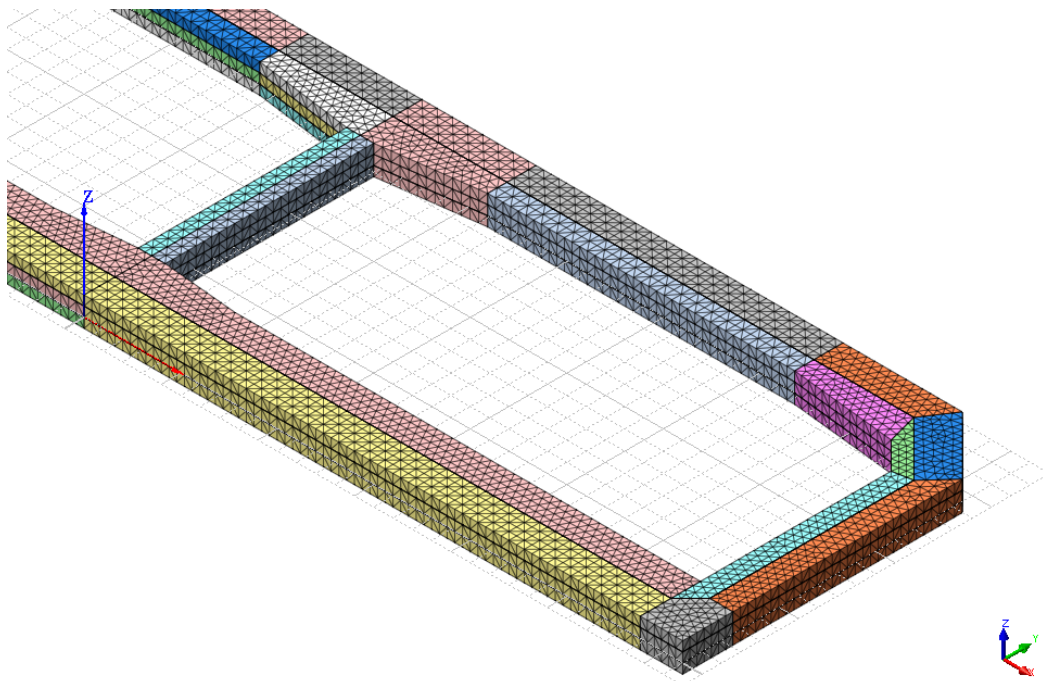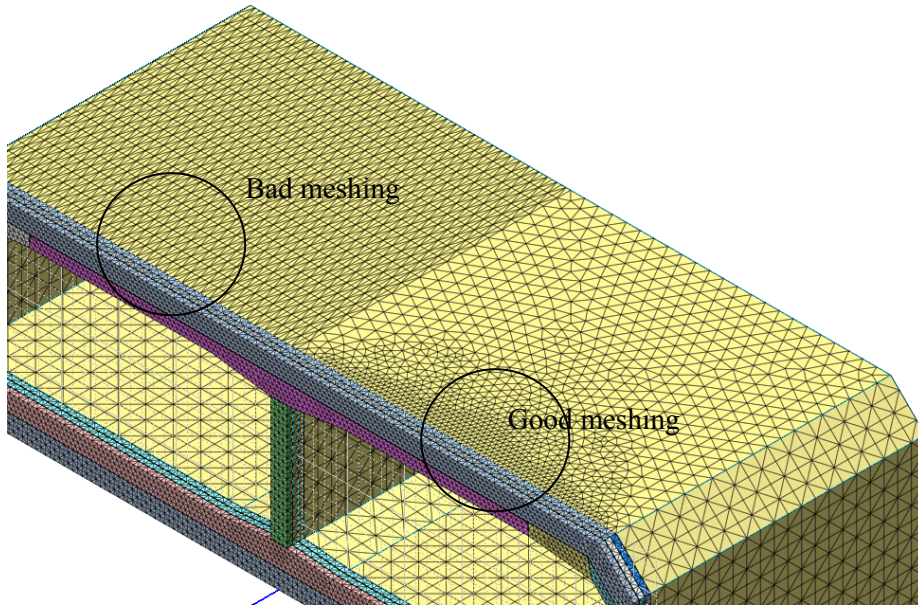

Figure 6.1- Tooth comprising of triads

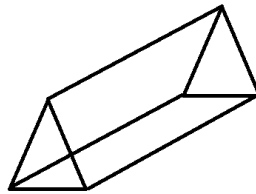**Figure 6.2-** Full tunnel made of triads

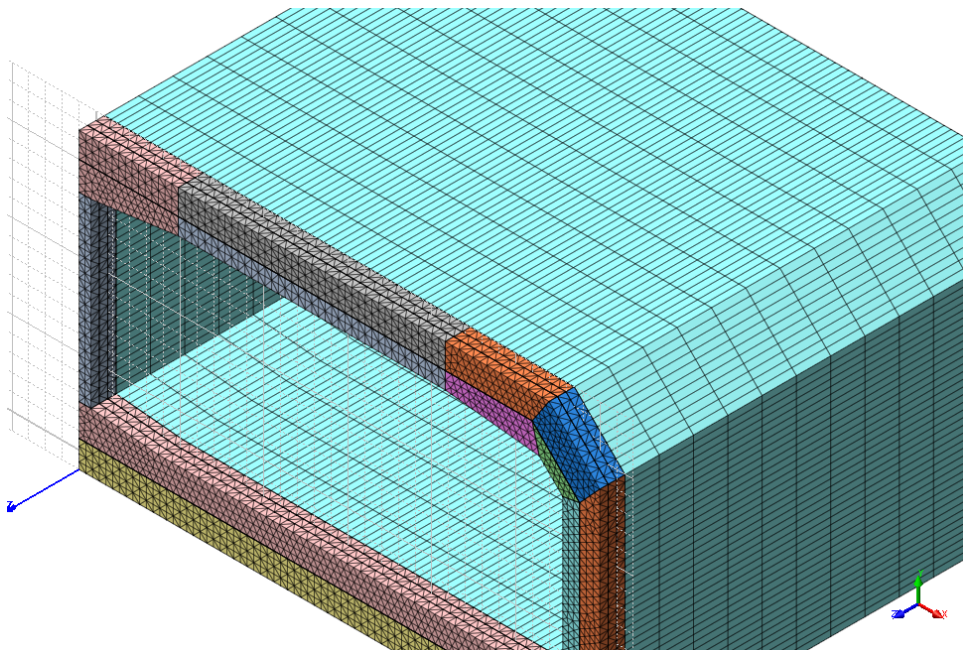**Figure 6.3-** Pyramid elements used for Figure 6.4

Figure 6.4- Full geometry with triads + pyramids

A major disadvantage with the model was discovered after the linear analysis of the model was carried out. The pressure due to water was applied and compressive stresses were noted at the tunnel connection. There were peaks found at certain locations of the tunnel, **Figure 6.5**. Clearly, this was not desired of the model. On further investigating the tunnel model, the mesh quality was observed. The quality of the mesh indicated very similar patters as were found in stress plot, as can be observed in **Figure 6.6**. Hence, the places where mesh quality was not very good, stress peaks were observed. Hence it was decided to change the element type used to bricks.
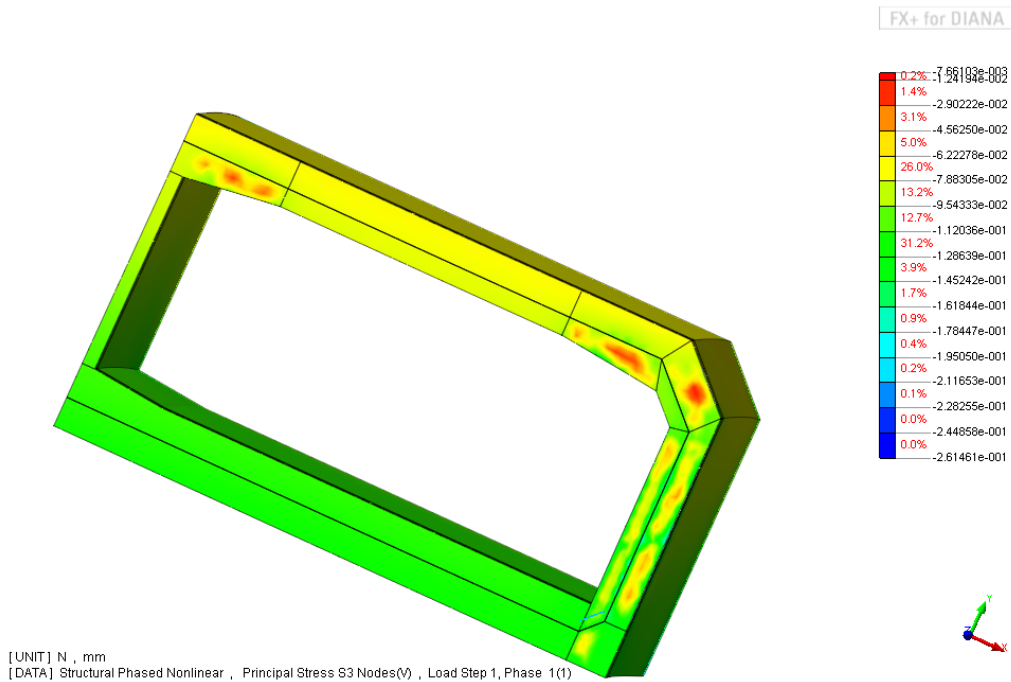
Figure 6.5- Compressive Stress on application of water pressure at tooth (peaks observed)
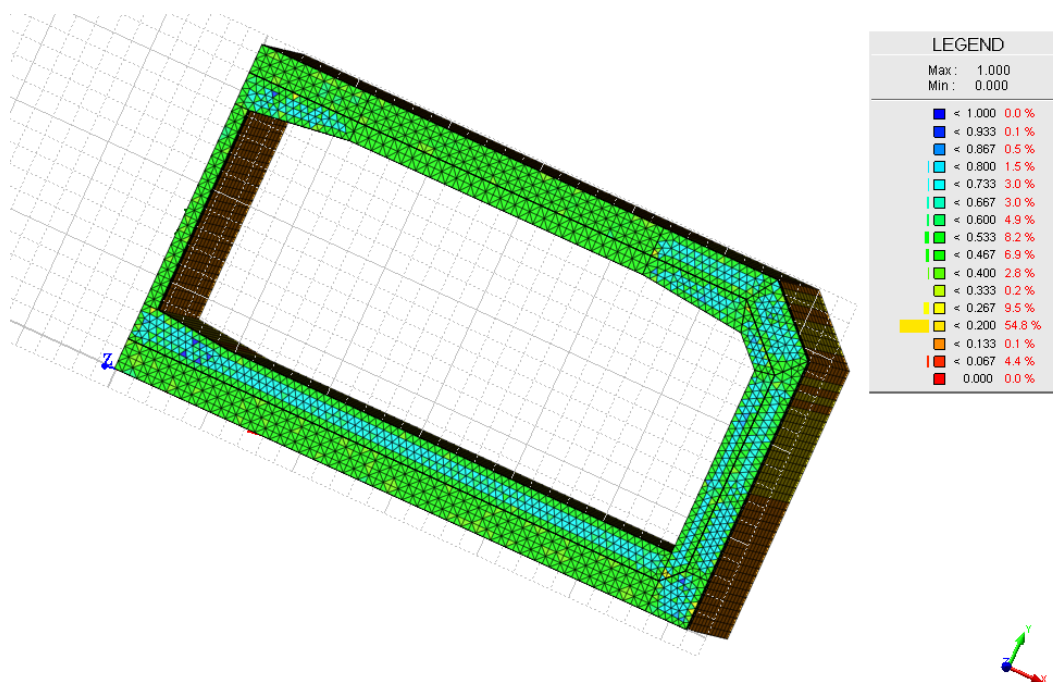

Figure 6.6- Mesh quality check-indicating similar pattern as Compressive Stress

Cubic mesh was then adopted for the further analysis. The model was made in the similar fashion as explained before. Except that the mesh was not protruded to 3-D, but the solids were copied and pasted along the entire length of the tunnel on both sides. By this, there was no difference between the sizes of the elements along the length of the tunnel. If the mesh was made coarser, it would have speeded up the calculations. It was required to ensure that the length is long enough to distribute the loads applied at the end and short enough to be quick for the analysis. The final result which has been used in this thesis for all analysis is shown in the **Figure 5.4**. The tooth of the structure is highlighted in **Figure 6.7**. A 2mm gap was kept between the two tunnel segments as shown in **Figure 6.8**.
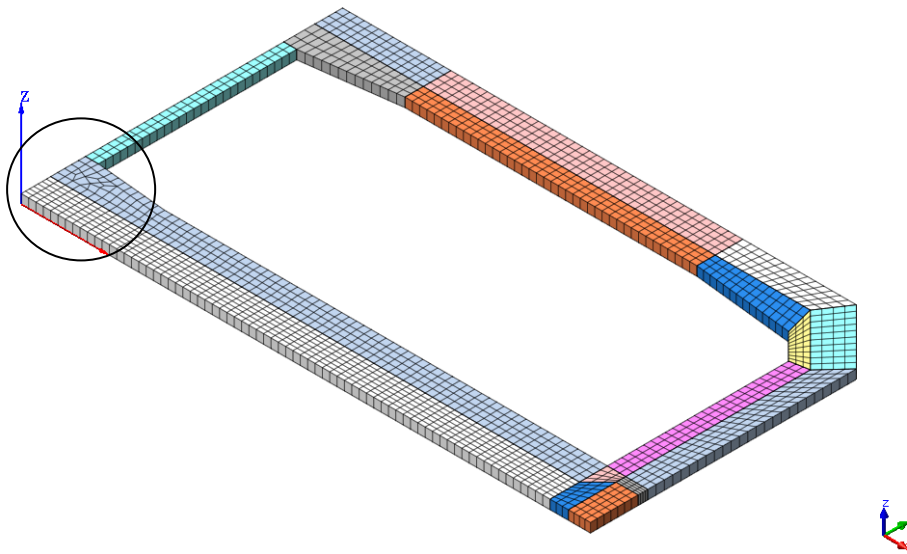
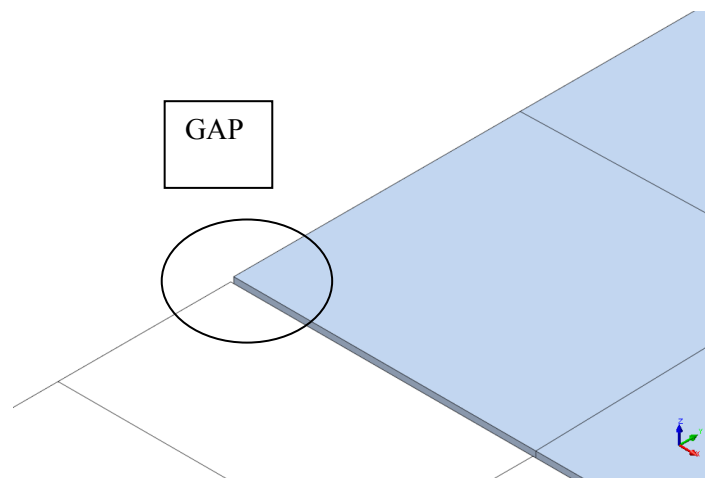**Figure 6.7-** Final mesh made with brick elements

Figure 6.8- Gap of 2mm between the tunnel tooth (this part is circled in **Figure 6.7**)

Even after the model was cut down to half, it took a long time to run the analysis. Every iteration in the analysis took about 60 min. So even with a very few load steps, the analysis was running easily into a couple of hours.

For all the analysis, this model (**Figure 5.4**) was used and no further changes were made. A close look into the geometry of the model, **Figure 6.9** shows the skewed nature of brick elements. Another aspect which should be highlighted here is the 2mm gap which exists between the shear keys of the tunnel. Interface elements were modeled in this 2mm gap at the tooth. When the tooth elements were copied in both directions along the length, this 2 mm gap persisted for the rest of the tunnel. Hence, with the help of very thin concrete elements, this gap was filled. This has been discussed with figures in the **Appendix E2**. These concrete elements are not well shaped due to the high aspect ratio between their width and length. It is a possibility that this could be one of the reasons why some analysis stopped prematurely.

One way in which this could be solved is by making two geometrical models on each side of the tooth. However, this would have consumed a lot of time and there would be no time left for the analysis. Hence, it was decided to use the model with the thin concrete elements.
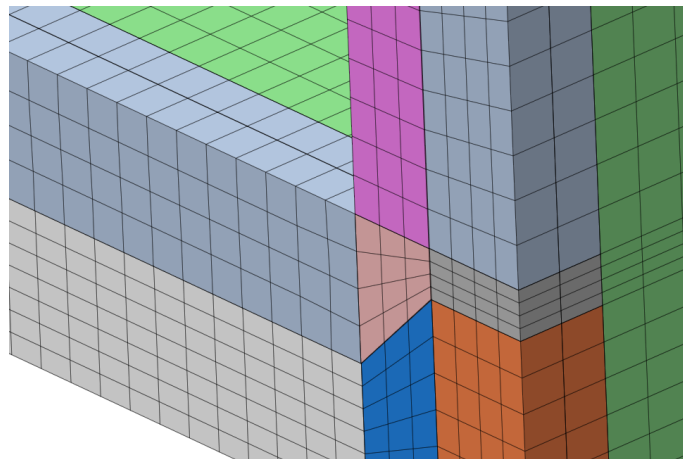

Figure 6.9- Skewed elements at the corners of the tunnel

6.4 Challenges faced while making the interface

Making the interface for the 3-D model was one of the toughest parts in the modeling. The general convention used for making interface is to protrude the mesh in a certain direction and to convert the elements protruded into interface elements. However, in the current tunnel model, the interface had to be modeled in both directions x-and y and 1-direction protrusion couldn't be used. Therefore, first the gaps were filled with solids with the same thickness of 2mm. Then these solids were converted into interface elements as shown in **Figure 5.10**.

6.5 Challenges faced while analyzing the model

As it has already been explained earlier, every iteration took about 1 hour of simulation time. Hence, a few load steps could lead to the analysis running into days. Hence it was important to keep the number of load steps low. The number of iterations for the simulations also had to be compromised. For non-linear analysis, the numbers of iterations are suggested to be around 50. However, due to lack of time, the maximum iterations were restricted to 5.

6.6 Summary

Important challenges about modeling in FX+ and how to overcome them have been discussed in this section. It is hoped that the reader gets a holistic overview of the problems which could be encountered when dealing with 3-D Finite element analysis.

Chapter 7

Conclusions and Recommendations

7.1 Conclusions

1) *Shear stress is concentrated at the walls of the tunnel cross-section at the segment connection.*

When water pressure and shear force along with a compensating bending moment were applied at the end of one segment of the tunnel, it was found that the shear stress is concentrated in the walls of the immersed tunnel (**section 5.12**). The effective-width model which was assumed by Schols [3] was hence validated by this study. Almost 9% of the total shear force passes through other parts of the tunnel. In the study by Schols [3], the contribution of these parts was considered to be zero.
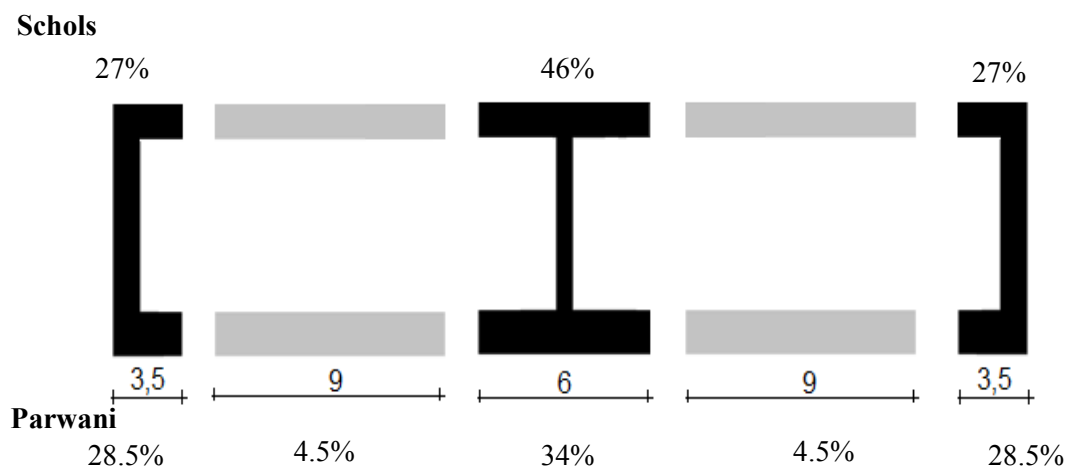
Figure 7.1- Percentage of shear force that passes through parts of the cross-section cross-section (Comparison of results with the effective width concept of Schols [3]), dimensions [m]

The percentage of the shear force which passes through the walls was found to be almost evenly divided between the walls. Almost 30-35% of the total force passes through each of the outer walls and one inner wall (**Figure 7.1**). The thickness of the middle/inner wall is the least making it most prone to damage/cracking. The highest tensile stresses were also found in the inner wall of the tunnel which makes it the critical element in the linear analysis of the tunnel.

2) *The tunnel segment connection is capable of carrying the estimated shear force in a linear analysis.*

It was shown that the segment connection of the tunnel in the finite element model is capable of taking the shear force which arises from the differential settlement of the segments (section **5.14** and **5.18**). In the analysis described in the section **5.14**, there is pure shear at 0.5 load step (aim is to reach 0.5 load step only). Since the analysis could continue beyond 0.5, we can say the top tooth is effective in transferring the shear force that occurs on site.

In the next analysis discussed in the section **5.18**, the bending moment direction (due to water) created compression in the direction of the shear force that is loading the bottom tooth in the section **5.18** . In this analysis also, the model could go beyond the expected load step of 0.5 in linear analysis. This implies that the tunnel is able to take up the expected amount of shear force without cracking. Hence, if the current tunnel is subjected to shear in the top tooth or the bottom tooth, then we can conclude that the tunnel is safe.

In the section **5.16,** the aim was to load the bottom tooth in pure shear (without any compression like in the section **5.18**), the model could not reach 0.5 load step.

3) *The bending moment is more critical than the shear force for tunnel stability*

It was noted that in all the schemes discussed in Chapter 5, the bending moment was the most critical of one the two loads (shear force and bending moment). When the shear-force was applied alongside the additional bending moment (simultaneously in the same step), divergence was obtained much earlier. This was observed in section **5.15** and **5.17**.

4) *The segment connection cannot take the expected bending moment in a linear analysis*

The bending moment expected in the tunnel was calculated in Chapter 4 as 46000 kNm. The bending moment which could be carried by the tunnel in the schemes was noted for each scheme discussed in Chapter 5. It was found that the Finite Element model of the tunnel is not capable of resisting the expected bending moment in a linear analysis. The rotations calculated in the tunnel analyses are 50-100 times smaller than the expected rotation on site. Since a detailed non-linear analysis could not be performed, the non-linear bending moment resistance of the connection could not be calculated.

7.2 Recommendations and future work

1) Smaller load steps and more iterations

To be able to follow the cracking of the tunnel, it is recommended to use very small load steps in DIANA. Another improvement could be achieved by increasing the number of iterations for each load step in the analysis. Around 100 load steps with 50 iterations each makes a good non-linear analysis (a similar number was used in the 2-D analysis in chapter 2). This was not done in 3-D due to the high amount of time required for analysis.

2) Use of well shaped elements

It is recommended to use elements which have very a good aspect ratio (length/width or length/height). In the current model, the tunnel corner (near the outer wall) is modeled with elements that do not have an optimal aspect ratio. This ratio is preferably between 0.5-1. Changing the mesh could lead to an improvement in results.

Next is the use of very thin elements in the concrete modeling, also explained in Chapter 6. They were modeled to fill the 2 mm thick gap between the segments along the length of the tunnel in both directions. These elements have a width and length of around 200 mm. These elements may introduce problems when the analysis proceeds into the non-linear part. Hence, it is recommended to remove these elements and replace them by a mesh with a better aspect ratio.

3) Incorporating the effects of torsion

In this study, the tunnel behavior when a rotation is applied in longitudinal direction (torsion) is not studied. However, the model is able to perform these analyses. It is recommended to take the effects of torsion into account as well while dealing with the tunnel analysis. Only half the tunnel cross-section was taken into this study due to time limitations. To study torsion behavior, the full tunnel cross-section should be modeled and analyzed.

4) Including the soil structure interaction in FEM modeling

Deformations are a major part of the current analysis. Hence it is recommended to include the soil-structure interaction by modeling the soil as elastic foundation.

It has been observed that the 3-D analysis stops early when the bending moment is applied to the structure. In such cases, it was observed that the analysis stops when there is tension in the interface. In reality, the structure is supported by sand underneath it and, as a result, there will be redistribution of forces in the elastic foundation. If the soil is modeled too, the analysis is expected to continue much further.

References

1. Immersed Tunnels (2013) R. Lunniss and J. Baber (2013).
2. Immersed tunnel settlements Part 1: Nature of settlements (2001) W.C. Grantz, Tunneling and Underground Space Technology, 16 (195-201).
3. Segmentvoegcapaciteit of Kiltunnel (2012) I. Schols , Master Thesis, TU Delft
4. Numerical simulation for large-scale seismic response analysis of immersed tunnel (2006) J.H.Ding, X.L.Jin, Y.Z.Gou, G.G.Li, Engineering Structures, 28 (1367–1377).
5. Tunnel structure analysis using the multi-scale modeling method (2012) C.Yuan, W. Puyong, J.Xianlong, W.Jianwei, Y.Yanzhi, Tunneling and Underground Space Technology, 28 (124-134).
6. Failure mechanism of tunnel lining joints and bolts with uneven longitudinal ground settlement (2013) Z. Wang, L. Wang, L. Li, J. Wang, Tunneling and Underground Space Technology, 40 (300-308).
7. Fast frequency-domain analysis method for longitudinal seismic response of super-long immersed tunnels (2013) M. Huang and H. Liu, International Conference on soil mechanics and Geotechnical Engineering, 18 (1715-1718).
8. Immersed Tunnel Techniques – 2 (1997) C.R.Ford
9. Immersed tunnel settlements Part 2: Case Histories (2001) W.C. Grantz, Tunneling and Underground Space Technology, 16 (203-210).
10. Finite element analysis of reinforced concrete structures under monotonic loads (1990) H. G. Kwak, F. C. Filippou, Report, University of California, Berkeley.
11. Comparison of Nonlinear Finite Element Modeling Tools for Structural Concrete (2006) S. Johnson, Report, University of Illinois at Urbana Champaign.
12. Comparative study of crack models (2002) J.G.Rots, Finite element analysis in Engineering Applications, DIANA Conference, Tokyo.
13. Improving the iterative methods in TNO DIANA using physical properties of the underlying model (2013) A. Sangers, Master thesis, TU Delft.
14. Advanced modeling of innovative bored tunnel design Amsterdam North South line (2002) W.H.N.C.V. Empel, F.J. Kaalberg, Finite element analysis in Engineering Applications, DIANA Conference, Tokyo.
15. Design philosophy of concrete linings for tunnels in soft soils (2002), C.B.M. Blom, PhD Thesis, TU Delft.
16. Experimental and analytical study of the structural response of segmental tunnel linings based on an in-situ loading test. Part 2: Numerical simulation (2011) O. Arnau and C. Molins, Tunneling and Underground Space Technology, 26 (778-788).
17. DIANA-User's Manual for Release 9.4.4 (2012), TNO Building and Construction Research.
18. The strut and tie model of concrete structures (2001). C.C. Fu, University of Maryland.
19. Design examples for strut-and-tie models (2011), Report by International Federation for Structural Concrete.

Images-

1. http://en.wikipedia.org/wiki/Submerged_floating_tunnel
2. http://blog.ramboll.com/fehmarnbelt/globalisation/how-is-the-fehmarn-tunnel-constructed-underwater.html
3. http://www.femern.com/home/construction-phase/tunnel-elements

Images-

Appendix A1

The Kiltunnel alignment showing the elements 2,3 and 1 from left to right. Each element is divided into segments represented by a,b,c,d and e and they have been used in **Figure 1.12** and **Figure 1.13**.
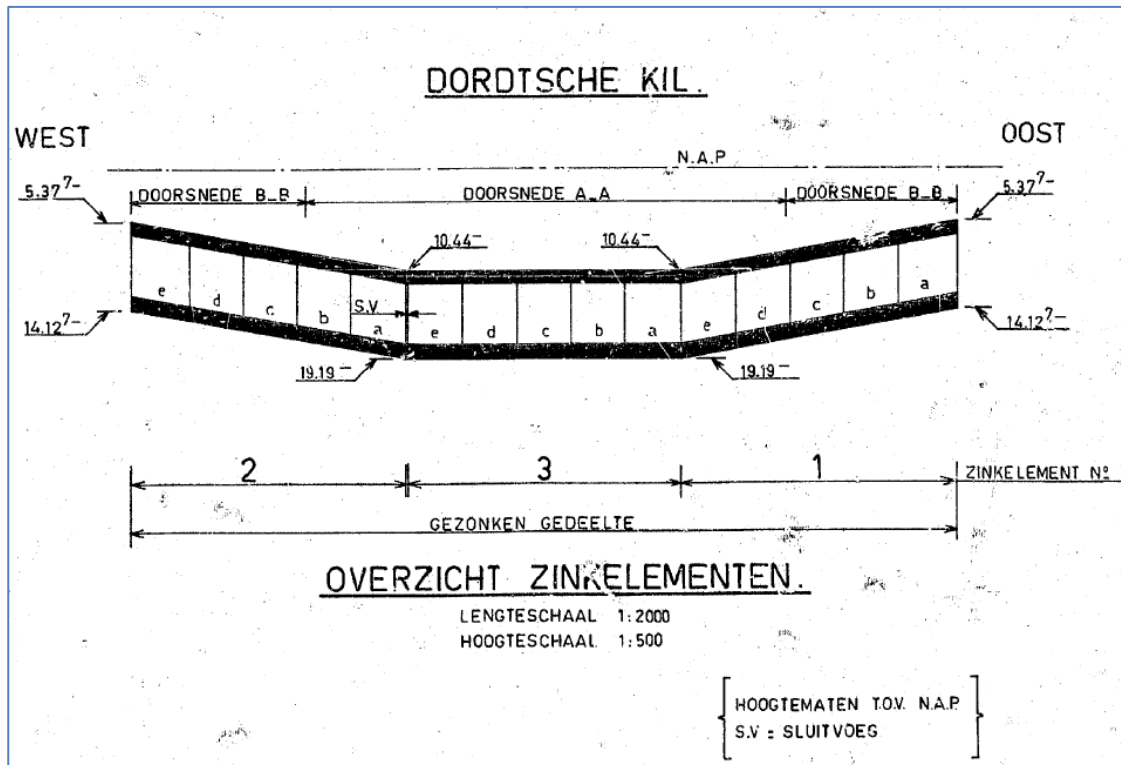
Appendix B1

In chapter 2, in section 2.5, analysis 1 has been discussed. This analysis is carried out for a single shear key. The interesting points in the analysis are discussed in detail. The plot for Concrete tensile stresses, the concrete compressive stress, the reinforcement stresses and the crack width is plotted for points 1, 2 and 3 as shown in the figure. These steps are 35, 45 and 48 in the analysis and have been discussed in this Appendix.
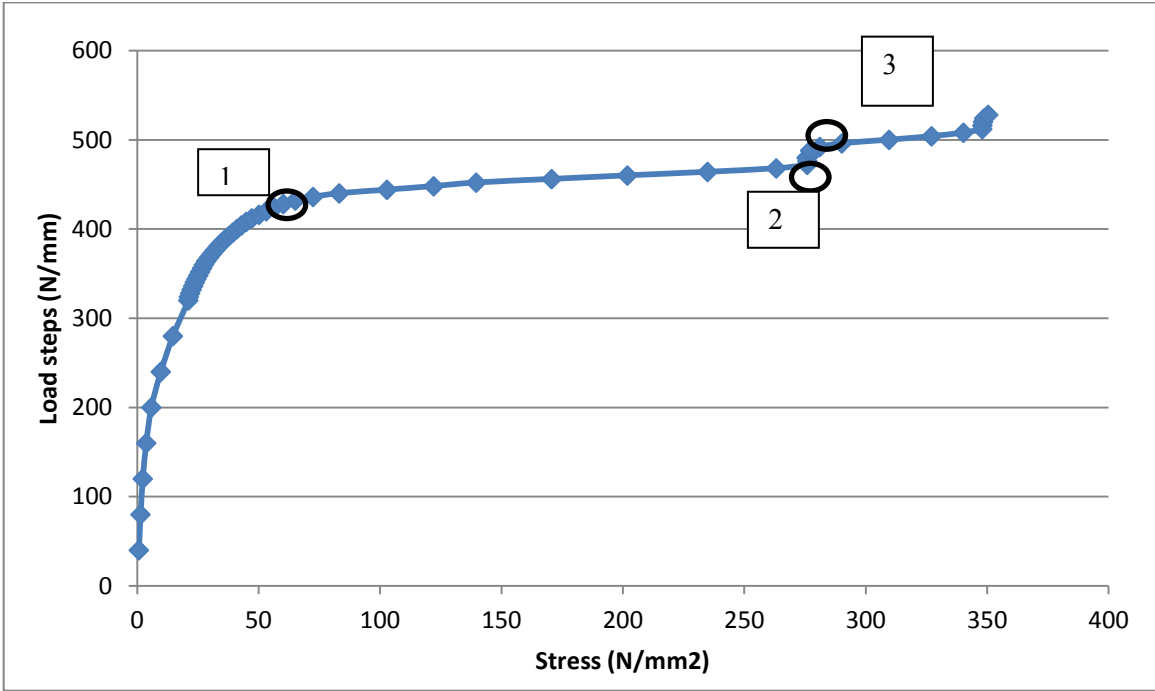
For point 1 → Step 34, Load = 424 N/mm

- Reinforcement stresses
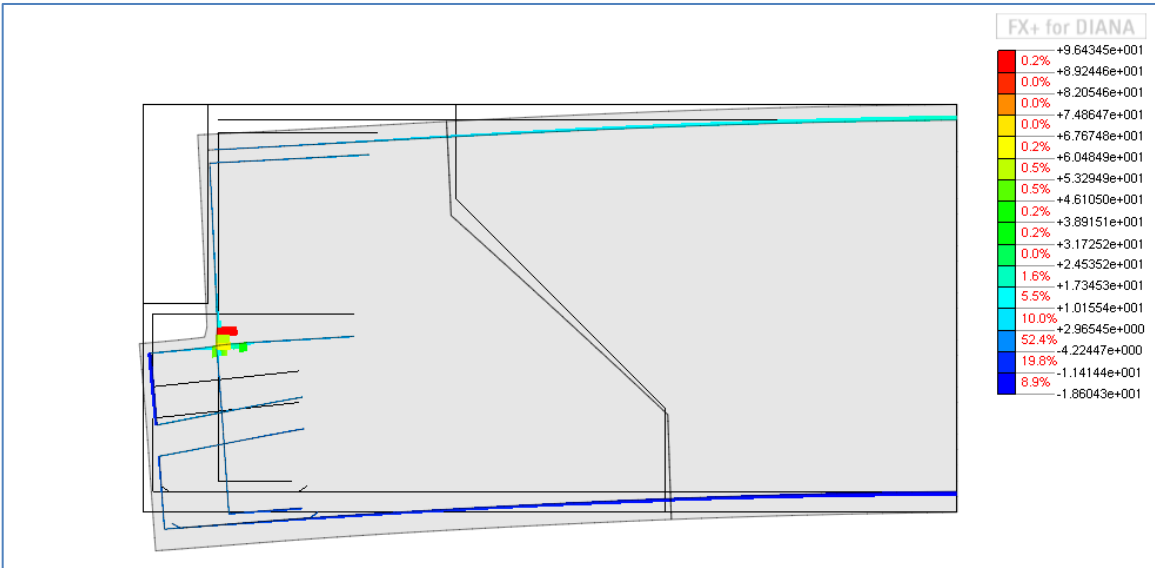
- Tensile stresses- step 34
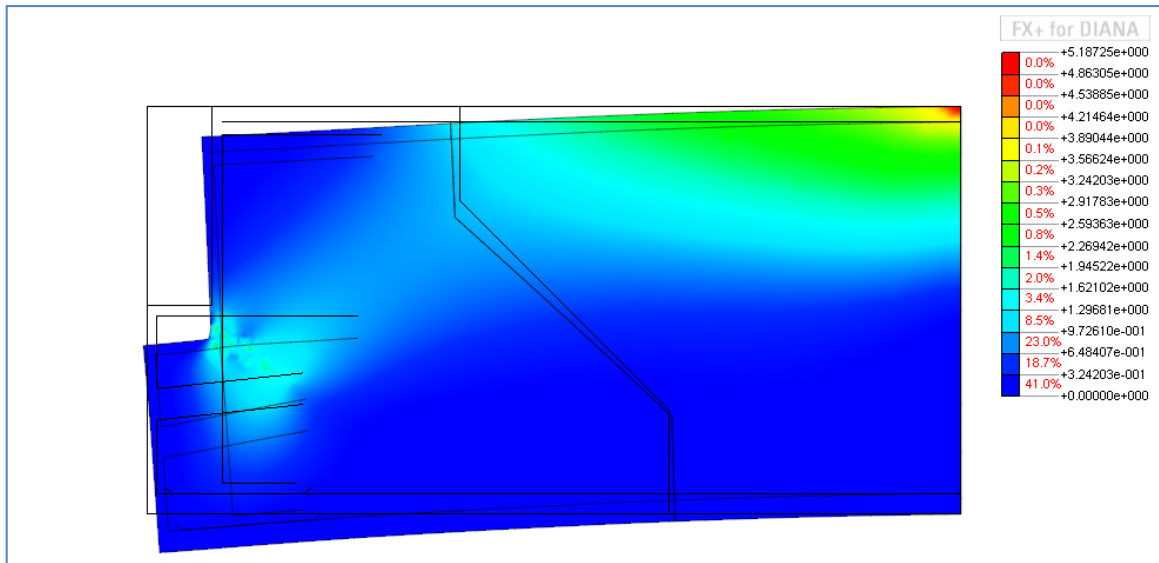
- Compressive stresses-step 34
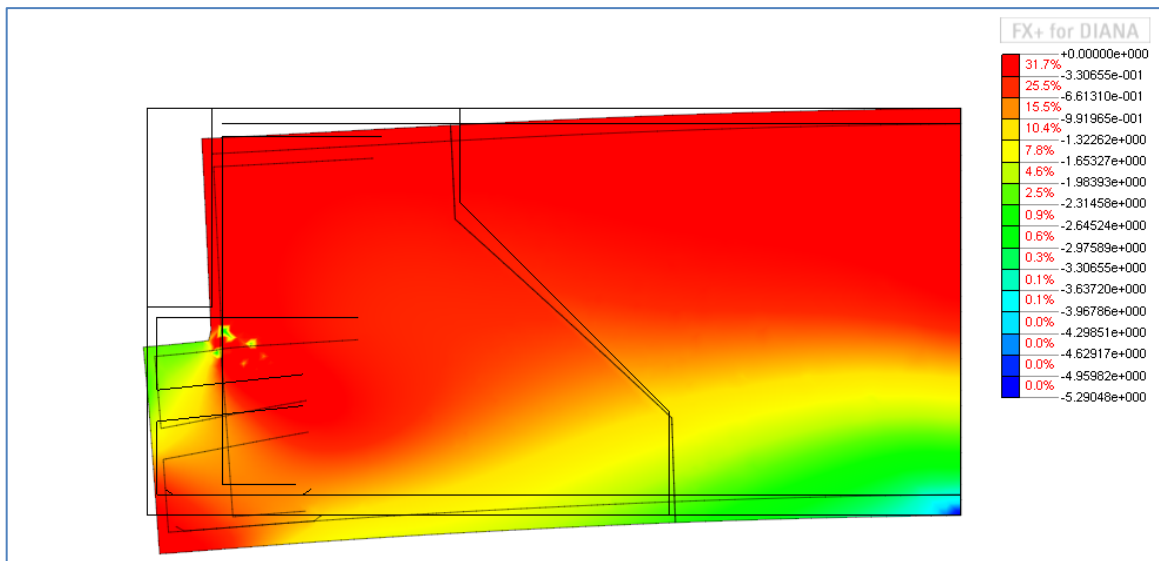
- Crack propagation- step 34
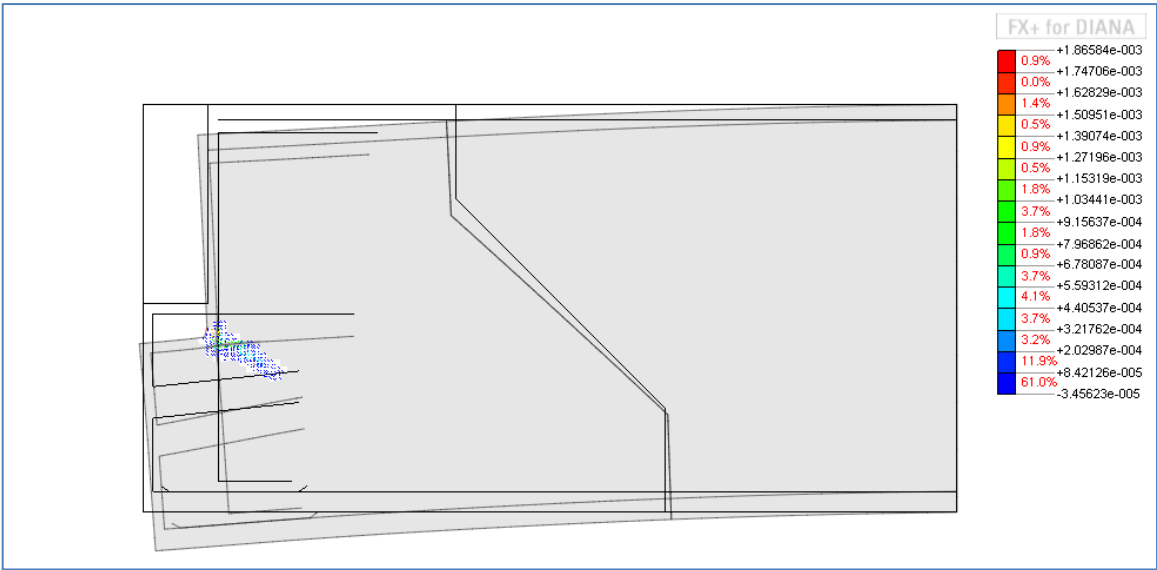
For point 2 → Step 45, Load = 468 N/mm

- Reinforcement stresses
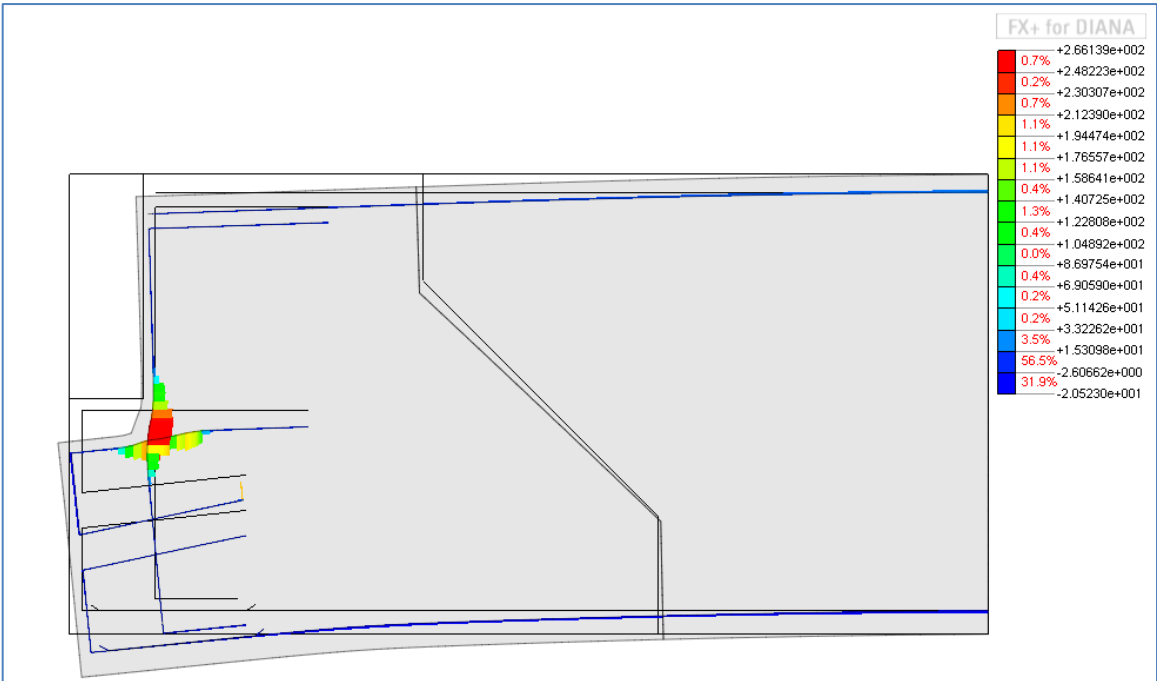
- Tensile stresses- step 45
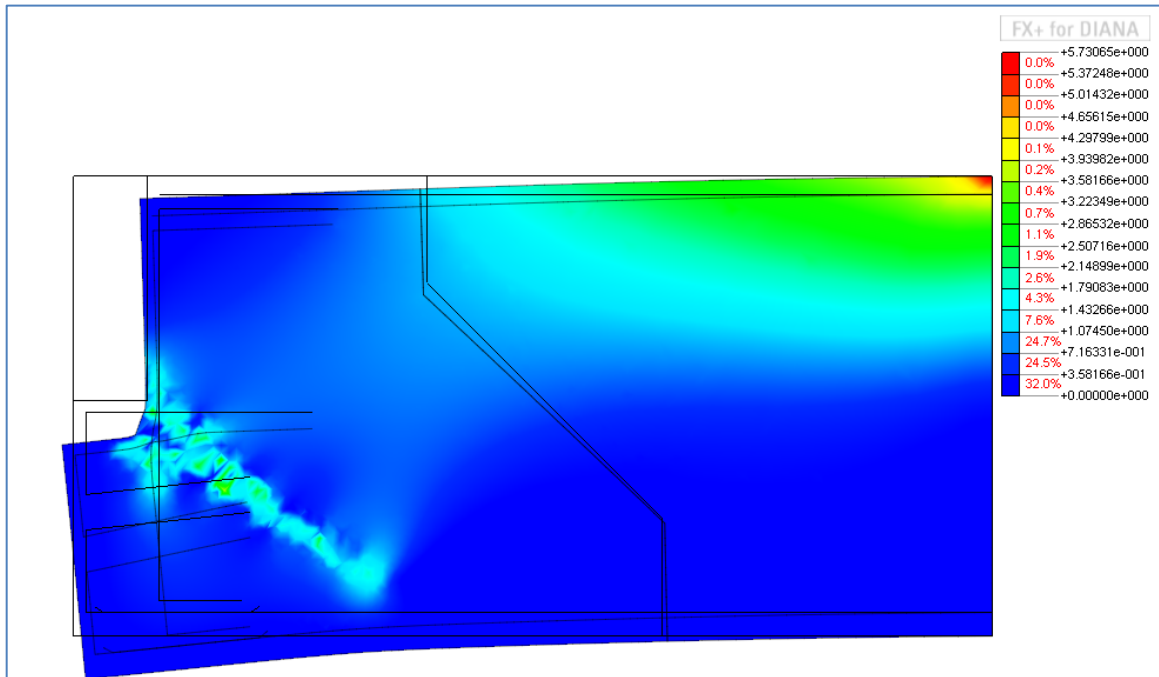
- Compressive stresses- step 45
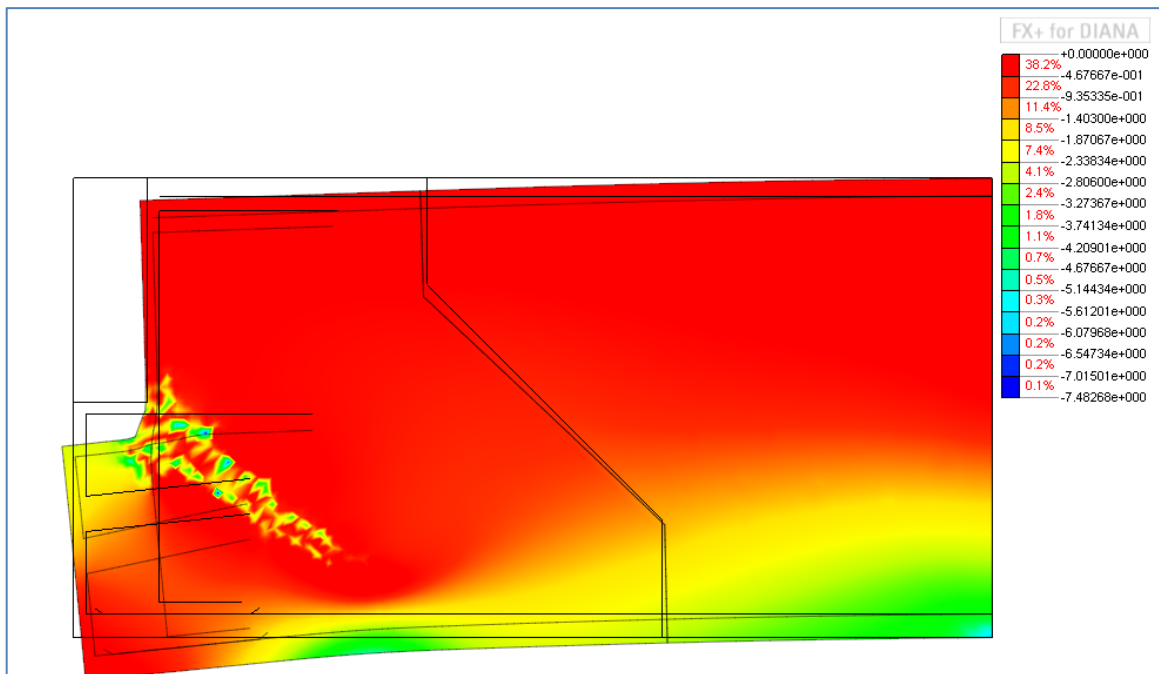
- Crack propagation- step 45
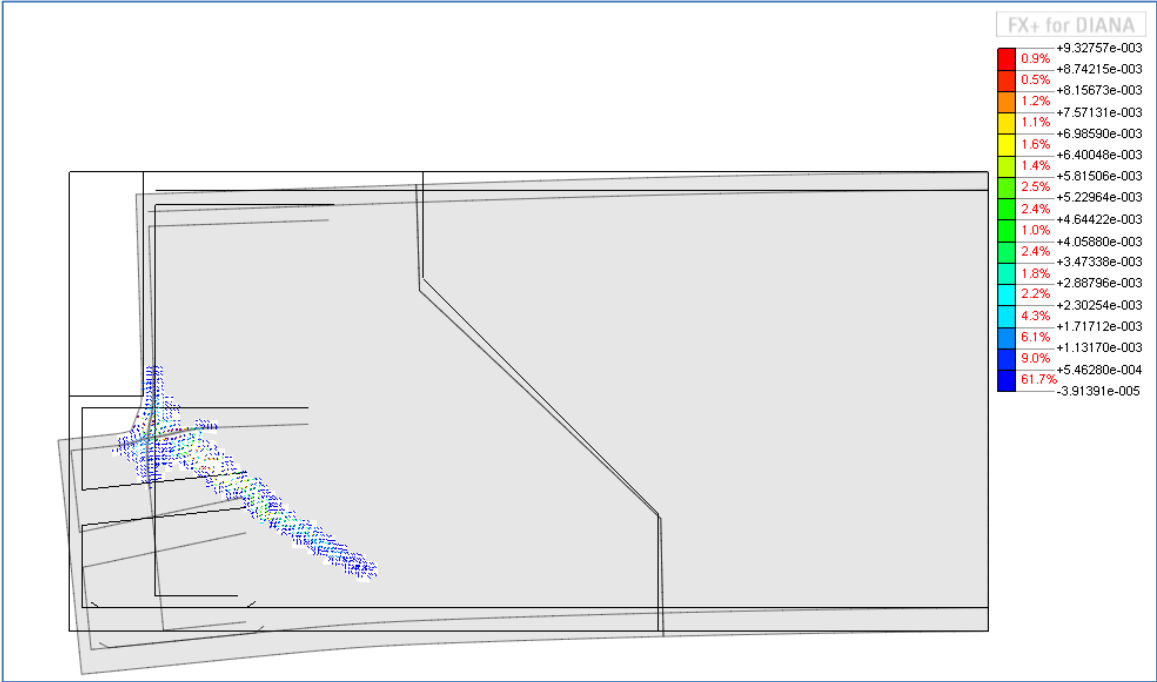
For point 3→ Step 48, Load = 480 N/mm

- Reinforcement stresses- step 48
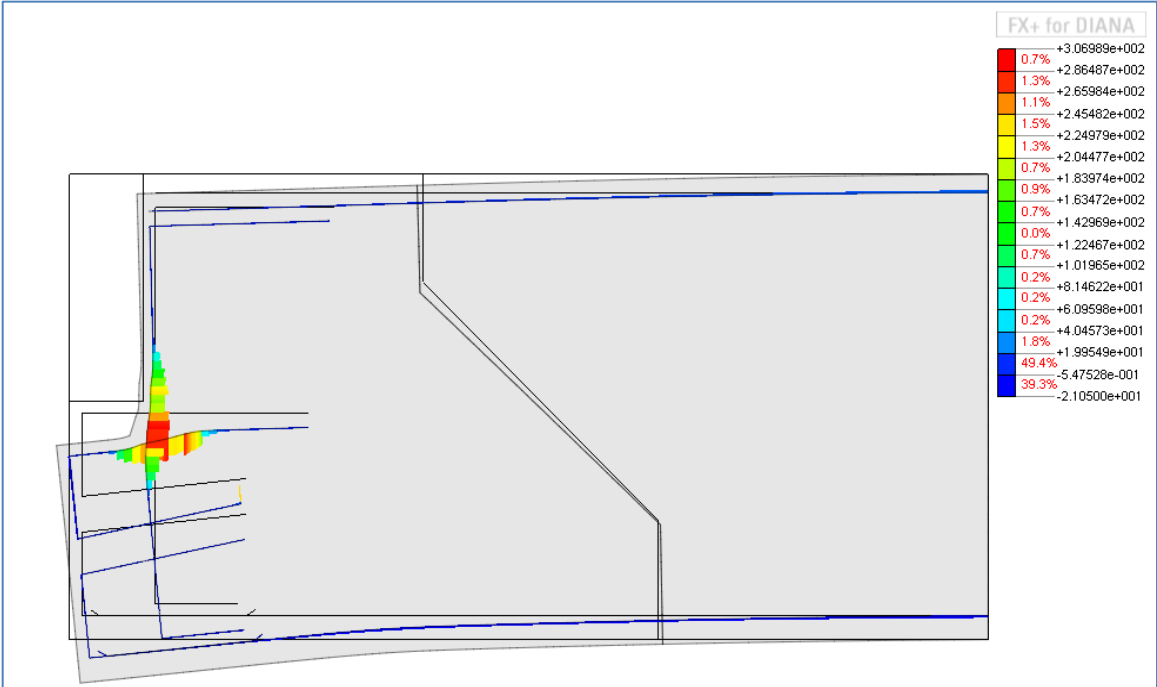
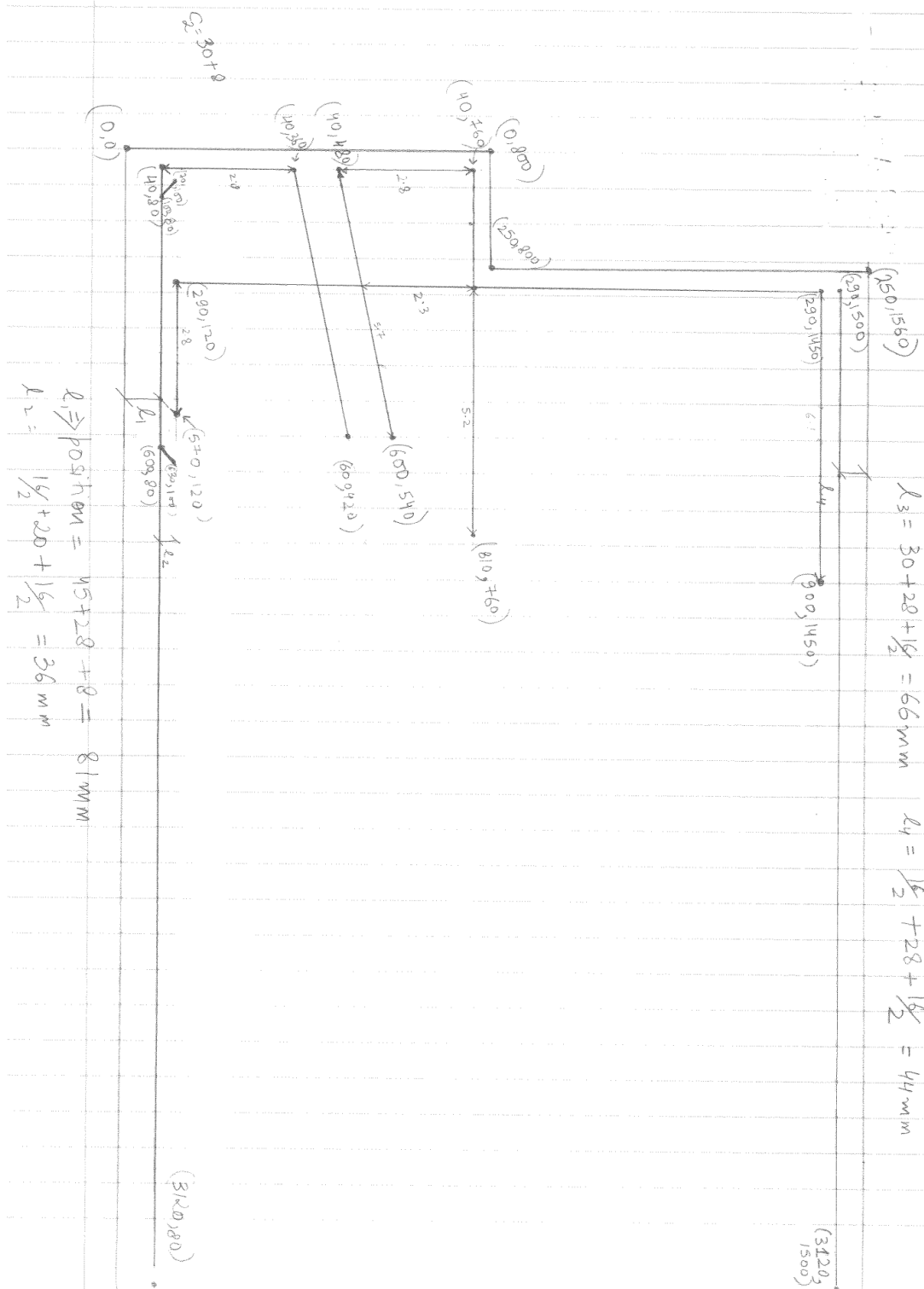- Tensile stresses- step 48
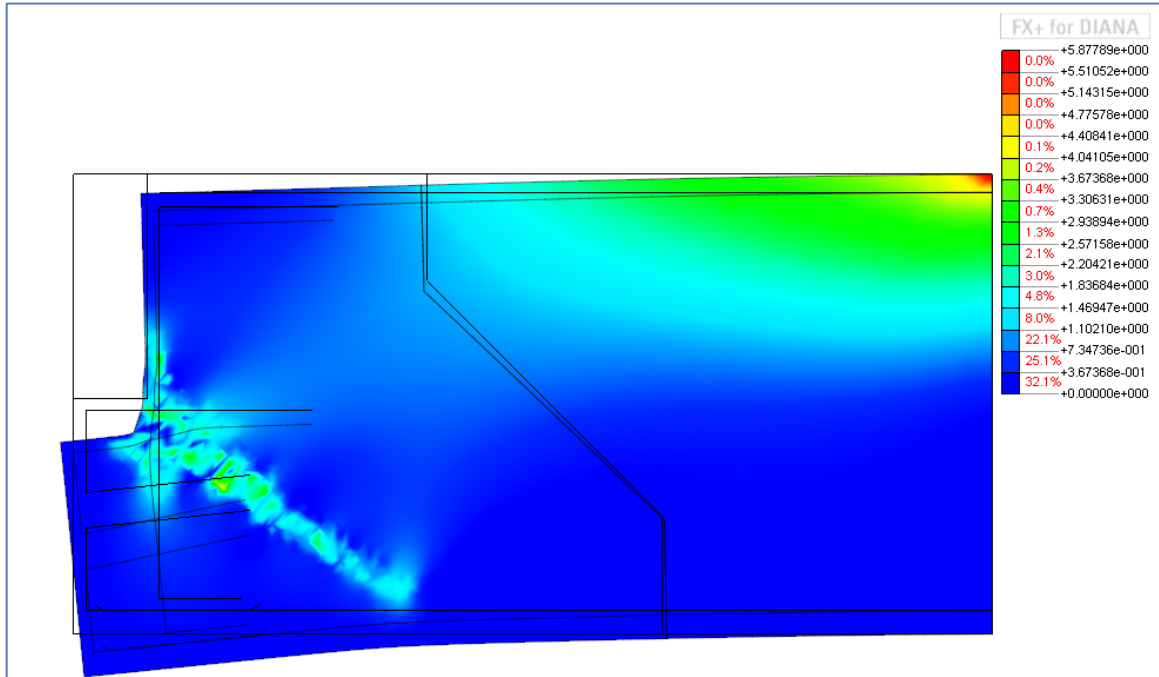
- Compressive stresses- step 48
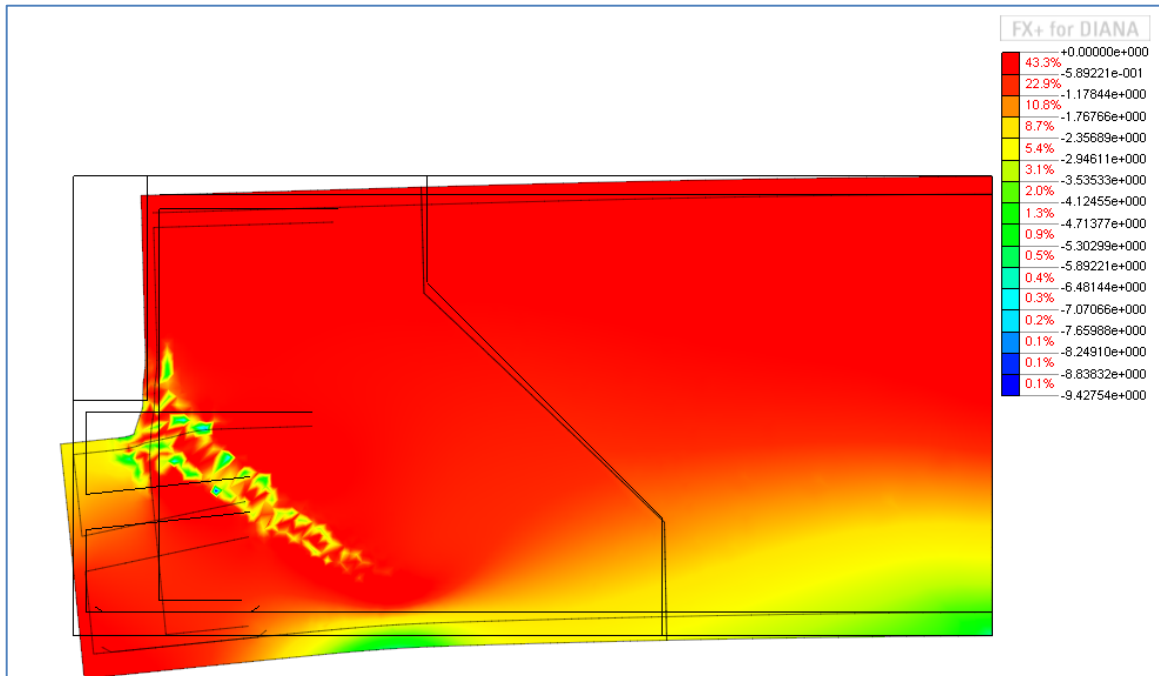
- Crack propagation- step 48
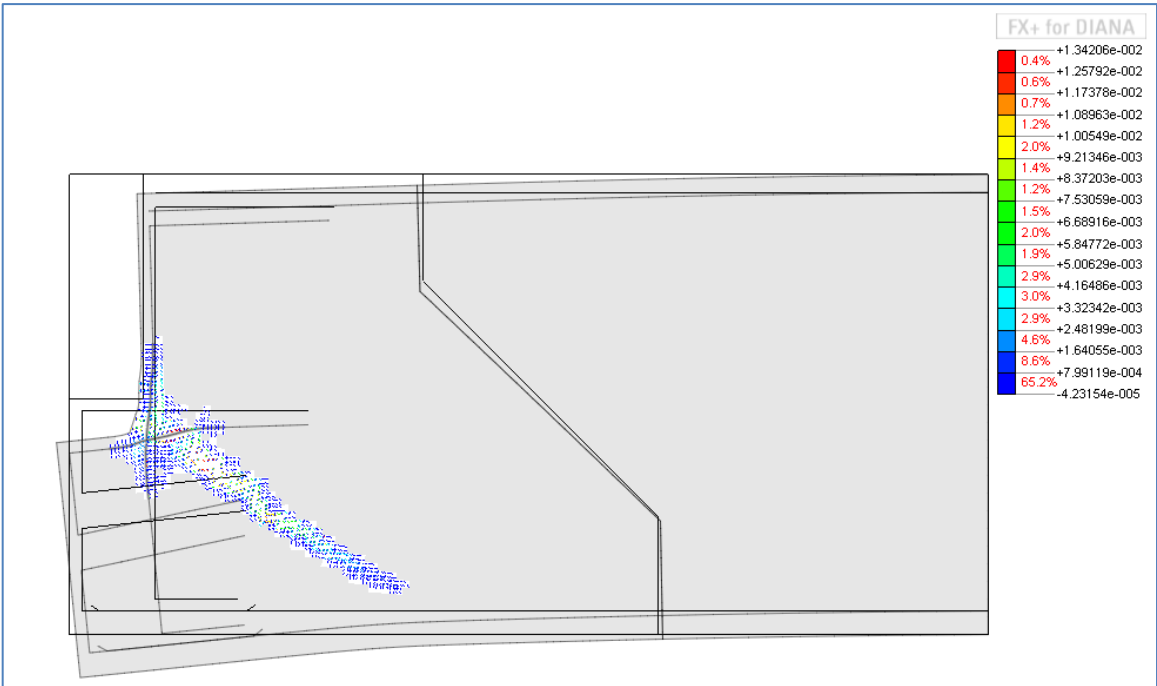
Appendix B2

The geometry of single shear key, analyzed in the strut and tie model in chapter 2

Appendix C1

The cross-section of the Kiltunnel, used in Chapter 4 and 5
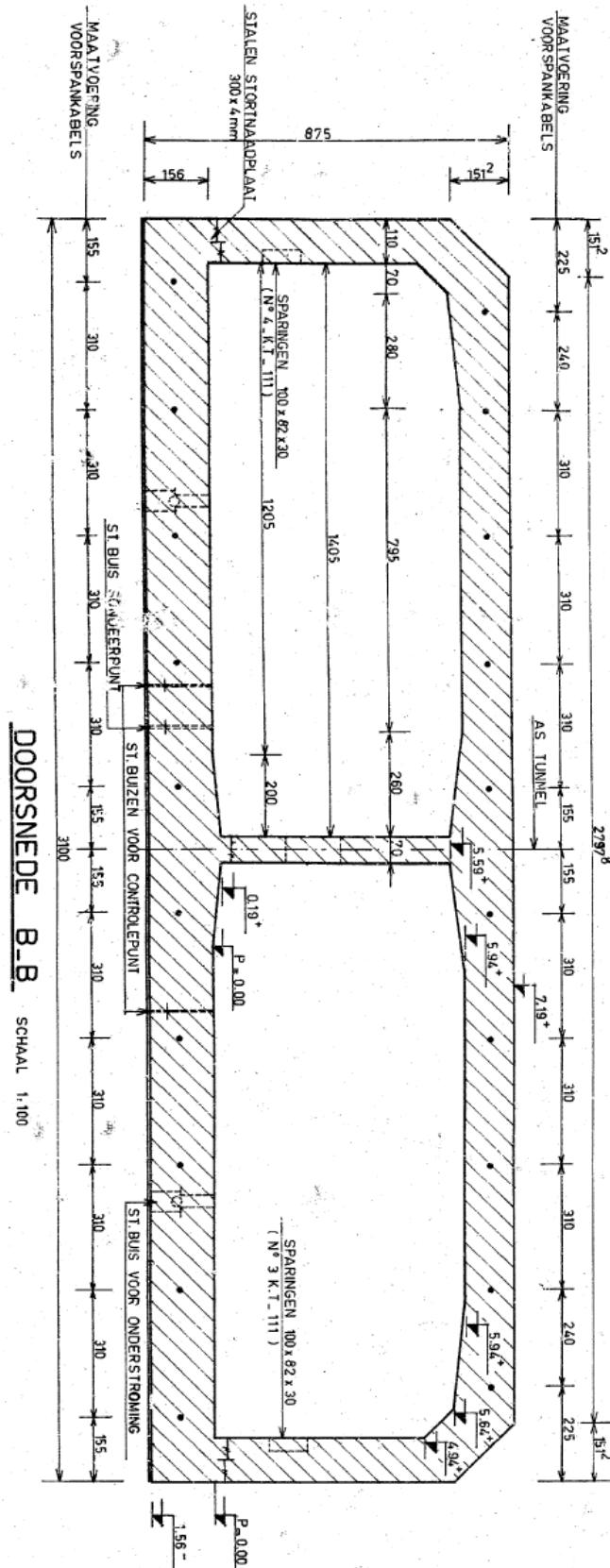
Appendix D1

An excerpt from **.dat file** showing the material properties used for concrete, steel, bitumen interface and the stiff plate at the end

```
'MATERI'
 1 NAME   CONCRETE //concrete properties
   YOUNG   3.40000E+004
   POISON  2.00000E-001
   TENSTR  1.50000E+000
   TENCRV HORDYK
   TOTCRK ROTATE
   GF1    7.50000E-002
 2 NAME   BITUMEN // interface properties
   DSTIF   1.70000E+004  1.53000E+004
   FRICTI
   FRCVAL  0.00000E+000  9.00000E-001  0.00000E+000
   GAP
   MODE2  0
 3 NAME   STEEL // steel properties
   YOUNG   2.10000E+005
   POISON  2.00000E-001
   YIELD  VMISES
   HARDIA  3.48000E+002  0.00000E+000  4.35000E+002  4.33000E+000
 4 NAME   STIFFELEMENT // stiff plate properties
   YOUNG   2.00000E+011
   POISON  2.00000E-001
```

**The .dcf file for execution**

```
*FILOS
 INITIA
*NONLIN
 EXECUT  LOAD  LOADNR 1 //Load-1 water pressure-as 1 load step
 BEGIN EXECUT
  BEGIN LOAD
   LOADNR 4 //Load 2- shear + bending moment
   STEPS  EXPLIC  SIZES 0.1(3) 0.02(35) //load steps
  END LOAD
  BEGIN ITERAT
   BEGIN CONVER
    DISPLA  OFF
    BEGIN ENERGY // energy and force norms
     CONTIN
     TOLCON 0.001
    END ENERGY
    FORCE  CONTIN
   END CONVER
```

```
    MAXITE 5 // maximum iterations is 5
    METHOD  NEWTON  MODIFI // newton raphson modified
  END ITERAT
END EXECUT
BEGIN OUTPUT
 FXPLUS
  FILE FULL87
END OUTPUT
*END
```
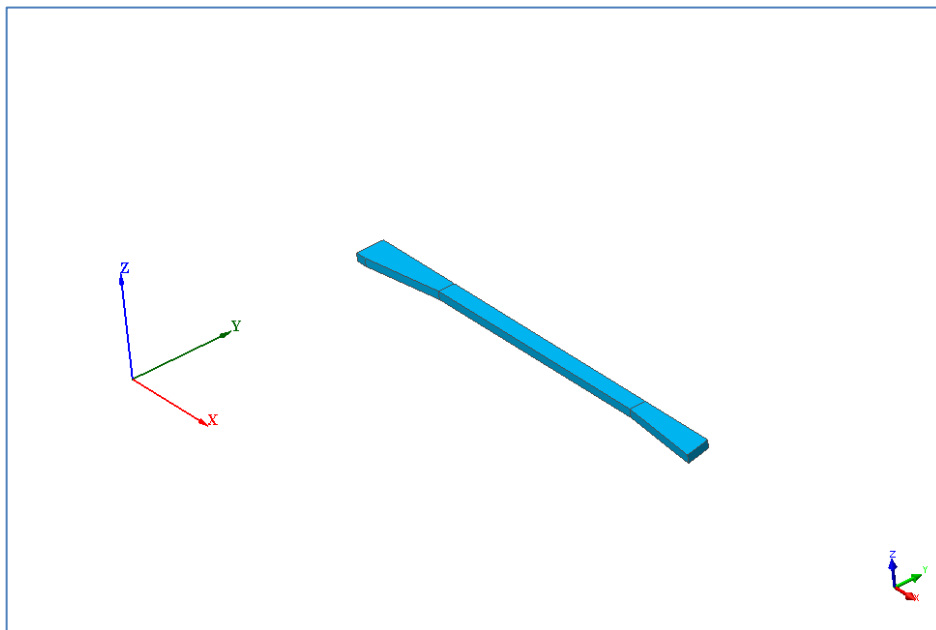
Appendix E1

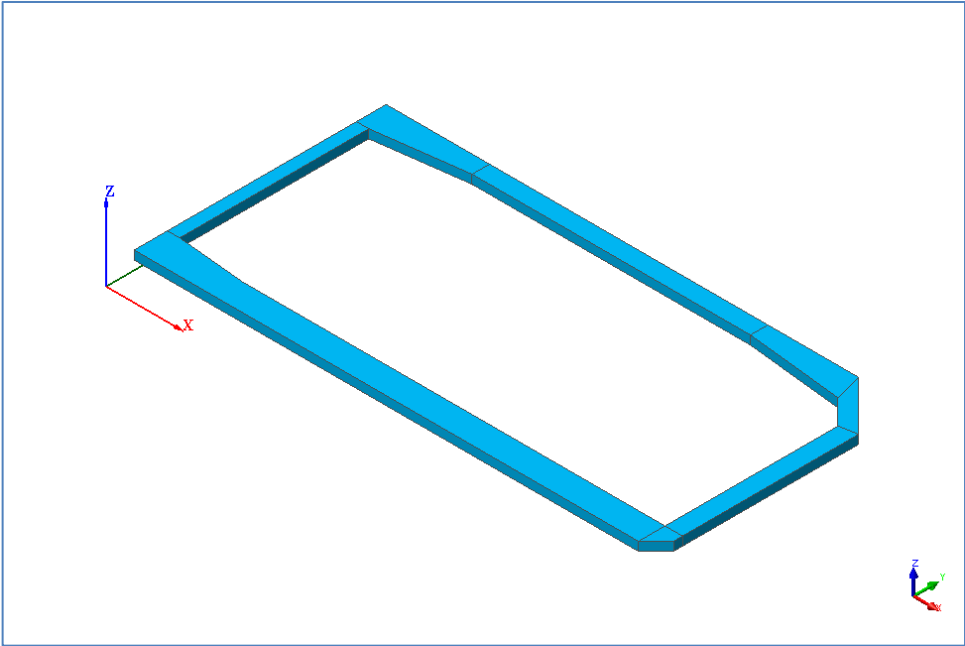Steps in the making of the 3-D model, discussed in Chapter 6.
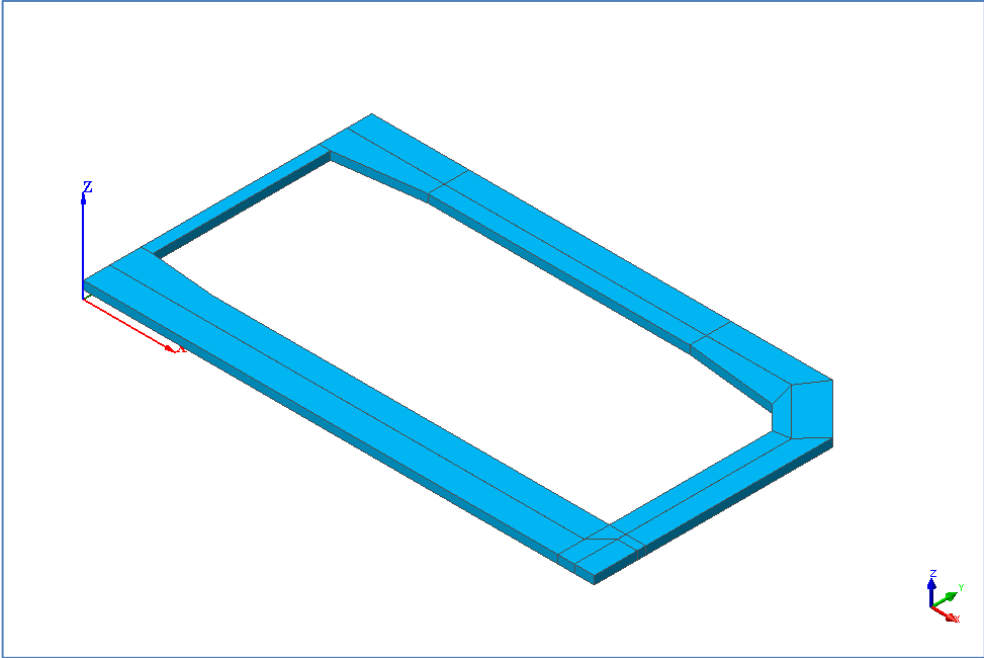
Step 1- Making of the inner tooth
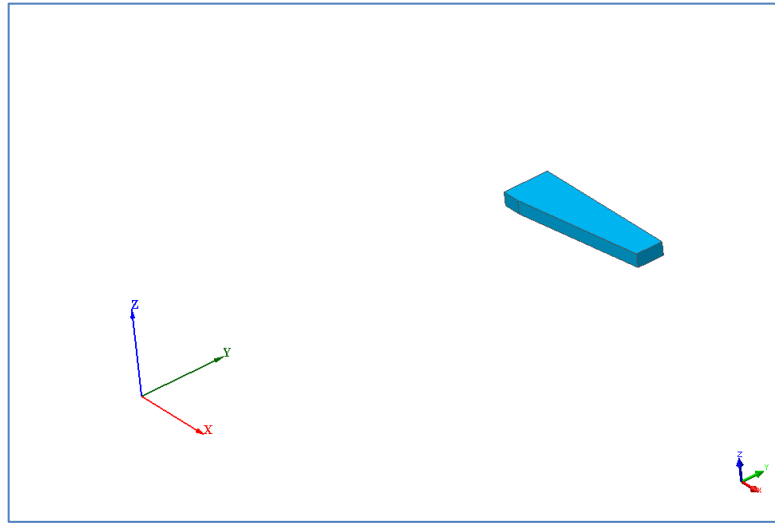
Step 2- Continuation of the inner tooth
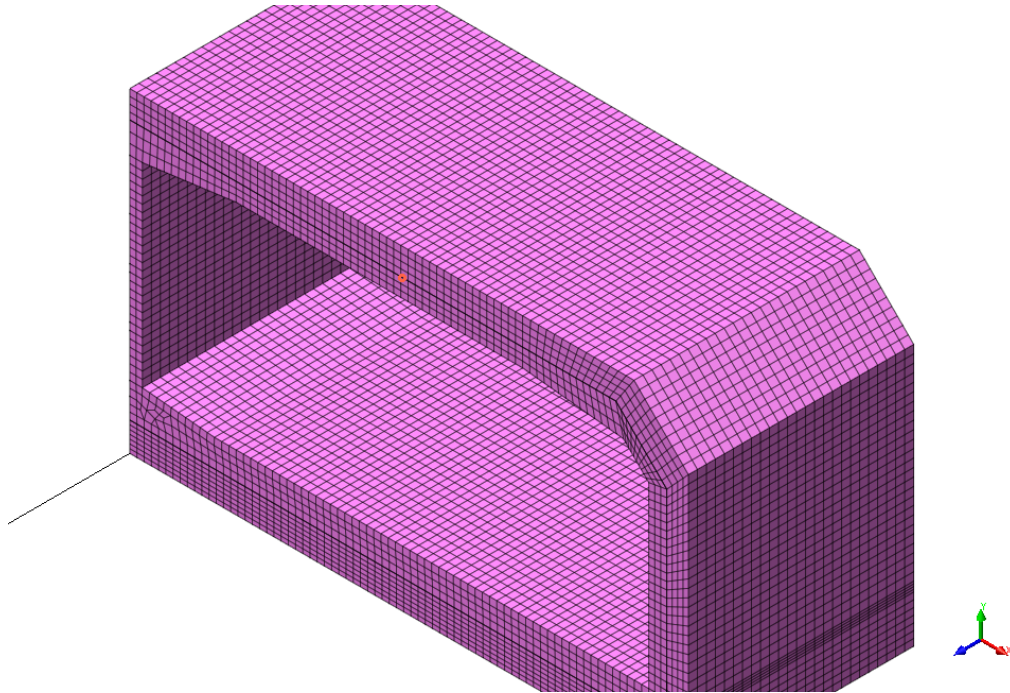
Step 3- Completion of the inner tooth

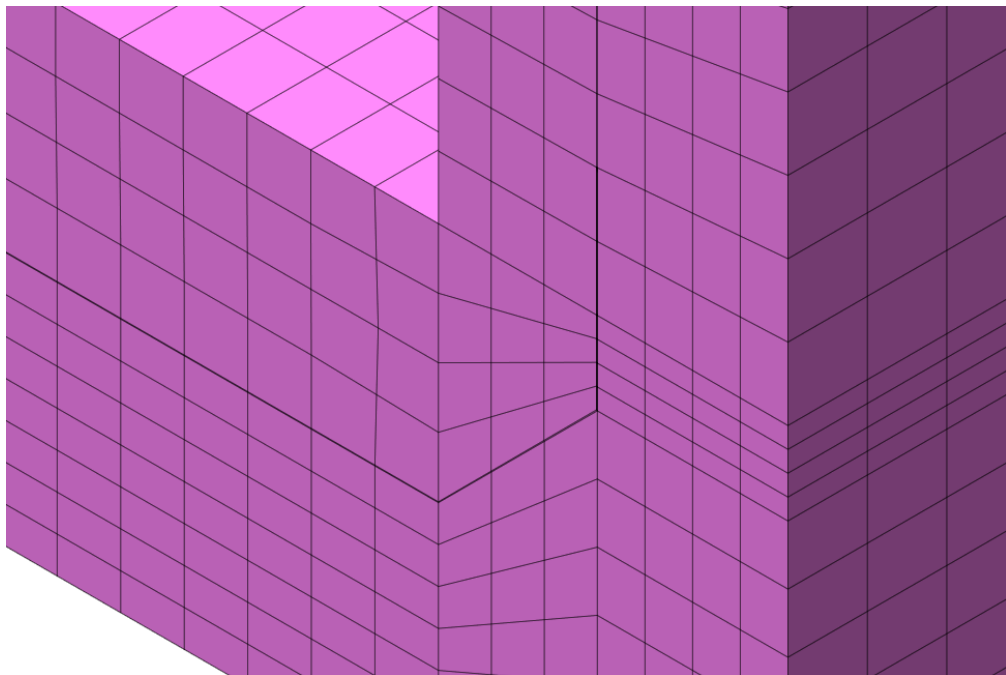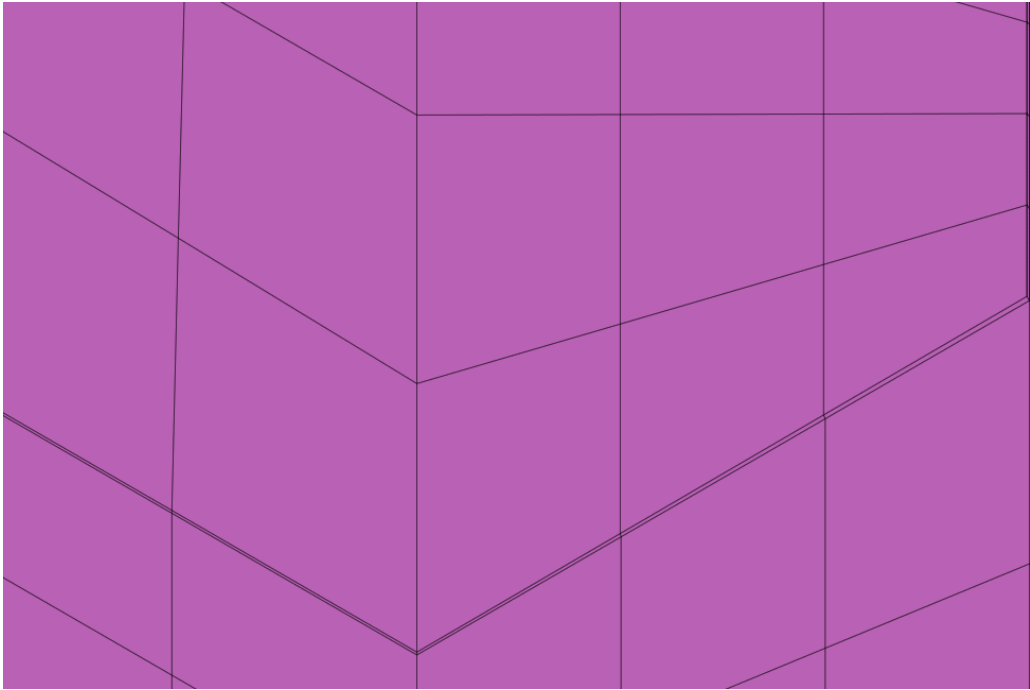**Step 4-** Completion of the outer tooth

Appendix E2

Closer look at the geometry of the tunnel and thin concrete elements, which may cause divergence in the structural analysis.

Section of tunnel-beyond the tooth

Magnified view near the outer wall

2mm thin elements in the concrete- shown near the outer wall